

Effects of redox variability and early diagenesis on marine sedimentary Hg records

Joost Frieling¹, Tamsin A. Mather¹, März Christian², Hugh Jenkyns¹, Hennekam Rick³, Reichart Gert-Jan⁴, Slomp Caroline⁴, and Niels Van Helmond⁴

¹University of Oxford

²University of Leeds

³NIOZ

⁴Utrecht University

February 22, 2024

Abstract

Volcanism is the dominant natural source of mercury (Hg) to the atmosphere, biosphere, ocean and sediments. In recent years, sedimentary Hg contents have emerged as a tool to reconstruct volcanic activity, and particularly activity of (subaerially emplaced) large igneous provinces (LIP) in geological deep time. More specifically, Hg has shown potential as a useful proxy to illuminate the previously elusive impact of such large-scale volcanism on marine and terrestrial paleo-environments. While Hg is now widely applied as volcanism tracer, non-volcanic factors controlling sedimentary Hg content are generally not well constrained. Part of this uncertainty stems from our inability to directly observe a natural unperturbed “steady-state” environment as a baseline, as the modern Hg cycle is heavily influenced by anthropogenic activity. Here we focus on the effects of ambient redox conditions in the water column and shallow sediments (early diagenesis), quantify their influence on the geological Hg record and thereby constrain their potential impact on the use of Hg as a proxy for deep-time volcanic activity. Constraining these factors is of critical importance for the application of Hg as a proxy. Many periods in the geological past for which records have been generated, such as the Mesozoic Oceanic Anoxic Events, are marked by a variety of high-amplitude environmental perturbations, including widespread deoxygenation and deposition of organic-rich sediments. We estimate the impact of redox changes and early diagenesis on the geological Hg record using a suite of (sub)recent–Pleistocene and Upper Cretaceous sediments representing oxic to euxinic marine conditions. Our sample set includes a transect through an oxygen minimum zone and cores that record transient shifts in oxygenation state, as well as post-depositional effects – all unrelated to volcanism, to the best of our knowledge. We find substantial alterations to the Hg record and the records of organic carbon and total sulfur, which are typically assumed to be the most common carrier phases of Hg in marine sediments. Moreover, these biases can lead to signal-alterations on a par with those interpreted to result from volcanic activity. Geochemical modifications are ubiquitous and their potential magnitude implies that the factors leading to biases in the geological record warrant careful consideration before interpretation. Factors of particular concern to proxy application are (1) the disproportionate loss of organic carbon and sulfur compounds relative to Hg during oxidation that strongly modulates normalized Hg records, (2) the evasion of Hg in anoxic and mildly euxinic sediments and (3) sharp focusing of Hg during post-depositional oxidation of organic matter.

1. Introduction

1.1 Hg in sedimentary records and its use as a proxy

In recent years, sedimentary mercury (Hg) has rapidly gained widespread attention due to its proposed use as a proxy for volcanic activity, particularly the volcanism associated with (subaerial) emplacement of large igneous provinces (LIPs) in the geological deep past ($>>10^6$ years) (e.g. (Sanei et al., 2012; Grasby et al., 2013; Percival et al., 2017; Kender et al., 2021)). This approach is based on the predominance of

volcanic-derived Hg prior to the emergence of anthropogenic fluxes (Pyle and Mather, 2003; Fitzgerald et al., 2007; Pirrone et al., 2010). Particular attention has been given to periods in geological time during which subaerial LIPs are thought to have been highly active, based on other sedimentary proxies (such as Os isotopes and (trace) metal enrichments; e.g., (Cohen et al., 2004; Snow et al., 2005; Du Vivier et al., 2014)) as well as direct dating of volcanogenic deposits (e.g., Sprain et al., 2019). These periods of (subaerial) LIP activity have also been studied for their high-amplitude environmental perturbations, including global warming, increased weathering, loss of biodiversity, changes in terrestrial vegetation, soil erosion, extensive water column anoxia–euxinia and ocean acidification.

To make accurate inferences about volcanic LIP activity from Hg enrichments in stratigraphic records, the influence of other sedimentary changes on Hg and its carrier compounds needs to be resolved in appropriate detail. For example, it is well established that particulate and dissolved organic matter (OM) concentration is an important factor in governing the Hg levels in seawater (Wallace, 1982) and sediments (Fitzgerald et al., 2007; Gehrke et al., 2009). This relationship is due to the very high affinity of Hg^{2+} for OM, which commonly leads to strong correlations between total organic carbon (TOC) and Hg (Outridge et al., 2007; Gehrke et al., 2009). While there are some indications that, under extremely high productivity regimes, dilution of Hg by organic matter might play a role (Machado et al., 2016), this appears to be uncommon in modern aquatic and sedimentary environments where Hg concentrations and Hg sequestration are positively correlated to (algal) OM abundance (profiles), although this relation is not necessarily linear (Wallace, 1982; Sanei and Goodarzi, 2006; Fitzgerald et al., 2007; Outridge et al., 2007; Bowman et al., 2016; Biester et al., 2018; Schütze et al., 2021; Cossa et al., 2022). To eliminate variation induced by changes in OM content, normalizing Hg contents against TOC in sedimentary records has become common practice in deep-time literature (e.g. Percival et al., 2015; Percival et al., 2017; Grasby et al., 2019; Jones et al., 2019; Shen et al., 2019b; Kender et al., 2021; Tremblin et al., 2022; Zhao et al., 2022a). The basis for this approach lies in that Hg in the sedimentary record is primarily bound to OM and only secondarily to other potential scavenging compounds (e.g., sulfides, forming compounds such as mercury sulfide (HgS) or Hg inclusion in pyrite, or adsorption to clays), especially in the presence of abundant OM (e.g., Fitzgerald et al., 2007 and references therein). In the absence of large Hg-cycle perturbations, the positive correlation between Hg and TOC, both at single sample localities (e.g., Percival et al., 2015; Shen et al., 2020) and at broader scales (e.g., Grasby et al., 2019) in the geological record, provides support for this generalization. However, the relation between Hg and TOC is in many instances not straightforward and since normalized Hg is not stable across all environments, the assumption that Hg/TOC (or otherwise normalized Hg) remains stable (in the absence of large-scale volcanic emissions) does not hold true for many deep-time records analyzed to date. Moreover, it has been established that, for example, other sedimentary Hg carrier phases such as sulfur (S) and pyrite can play an important role, especially in strongly euxinic conditions (Shen et al., 2019a, 2020; Wang et al., 2020). Through association with TOC, clays and S, Hg might appear to behave in a similar way to bio-essential, redox-sensitive and/or sulfide-forming trace metals (such as, for example, Mo, V, Ni, Cd, Zn), that may change phase associations following their deposition at the seafloor (e.g., Tribouillard et al., 2006; Brumsack, 2006).

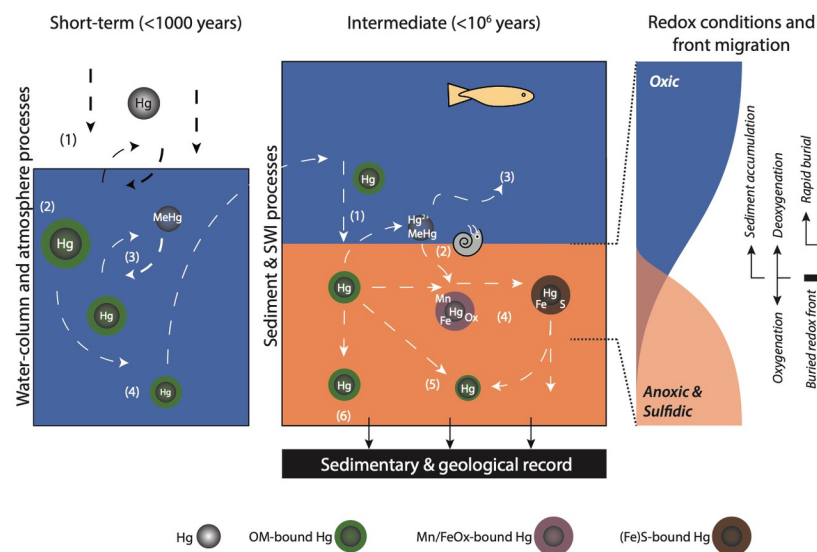


Fig. 1. Simplified diagram illustrating a selection of pathways that influence aquatic (marine) sedimentary mercury (Hg) and/or organic-matter cycling (green circles). Blue and brown/orange colors in middle panel indicate water and sediment, respectively.

Left-hand panel: atmospheric deposition and aquatic processes– (1) influx from rivers and atmosphere, (2) gas exchange in the surface layer (Mason and Sheu, 2002; Strode et al., 2007; Mason et al., 2012), (3) remineralization in the upper water column and methyl-mercury (MeHg) formation (Heimbürger et al., 2010), (4) progressive OM and Hg cycling and remineralization in the lower water column. Note that ageing deep water accumulates both C and Hg (Takahashi et al., 2002; Bowman et al., 2015, 2016).

Middle panel – processes potentially influenced by ambient oxygenation: (1) deposition of OM-bound Hg from the water column (Wallace, 1982) (2) bioturbation, diffusion and biologically driven cycling of OM and Hg near the sediment–water interface, (3) potentially resulting in Hg evasion (with MeHg or Mn/Fe (oxyhydr)oxides as intermediate phases) (Gagnon et al., 1997; Mikac et al., 1999; Hammerschmidt and Fitzgerald, 2004), (4) (temporary) binding to Mn/Fe (oxyhydr)oxides and sulfide minerals (Gagnon et al., 1997; Shen et al., 2020), (5) recalcitrant OM and Hg remaining after oxidation, (6) unaltered recording of Hg scavenged from the water column.

Right-hand panel - simplified reduction-oxidation (redox) front – controlling the position and intensity of processes depicted in the middle panel . The redox front, here illustrated from the sediment-water interface down, migrates upwards with sediment accumulation and deoxygenation, downwards with (re)ventilation and may be buried and fixed, for example when a mass-transport deposit such as a turbidite rapidly covers the sediment–water interface. The position of the redox front influences many (trace-) element records and, combined with processes shown in the middle panel, such as Hg binding to Mn/Fe (oxyhydr)oxides, sulfides and methylation, conceivably also shapes the sedimentary Hg record.

To date, variability in pre-industrial marine sediments, and particularly in deep-time records, related to the processes controlling coupled TOC, S and Hg burial remains poorly understood. These processes can be roughly divided into three categories. In the first category are processes that influence Hg and/or TOC before they enter the sedimentary record, such as the riverine flux of Hg and terrestrial OM, ocean–atmosphere exchange, and water-column processes (abundance of marine OM, remineralization, scavenging efficiency). The second category includes processes that take place during or shortly after the sedimentary record is formed, particularly early diagenetic and soft-sediment processes: redox behavior, remineralization and re-mobilization. The cycling of Hg, the position of the redox front and its migration ultimately determine the signal preserved in the sedimentary record (Fig. 1). Third, signal deterioration may occur in samples that

have been exposed for long periods on the Earth’s surface (Charbonnier et al., 2020). The potential for weathering to alter Hg records is high in arid regions that provide seemingly excellent outcrop material for less reactive compounds such as clays and carbonates (Keller et al., 2018, 2020; Racki et al., 2018; Sabatino et al., 2018).

Whereas unaltered material may be recovered given the right circumstances or through deep drilling, the short-term processes that lead to the original Hg deposition in the marine realm, as well as early diagenesis, potentially influence any geological record of Hg and OM. Therefore, these processes warrant careful consideration in terms of what their effects might be and how they might be recognized. Because Hg, TOC and other Hg-binding ligands are unlikely to be uniformly influenced by early diagenesis, and particularly by oxidation, TOC- or S-normalized records will be especially sensitive to these poorly constrained confounding factors. We here focus on the short-term post-depositional diagenetic alteration of Hg and its carrier phases and how such alteration might have influenced the sedimentary record.

1.2 Behavior of major Hg carriers: sedimentary TOC & S

The preservation of OM in sediments is a function of several factors, most notably plankton productivity, export carbon flux, ventilation of the overlying water and influx rate and type of siliciclastic material (Demaison and Moore, 1980; Pedersen and Calvert, 1990). Overall, less exposure to oxidants is expected to yield higher preservation potential of OM, including relatively labile compounds (Hedges and Keil, 1995; Hedges et al., 1999). At the same time, redox-sensitive elements are scavenged, released or remobilized at various depths in the water column and sediment (Calvert and Pedersen, 1993; Tribovillard et al., 2006).

In typical marine sediments since the Mesozoic Era, S has been deposited under non-sulfidic water-column conditions in a fairly constant ratio with organic carbon (C/S) of around ~ 3 –4 (Berner and Raiswell, 1983; Berner, 1989). However, in sulfidic settings, a larger proportion of sedimentary S might be present as sulfide minerals. Increased S sequestration is relevant as Hg, like many divalent metals (Morse and Luther, 1999), may be sequestered directly as a sulfide mineral (HgS) or as an inclusion in, for example, pyrite (Hg-FeS₂) (Shen et al., 2020; Wang et al., 2020). Moreover, during times of much lower (μ M-levels rather than mM) marine sulfate concentration than in the present-day ocean, the occurrence of widespread sulfidic conditions may have been limited (e.g. Lowenstein et al., 2001; Wortmann and Chernyavsky, 2007; Newton et al., 2011; Xu et al., 2018), and it is conceivable that, in some intervals during the Phanerozoic, the rate of pyrite burial was also temporarily limited (Wortmann and Chernyavsky, 2007; Algeo et al., 2015).

Overall, the preservation of both TOC and S is likely to be significantly controlled by the intensity and duration of bottom- and pore-water oxygenation. Under euxinic conditions, sedimentary S might show further enrichment relative to TOC, as S is also sequestered through formation of various metal sulfides. The trends that sedimentary TOC and S follow with changing ambient redox conditions are relatively well established and thereby provide useful simplifications until more detailed data become available. But it should be noted that Hg may not exclusively follow the classic OM- or S-bound path, as has been shown, for example, by Mo (Helz and Vorlicek, 2019).

1.3 Behavior of Hg in sediments – (de)oxygenation

Unlike many other divalent metals, Hg is not usually associated with any sulfate mineral (cf. Ba in barite), and it does not serve as an essential micro-nutrient (as do, for example, Fe, Cu, Mo, Ni), which could lead to direct metal-OM associations. Many other predominantly divalent heavy metals that are also associated with OM may bind to sulfide and are traditionally used as redox proxies themselves (e.g., Mo, Cd: Brumsack, 2006; Lyons et al., 2009; Tribovillard et al., 2006). Binding to sulfide minerals implies that these elements can be efficiently trapped in sulfidic (pore) waters. By contrast, it might be expected that sulfate-depleted anoxic conditions (see section 1.2) could lead to lower HgS and pyrite-associated Hg burial, relying on other carrier phases to sequester Hg. Although Hg speciation and element mapping data are very scarce for Pleistocene and older sediment samples (Shen et al., 2019a, 2020; Wang et al., 2020), the limited evidence suggests that Hg-S associations (specifically pyrite) are rarely dominant and perhaps less common than expected. Most deep-time studies that have argued for S-bound Hg inferred this association from stronger statistical

correlation of Hg and S compared to other tested parameters (e.g., Sanei et al., 2012; Shen et al., 2020; Zhao et al., 2022b). However, using statistical correlations to derive the (dominant) sedimentary host phase of Hg can be especially challenging as Hg carriers (TOC, S and clays) tend to be coupled or co-varying. For TOC and S, this covariation might primarily result from Hg binding to organic-S compounds such as thiols (Haitzer et al., 2002; Ravichandran, 2004), and HgS formation in sulfide-enriched (micro-) environments during OM remineralization (Pham et al., 2014; Manceau et al., 2015).

Moreover, some groups of micro-organisms, i.e., Fe- and sulfate-reducing and methanogenic bacteria and archaea, are capable of methylating Hg to avoid its toxic effects (Benoit et al., 1999; Fleming et al., 2006; Gilmour et al., 2013), while some methanotrophic bacteria can demethylate Hg (e.g., Lu et al., 2017). The mono- and di-methylated Hg (hereafter referred to collectively as MeHg) have been extensively studied because these Hg species are particularly toxic to higher organisms and subject to bio-accumulation in food webs (e.g., Morel et al., 1998; Fitzgerald et al., 2007; Merritt and Amirbahman, 2009; Cossa et al., 2022). Although some studies have hinted at MeHg presence in ancient rock archives (Rakociński et al., 2020), it seems unlikely many deep-time samples would retain ancient MeHg given the lability of this Hg species (Rydberg et al., 2008).

Compared to the rapidly scavenged dissolved Hg^{2+} , MeHg is considered more mobile in pore and bottom waters, which may result in significant Hg evasion from sediments (Hammerschmidt and Fitzgerald, 2004; Emili et al., 2011). The impact of Hg remobilization through MeHg formation on the geological record is worth exploring as methylation appears to be generally higher under oxygen-depleted conditions (Compeau and Bartha, 1985; Merritt and Amirbahman, 2009; Gu et al., 2011; Wang et al., 2021). MeHg formation also increases with abundant labile algal organic matter in the water column and sediment (Kim et al., 2011; Bravo et al., 2017; Jiang et al., 2018), factors that are often considered intimately coupled with low-oxygen conditions. If Hg-methylation is indeed a (more) common process in anoxic environments, sediments subjected to ferruginous or (mildly) sulfidic conditions may be expected to have comparatively low preservation potential for Hg, in apparent contrast to the more common assumption for deep-time studies that sulfidic waters may lead to Hg spikes (Grasby et al., 2019; Shen et al., 2020). While MeHg is usually not a large proportion of total Hg in modern (surface) sediments ($\sim 0.1\text{-}1\%$, e.g., Hammerschmidt and Fitzgerald, 2004; Fitzgerald et al., 2007), it can be argued that through net loss of MeHg to overlying waters, methylation of Hg can ultimately modulate total sedimentary Hg even if methylation is a slow process (Ogrinc et al., 2007; Emili et al., 2011).

It might be argued from these observations on Hg-methylation that the paradoxical scarcity of apparent Hg-sulfide complexes in the geological record could in part be a consequence of Hg methylation by sulfate reducers. HgS formation and pyrite inclusions could potentially be limited to (pore-water) environments where high concentrations of dissolved sulfide inhibit for Hg methylation by sulfate- and Fe-reducers (Compeau and Bartha, 1985; Merritt and Amirbahman, 2009). However, given that the vast majority of deep-time sedimentary Hg associations are inferred from statistical correlations, it is conceivable that even if sedimentary Hg was associated with S in sulfidic settings, this would remain obscured by the covariance of S with other host phases. Unfortunately, Hg speciation data, while fairly common for modern soil and sediment samples (e.g., Higuera et al., 2003; Sunderland et al., 2004; Cooke et al., 2009; Rumayor et al., 2017; Lim et al., 2020 and many others), is virtually absent for the deep-time rock record with a few notable exceptions (Shen et al., 2020; Wang et al., 2020). Whether Hg-S associations are truly scarce in the deep-time sediment records or remain systematically underappreciated may only be resolved when further dedicated Hg-speciation data become available for a range of geological samples.

Soft-sediment Hg redox studies, focusing on the mobility of Hg in polluted settings, also showed that, around active redox fronts, sedimentary Hg can be associated with Fe (oxyhydr)oxides through adsorption which, in turn, could imply that Hg mobility is affected by Fe and potentially Mn reduction and oxidation (Gobeil and Cossa, 1993; Mikac et al., 1999; Tribovillard et al., 2006). Data from post-depositionally oxidized turbidite sediments show Hg spikes at or around the buried oxidation fronts, which supports a degree of Hg adsorption to, and subsequent release from, Mn or Fe (oxyhydr)oxides (Merceone et al., 1999). Preserved Mn- and Fe-Hg

associations in the geological record appear to be rare. (Shen et al., 2020; Zhao et al., 2022b). Similar to Hg-S associations, the complication arises that with the currently available data these associations are generally only inferred via statistical correlation of Hg with Mn or Fe. Unlike Hg-S associations, scarce geological occurrence of Mn/Fe (oxyhydr)oxide-bound Hg (Shen et al., 2020) would align the notion that Hg adsorption to Mn/Fe (oxyhydr)oxides is an intermediate phase, whose preservation may be limited to buried redox fronts.

In summary, despite the somewhat uncertain long-term (10s to >1000s of years) and perhaps limited redox cycling of Hg^{2+} , we can expect some smoothing and alterations to the Hg signal relative to the burial flux with changing ambient redox conditions due to, for example, the mobility of MeHg and increased efficiency of Hg sequestration in sulfidic pore waters. Changes in ambient redox conditions have been recognized for many deep-time geological records, such as the Mesozoic Ocean Anoxic Events, several of which are also recognized as periods of LIP activity, both submarine and subaerial. Moreover, the progressive loss of TOC and S with oxidation (section 1.2) implies that normalization to TOC or S could introduce further uncertainty.

1.4 Aim and approach

Before applying the knowledge of Hg redox behavior in modern systems to the geological record, it is critical to recognize that this is based on recent and often polluted (soft) sediments (e.g., Fitzgerald et al., 2007; Gagnon et al., 1997). These sediments do not only have temporally and spatially highly variable and uncertain Hg influxes (e.g., Covelli et al., 2001; Leipe et al., 2013; Mason et al., 1994), but, even if not heavily polluted, are also subject to ongoing oxidation and redox-front migration. As these modern environments are continuously being geochemically modified, also on time-scales beyond those that can be observed in controlled environments (10s to >1000s of years), the findings obtained from them cannot be directly applied to signals that are recorded in ancient sedimentary Hg records. Moreover, as discussed above, syn-sedimentary oxidation leads to progressive loss of sedimentary OM and, after oxygen-depletion, increased sedimentary reduced S from sulfide minerals. As TOC and S are considered the most common Hg carriers these processes add a second layer of complexity to TOC- and S-normalized Hg records. Constraining the behavior of Hg and its relationship to the most common carrier phases (TOC, S) under variable redox conditions and understanding how these signals are recorded in sediments is fundamental for the use of (normalized) sedimentary Hg as a direct proxy for Hg-cycle perturbations and volcanic activity.

Understanding the role of chemical changes associated with early diagenesis and (an)oxic degradation is particularly important because many of the key intervals in geological deep time for which enhanced volcanic activity is discussed were also marked by high-amplitude variations in primary productivity, (local) oxygenation and TOC contents in accumulating sediment (Schlanger and Jenkyns, 1976; Jenkyns, 2010; Ernst and Youbi, 2017). Some soft-sediment studies show that Hg could have been enriched at, or actively moved away from, (extinct) redox fronts, and microbial Hg methylation could have resulted in active evasion from sediments (Mercione et al., 1999; Mikac et al., 1999; Fitzgerald et al., 2007, Fig. 1). Consequently, we here consider resolving the paired geochemical behavior of Hg itself, and of its potential carrier phases, during early diagenesis. This knowledge is fundamental for the reliable use of Hg and normalized Hg as proxies for enhanced volcanism in geological deep time. Moreover, global, regional and local biogeochemical models that include or focus on the long-term (sedimentary) Hg cycle (e.g., Amos et al., 2013; Amos et al., 2015; Fendley et al., 2019; Dal Corso et al., 2020) benefit greatly from further data-driven constraints on how Hg is sequestered on geological timescales. Ultimately, well-constrained models might facilitate inverse modelling of Hg fluxes and hence volcanic (Hg) emissions.

We designed our study to elucidate various influences of changing redox conditions on Hg, TOC and S (and hence the most widely reported host phases of Hg records in the natural environment). To bridge the gap between soft-sediment processes and signals recorded in geological deep time, we generated new Hg and TOC data for a total of 10 depositional settings, 6 (sub)recent-Pleistocene and 4 Late Cretaceous ones (Fig. 2), representing a wide range of (paleo-)redox conditions and depositional environments (Fig. 2, Table 1). We relate these measurements to published major- and trace-element chemistry and associated inferred redox conditions. We seek to eliminate major influences on the Hg flux other than locally produced marine OM,

changes in local oxygenation and inherited effects. To do so, we focus on geological intervals without known substantial subaerial LIP activity or nearby submarine LIP activity that may influence Hg records (Percival et al., 2018), and localities without substantial or variable input of terrestrial higher plant material that may have influenced Hg records (Them et al., 2019; Dal Corso et al., 2020). The main objectives of this study are to (1) establish whether variable oxidation leads to alteration in Hg and normalized Hg, (2) subsequently quantify any observed biases resulting from variable oxidation, and (3) resolve the origins of these biases

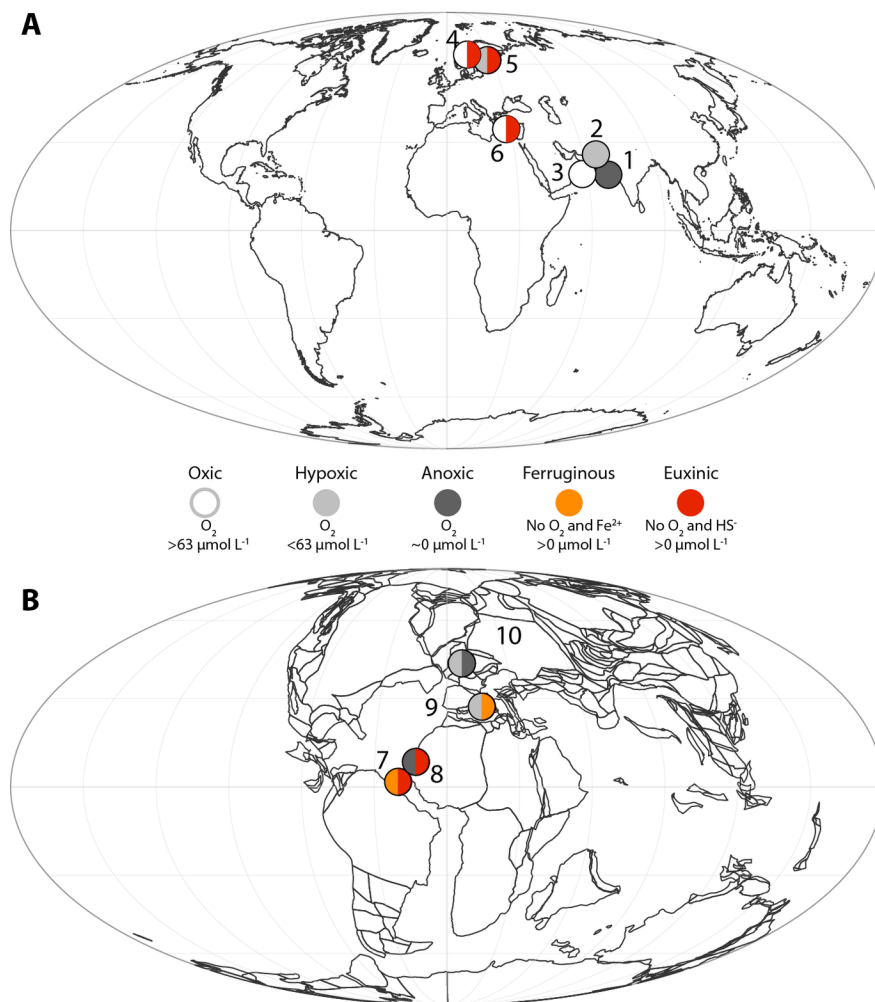


Fig. 2. Maps of site locations. **A.** Holocene–upper Pleistocene sites: (1, 2 and 3 Stations 1B, 6B and 10, Arabian Sea, (4 and 5) LL19, F80, Baltic Sea, (6) 64PE406-E1, Eastern Mediterranean Sea. **B.** Plate reconstruction for 90 Million years ago (Ma) with Cretaceous sites (7) ODP1261A Coniacian–Santonian Oceanic Anoxic Event (OAE3; ~ 86 Ma) 3, (8) Cenomanian–Turonian (OAE2; ~ 94 Ma) Tarfaya Basin core S57, Morocco, (9) Late Cenomanian, Furlo, Italy and (10) Cenomanian–Turonian (OAE2) South Ferriby, United Kingdom. Colored symbols depict reconstructed bottom-water oxygenation from oxic (white), hypoxic (light grey – lowered oxygen conditions; $[O_2]_{aq} < 63 \mu\text{mol L}^{-1}$), anoxic (dark grey – oxygen-depleted conditions $\sim 0 \mu\text{mol L}^{-1}$), ferruginous (orange – no oxygen and Fe^{2+}) to euxinic (red – no oxygen and free HS^-). Differently colored semi-circles for a single site illustrate the approximate range of oxidation regimes within the analyzed sequence.

2. Materials & Methods

Materials – site descriptions

2.1 Site selection

We first study the influence of natural long-term (10s to 1000s of years; Lengger et al., 2014) oxidation in a multi-core depth transect through the Arabian Sea oxygen minimum zone (OMZ) where it intersects the sea floor (Kraal et al., 2012). The three short (0-25 cm depth) cores (Stations 1B, 6B and 10; see also Kraal et al. (2012)) represent anoxic, hypoxic and oxic conditions respectively, and with the exception of Station 1B, where OM breakdown results from anaerobic processes, the uppermost sediments are subject to continued aerobic degradation. The observed differences between these sites can be attributed to oxidation in the water column and sediment and make the Arabian Sea OMZ an ideal testing ground for oxidation-induced sedimentary signals, including those in Hg and its carrier phases (see e.g., Kraal et al., 2012; Koho et al., 2013; Lengger et al., 2014 and Supplementary material 1.1).

Compared to the Arabian Sea multi-core data, the Baltic and Mediterranean Sea sediments cover transient redox variability, similar to those reconstructed for many deep-time Hg records, and allow us to test how these changes in oxygenation shape the geological record of Hg and Hg carriers. To this end, we analyzed gravity core material from the Baltic Sea, representing a time-series of the past 8 kyr (Supplementary material 1.2) (Jilbert and Slomp, 2013). These two cores, from the Fårö Deep (core F80) and Northern Gotland Basin (LL19), record oxic to euxinic bottom-water conditions and several transitions from oxic to euxinic conditions and *vice versa*, within the same core (e.g., Jilbert and Slomp, 2013; van Helmond et al., 2018). The Baltic Sea cores thus provide insight as to how transitions in oxygenation might influence single sedimentary Hg records and to what extent such signals are preserved in the geological record. In addition, a multi- and piston-core composite site 64PE406E-1 in the Mediterranean Sea (Supplementary material 1.3), containing several sapropels (sapropel S1 and S5 are used here, see e.g., Rohling et al., (2015) for a review of the Mediterranean sapropel records), is studied to further assess the influence of deoxygenation, post-depositional oxidation of organic-rich sediments and paleo-redox fronts (Mercone et al., 1999; Hennekam & van der Bolt et al., 2020; Sweere et al., 2021).

Lastly, we analyze four Upper Cretaceous successions to test whether the signals found in the oxic to sulfidic unconsolidated sediment are transferred to the rock record – on which sedimentary Hg studies targeting deep-time volcanic activity are based. For this purpose, we selected one Coniacian–Santonian black shale record from Ocean Drilling Program (ODP) Hole 1261A (März et al., 2008) (Supplementary material 1.4) recording cyclic alternations from ferruginous to sulfidic bottom-water conditions, and three upper Cenomanian to lowest Turonian successions (Furlo, Italy, South Ferriby, UK and Tarfaya core S57, Morocco) marked by high-amplitude variations in oxygenation (e.g., Poulton et al., 2015; Owens et al., 2017; Clarkson et al., 2018 and Supplementary material 1.5-1.7). The Cenomanian–Turonian successions might have been affected by contemporaneous LIP activity, but because the LIPs in question are thought to have been largely subaqueously emplaced and at substantial distance to the studied sites, the Hg-cycle perturbation is thought to be geographically confined even during periods of intense volcanism (Scaife et al., 2017; Percival et al., 2018).

Site	Core/Locality	No. on map	Period	Environmental setting	Oxygenation regime(s)	Sediment accumulation rate	Data from literature (quoted data only)	Key references	Data generated for this study	Study aim	Isolated factors	Expected processes
Murray Ridge, Arabian Sea	Station 1B	1	Holocene	Open marine, overlying zone $0-200\text{m}$ water depth	Anoxic	Moderate (1-10 cm/kyr)	TOC, trace elements (part), pore-water chemistry, in-situ oxidation	Kraal et al. (2012), Lengger et al. (2014)	Hg	Resolve Hg & TOC accumulation in anoxic through oxygen-depleted to oxic conditions, and relate to oxygenation in other sites with similar export flux (S1, S5, and S5). Includes temporal & spatial variability as a factor in shaping Hg records	Oxygenation	Hg sequestration with organic matter, subsequent slow breakdown of organic matter and impact on Hg/TOC
Murray Ridge, Arabian Sea	Station 6B	2	Holocene	Open marine, overlying zone $1-1500\text{m}$ water depth	Hypoxic	Moderate (1-10 cm/kyr)			Hg	Hg sequestration with organic matter, subsequent slow breakdown of organic matter and impact on Hg/TOC		
Murray Ridge, Arabian Sea	Station 10	3	Holocene	Open marine, overlying zone $0-3000\text{m}$ water depth	Oxic	Moderate (1-10 cm/kyr)			Hg	Hg sequestration with organic matter, subsequent slow breakdown of organic matter and impact on Hg/TOC		
Northern Gotland Basin, Baltic Sea	LL19	4	Mithropocene/Judicocene	Restricted, marginal sea ($1-20\text{m}$ water depth)	Oxic/hypoxic to euxinic	Very high (>50 cm/kyr)	TOC, trace elements	Albert & Slomp (2013), van Helmond et al. (2018)	Hg	Resolve Hg & TOC accumulation during transition from oxic/euxinic to euxinic conditions and vice versa, includes temporal variability. LL19 and F80 together provide control on potential spatial variability.	Transient variability in oxygenation	Hg sequestration with organic matter and sulfur, Hg fluxing with sulfides, Hg evasion through methylation
Fårö Deep, Baltic Sea	F80	5	Mithropocene/Judicocene	Restricted, marginal sea ($1-200\text{m}$ water depth)	Oxic/hypoxic to euxinic	Very high (>50 cm/kyr)			Hg	Hg sequestration with organic matter and sulfur, Hg fluxing with sulfides, Hg evasion through methylation		
Eastern Mediterranean	64PE406E-1	6	Holocene-late Pleistocene	Open marine (Hobocene-late Pleistocene)	Oxic to euxinic	Moderate (1-10 cm/kyr)	TOC (part), trace elements	Bull et al. (2010), Hemmink & van der Bolt et al. (2020), Sweere et al. (2021)	Hg, TOC (part)	Resolve Hg & TOC accumulation during transition from oxic/euxinic to euxinic conditions, includes temporal variability and post-depositional oxidation including buried redox fronts.	post-depositional oxidation	Hg sequestration with organic matter and sulfur, Hg fluxing with sulfides, Hg evasion through methylation, Hg fluxing during post-depositional oxidation in oxic zone location
Demarara Rise, Equatorial Atlantic	ODP1261A	7	Coniacian-Santonian	Open marine (semi-restricted)	Ferruginous to euxinic	Low-moderate ($1-1\text{ cm/kyr}$)	TOC, trace elements	März et al. (2008)	Hg, TOC (part)			
Morocco	Tarfaya S57	8	OAE2 interval	Open marine, overlying zone(?)	Ferruginous to euxinic	Low-moderate ($1-1\text{ cm/kyr}$)		Talbot et al. (2004), Probst et al. (2013)	Hg, TOC			Test if geological data (time sedimentary succession, record similar effects as seen in Holocene-Pleistocene records) and if these effects can be traced to individual processes
Italy	Furlo	9	Cenomanian (pre-OAE2)	Open marine	Hypoxic to euxinic	Very low-low ($1-1\text{ cm/kyr}$)		Jenkins et al. (2007), Owens et al. (2017)	Hg, TOC			
United Kingdom	South Ferriby	10	OAE2 interval	Marginal sea	Oxic to hypoxic/oxic	Very low ($1-1\text{ cm/kyr}$)		Jenkins et al. (2007), Pagar van der Bruggen et al. (2013)	Hg, TOC			

Table 1. Overview of studied localities. For a more detailed description of each record we refer to section 1 of the supplementary text.

2.2 Methods

2.2.1 Hg analyses

Mercury (Hg) analyses were conducted with a Lumex 915+ device, attached to a pyrolysis unit (PYRO-915) at the University of Oxford. For each sample, approximately 50–200 mg of homogenized powdered sediment was pyrolyzed at 700 °C and ~60% of samples were analyzed in duplicate to assess reproducibility. Calibration of the Lumex 915+ unit was performed using a paint-contaminated soil standard (NIST2587), which contains 290 ppb (ng/g) Hg. Reproducibility, estimated through both standard and replicate sample measurements, was generally better than 10%, falling to approximately 5% at higher Hg contents. A few samples with very low Hg contents (<5 ppb), around and below the detection limit, have analytical uncertainty >10%. With the exception of the Mediterranean core (64PE406E-1) all Hg was analyzed on sample powders that have also been analyzed for TOC, S and trace elements. For 64PE406E-1, we utilize a combination of calibrated Mo concentrations from XRF scanning (Hennekam et al., 2020) and new and existing dedicated TOC measurements on the same powders that were analyzed for Hg.

2.2.2 Determination of organic and inorganic carbon

For black shales and samples expected to be relatively rich in organic carbon, total organic carbon (TOC), hydrocarbon yield of the organic matter and inorganic carbon were assessed with a Rock-Eval 6 device (Lafargue et al., 1998; Behar et al., 2001) at the University of Oxford. For every 10 samples, at least one in-house standard of homogenized sediment with pre-determined values was analyzed to assess reproducibility. The reproducibility of parameters of interest (TOC, T_{\max} , Hydrogen Index (HI), Oxygen Index (OI), mineral carbon) was always better than 10% and typically better than 5% of the measured value, based on repeated measurements of the in-house standard. The hydrogen index (HI) and oxygen index (OI) are used as in, e.g., Behar et al., (2001); briefly, the mass of released hydrocarbons (“S2”) and CO₂ (“S3”) during standard pyrolysis in mg is multiplied by 100 and divided by TOC to obtain HI and OI, respectively. Analyses of a decarbonated standard (~48% carbonate) suggest that TOC, S2, S3 and consequently HI and OI were not significantly impacted by low-temperature decomposition of carbonates (Hazra et al., 2022). As all tested samples are dominated by marine organic matter (see Supplementary materials (S1.2-1.7)), we interpret HI and OI primarily as indicator of organic matter degradation. For the samples that were previously analyzed for TOC after an acid-washing procedure (März et al., 2008) and here analyzed with RockEval (ODP1261A), average TOC is slightly higher ($8.2 \pm 1.4\%$) for acid-washed than for bulk RockEval analysis ($7.5 \pm 1.3\%$), confirming there is minimal influence of methodology on the measured TOC content (Nieuwenhuize et al., 1994).

Organic-lean carbonates from the Furlo section were analyzed on a Strohlein Coulomat 702 at the University of Oxford. Total carbon of the bulk sediment was determined by analyzing 20–40 mg of untreated homogenized powdered material, while a second 20–40 mg aliquot was heated to 450 °C in a combustion furnace overnight to remove organic carbon. The difference between the two measurements indicates the TOC, whereas the heated aliquot represents the total inorganic carbon fraction (TIC). Long-term analytical reproducibility based on an in-house pure carbonate standard was determined to be ~0.1% C.

A subset of samples (25) from the 64PE406-E1 multi- and piston core were analyzed for TOC at Royal Netherlands Institute for Sea Research (NIOZ). Samples were dried, homogenized, decarbonated with 2M HCl and subsequently dried and homogenized again, followed by measurement on a Thermo-Interscience Flash EA1112 Series Elemental Analyzer. Based on replicate analyses of standard materials the accuracy is ~0.3% for TOC, with a detection limit of ~0.1%.

2.2.3 Determination of Pb and Zn

For a small subset of samples from the Arabian Sea, sedimentary lead (Pb) and zinc (Zn) content were determined by analyzing the 1M HCl total digestion extracts of Kraal et al. (2012) on an Inductively

Coupled Plasma Mass Spectrometer (Thermo Fisher Scientific XSERIES 2 ICP-MS) at Utrecht University. The accuracy (recovery), based on QCs, was 99% for both Pb and Zn. Average analytical uncertainty based on sample replicates was 1.4% for Pb and 3.6% for Zn.

3. Results

3.1 Natural long-term oxidation – Arabian Sea

At the three Arabian Sea stations, Hg contents are highest at the top of Station 1B (the shallowest water station), with a maximum of 150 ppb, and lowest (23 ppb) for the lowermost sample of the Station 6B core (Fig. 3). Station 10 (greatest water depth) shows rather stable Hg contents (50–90 ppb). The elevated Hg contents at the top (<10 cm) of the anoxic station (1B) seem to suggest some influence of anthropogenic pollution. There are, however, several reasons why we consider anthropogenic contamination unlikely even at the top of the Station 1B core. For example, the elevated Hg does not appear in similar fashion at the other locations, the average accumulation rates ($\sim 5\text{--}10\text{ cm kyr}^{-1}$) would imply significant Hg perturbation prior to the industrial revolution (Koho et al., 2013) and there is a complete absence of anomalous values in other commonly Hg pollution-associated heavy metals such as Pb, Zn (Supplementary data). Lastly, there is no clear evidence for a trend break in Hg or Hg/TOC similar to the youngest part of the Baltic Sea cores (Fig. 3A, C); in the Arabian Sea Station 1B and 6B Hg content gradually decreases with depth. Hg overall correlates positively with TOC when all data from the three stations are combined ($R^2 \sim 0.3$; Supplementary Fig. 1A), and the strength of the correlation increases when the two deeper water stations are considered individually ($R^2 \sim 0.7$ for the intermediate site (6B) and $R^2 \sim 0.45$ for the deep-water site (10)). Remarkably, a negative correlation ($R^2 \sim 0.7$) with TOC is found at the shallowest water Station 1B.

Mercury and Hg/TOC for the shallowest water station (1B) show a strong decreasing trend with depth, as Hg decreases from 150 to 60 ppb while TOC increases from $\sim 5.5\%$ to 7.5% (Fig. 3A). Mercury at the intermediate station (6B) shows a similar, albeit much shallower, trend (Fig. 3C) but clear depth-dependent trends in Hg/TOC are not recorded here or at Station 10 (Fig. 3C, E). At Station 1B, the absence of dissolved Mn (assumed to be Mn^{2+}) and presence of dissolved Fe (assumed to be Fe^{2+}) shows that reduction of Fe-oxides is presumably the primary pathway for the (microbial) degradation of organic matter throughout the studied interval (Fig. 3B) (Kraal et al., 2012). Kraal et al. (2012) also determined that Mn-oxide reduction is more prevalent at Station 6B and becomes the dominant anaerobic pathway for (microbial) degradation of organic matter at Station 10 (Fig. 3D, F).

Across the site transect, average Hg/TOC increases markedly with oxygenation; we find Hg/TOC of 15 ± 6 ppb/% (mean, standard deviation) at the shallowest (anoxic) site (Station 1B) (Fig. 3A), rising to 32 ± 5 at the intermediate (6B) (Fig. 3C) and 96 ± 12 at the deepest, most oxic site (10) (Fig. 3E). Arguably, the lowermost (i.e., greatest core depth) recovered sediments, where trends with depth are minimal in Hg and TOC, are most representative of the burial signal. Focusing on the lowermost 10 cm of each core, we find a further decrease in Hg/TOC in the anoxic site to 8.7 ± 0.9 , whereas Hg/TOC at the other sites remains virtually unchanged from top to bottom of the analyzed interval.

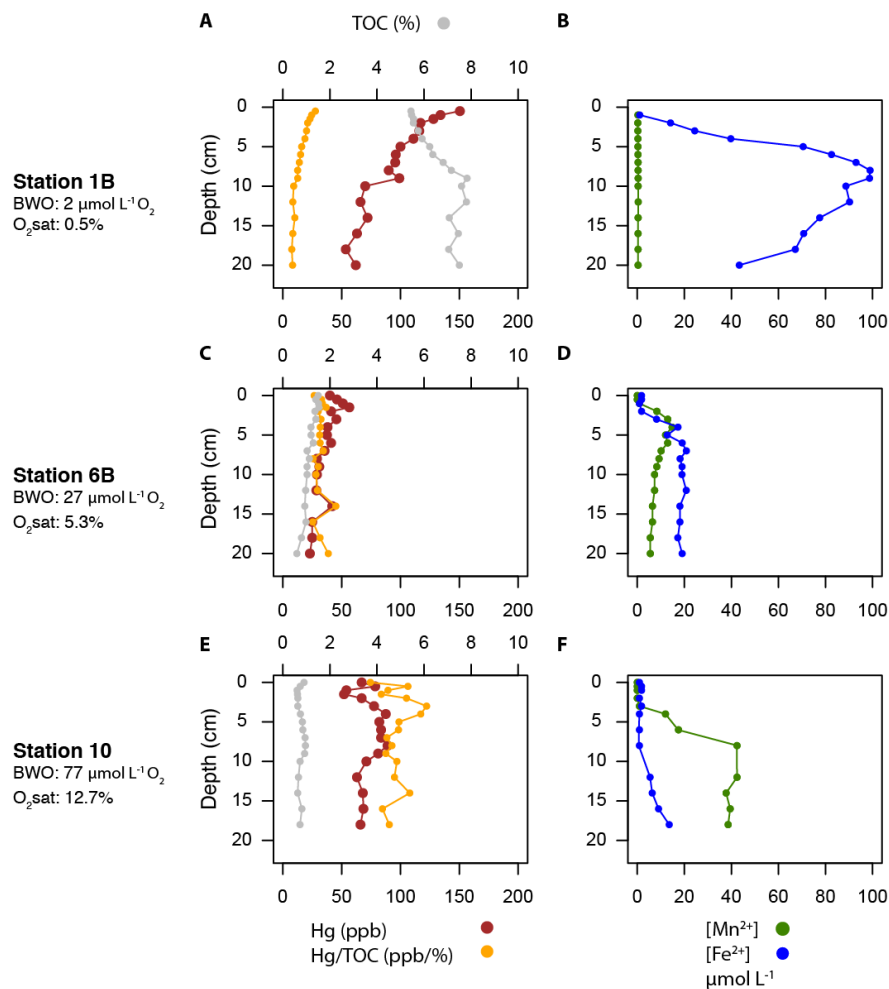


Figure 3. Hg, TOC and sediment and pore-water chemistry for the Holocene (~0-4 ka) Arabian Sea stations. A, C, E. Hg, TOC and Hg/TOC for Station 1B, 6B and 10 respectively. **B, D, F.** Mn^{2+} and Fe^{2+} concentrations in pore-waters. Bottom-water oxygen concentration (BWO) and saturation (O_2 sat) for each station (Koho et al., 2013). TOC and pore-water data were published in Kraal et al. (2012).

3.2 Influence of transient changes in oxygenation: Baltic Sea soft sediments

The Holocene sediment cores F80 and LL19 from the Baltic Sea (See Table 1, see Supplementary text 1.2 for details on age-depth models and previous studies using F80, LL19) show identical trends in TOC-normalized Hg and Hg content throughout. In the pre-industrial (<1750 calendar years common era (CE); based on the detailed age model of Jilbert and Slomp, 2013), sedimentary Hg content did not exceed 40 ppb, whereas it reached a maximum well above 200 ppb around ~1980 CE. Core F80 seems to record a subtle increase in Hg and Hg/TOC from about 1100-1200 CE, suggesting that, for example, small-scale early industrial activity or deforestation around the Baltic Sea may have influenced Hg influx at our sites, as is also supported by the Pb record in the study by van Helmond et al. (2020). The pre-industrial Holocene Hg and TOC contents in our cores are very similar to those obtained during earlier work in the Baltic Sea that focused mainly on the recent centuries and effects of modern anthropogenic Hg pollution (Leipe et al., 2013).

Before the main period of anthropogenic Hg emissions (<1750 CE), Hg loading in the oxic-anoxic sediments, based on correlation with TOC, appears to be almost completely controlled by their TOC contents

(Supplementary Fig. 2A, C). In some anoxic–sulfidic intervals, TOC spikes above 10%, whereas the more oxic intervals generally have 1–2% TOC (Jilbert and Slomp, 2013). Hg/TOC averages ~ 3.8 – 5.5 ppb/% in the anoxic to sulfidic intervals and averages 6.4 (F80) to 8.6 (LL19) in the more oxic intervals (Fig. 4, 6B, C). The non-sulfidic intervals at F80 show elevated Mo and lower Hg/TOC compared to the same intervals in LL19 (Fig. 4). This pattern may signal continued oxygen deficiency at F80 even during the most oxic phases, which is supported by sedimentary Re content data (van Helmond et al., 2018). Prior to the emergence of overwhelming Hg pollution (1750 CE), negative correlations between both Hg and Hg/TOC and redox-sensitive elements (Mo, U, Cd etc.) are ubiquitous. This illustrates such redox-sensitive elements are usually also enriched or proportional with the TOC increase, whereas the rise in Hg is smaller than that in TOC (Fig. 4). This relationship implies that the correlation of other TOC-bound elements with Hg is generally positive and that the correlation of these elements with Hg/TOC is negative, as also indicated by the decreasing Hg/TOC with TOC. The negative correlation between sulfide-bound elements (Mo) and Hg/TOC weakens with increasing Mo, which suggests a non-linear connection between anoxic and especially sulfide-enriched (pore) waters and decrease in Hg/TOC (Fig. 4E, F).

3.3 Influence of post-depositional oxidation: Mediterranean Sea soft sediments

The sapropels S1 and S5 in sediments from the Eastern Mediterranean Sea show increased Hg contents (Fig. 5). However, (slightly) subdued or stable Hg/TOC values appear in the anoxic intervals (high Mo, high Ba; for details on oxygenation during sapropel deposition see, e.g., Hennekam et al., 2020; Clarkson et al., 2021; Sweere et al., 2021), similar to the Arabian and Baltic Sea records. Background Hg contents in the oxygenated (low Mo, low Ba) sediments are ~ 10 ppb, increasing to relatively stable values around ~ 50 ppb (S1) and ~ 100 ppb (S5) within the sapropel layers. The profiles also show second-order variability both below and above the sapropel layers. For example, the top of both S1 and S5 is marked by a clear spike in Hg contents (up to ~ 100 ppb in S1 and 250 ppb in S5), approximately double the Hg contents observed in the lower part of the sapropels. These spikes are not paralleled by a further increase in TOC, which remains stable around the average of the sapropel interval (values around $\sim 2\%$ in S1 and ~ 5 – 6% in S5), above background values of ~ 0.5 – 1% . In general, the preserved Hg/TOC ratios are more variable (Fig. 5C, 6D) during deposition of background sediments than during sapropel deposition. Whether Hg/TOC during background deposition are higher compared to sapropel deposition, as suggested by the trends across the onset of sapropel S5, cannot be confidently determined with the available data.

Intriguingly, Hg/TOC for S1 is higher (~ 25 ppb/%) than for S5 (~ 17 ppb / %), which may be linked to more intense deoxygenation during S5 (Sweere et al., 2021). In the oxidized part of S1, where high Ba is considered to follow the original extent and intensity of the sapropel (e.g. van Santvoort et al., 2002) (*ca.* 28 – 23.5 cm depth, 8.3 – 6.5 ka), Hg spikes and Hg/TOC remain at a relatively elevated level. This pattern contrasts with TOC, of which a substantial part has been removed during post-depositional oxidation: the oxidized part of S1 records 0.8% TOC, whereas the unoxidized part records 2%. A similar effect appears to occur at the upper 3–4 cm of S5 (*ca.* 122 ka).

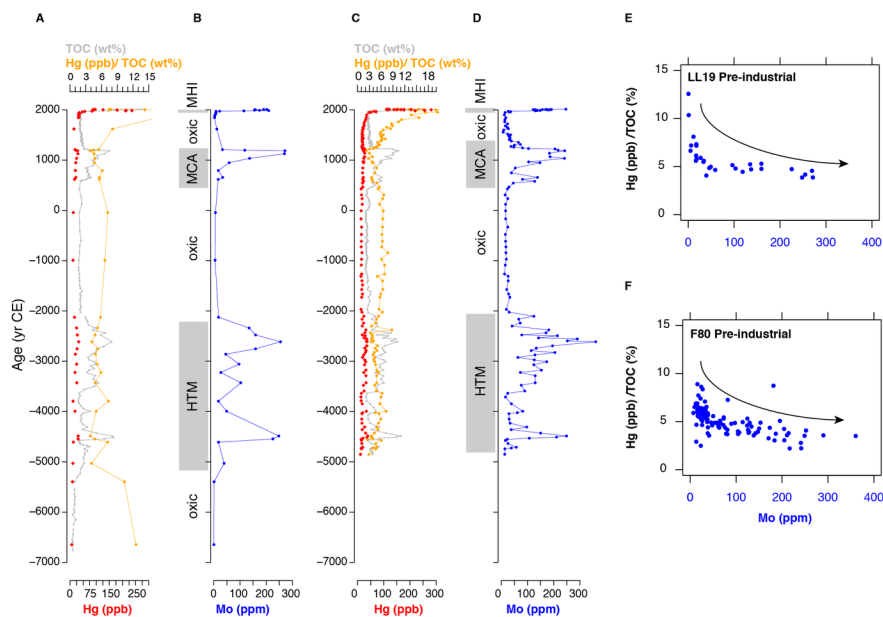


Figure 4. Hg, TOC, and trace-element records for Baltic Sea cores LL19 and F80 for the Holocene (~0-8 ka). **A.** Hg, TOC and Hg/TOC for core LL19, North Gotland Basin. **B.** Molybdenum (Mo) contents for LL19 (data from van Helmond et al. 2018). **C.** Hg, TOC and Hg/TOC for core F80, Fårö Deep. **D.** Mo contents for F80 (data from van Helmond et al. 2018). Abbreviations – MHI: Modern hypoxic interval, MCA: Medieval Climate Anomaly, HTM: Holocene Thermal Maximum, CE: Common Era. **E.** Pre-industrial (<1750CE) Hg/TOC vs Mo for core LL19, **F.** Same as panel E, for core F80.

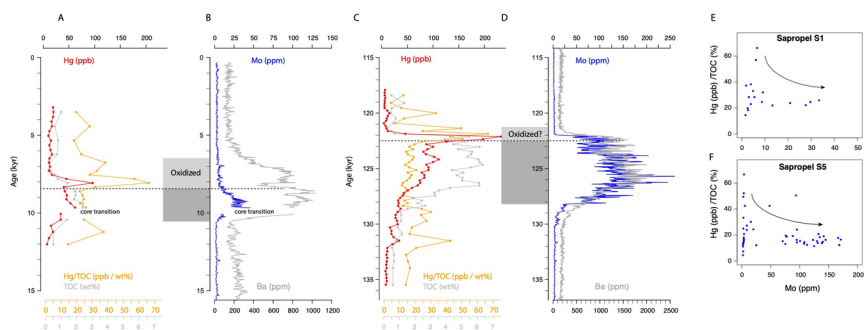


Figure 5. Hg, TOC and trace-element records for 64PE406-E1 through intervals encompassing Sapropel S1 (deposited *ca.*10.5–6.1 ka) and S5 (deposited *ca.* 128.3–121.5 ka). **A.** Hg, TOC and Hg/TOC for sapropel S1. **B.** Molybdenum (Mo) and barium (Ba) contents in ppm from calibrated high-resolution XRF scanning (data published in Hennekam & van der Bolt, et al. 2020). **C.** Hg, TOC and Hg/TOC for sapropel S5. **D.** Mo and Ba in ppm from calibrated high-resolution XRF scanning (data published in Hennekam & van der Bolt et al., 2020). Dark shaded boxes show the extent of the existing sapropel and light shading shows the extent of post-depositional oxidation. **E.** Hg/TOC vs Mo for the sapropel S1 interval. **F.** Same as panel E, but for sapropel S5.

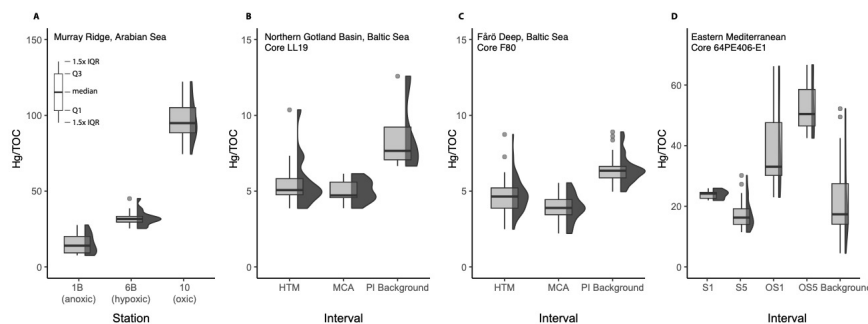


Figure 6. Summary of observed Recent to upper Pleistocene Hg/TOC in the Baltic, Arabian and Mediterranean Sea cores. **A.** Hg/TOC for the Arabian Sea stations, going from anoxic (1B) to oxic (10). **B.** Hg/TOC for the Holocene Thermal Maximum (HTM) and Medieval Climate Anomaly (MCA) euxinic and pre-industrial (PI) oxic background intervals for core LL19. **C.** As panel B but for core F80. **D.** Hg/TOC for Site 64PE406-E1, Eastern Mediterranean, split by oxidation regimes: sapropels “S1”, “S5”, their oxidized tops, “OS1” and “OS5”, and background.

3.3 Influence of transient oxygen variability: the deep-time sedimentary record

3.3.1 Coniacian–Santonian, Ocean Drilling Program (ODP) Site 1261A

The Coniacian–Santonian sediments at Demarara Rise ODP Leg 207 Site 1261 Hole A (Shipboard Scientific Party, 2004) (Fig. 7) show generally high to very high TOC (4–12%) and moderate Hg content (20–140 ppb), compared to geological averages (~60 ppb for shales, ~30 ppb for limestones, Grasby et al., 2019). We find no obvious correlation between Hg and TOC or Hg and S (Supplementary Fig. 3), and see a pronounced cyclicity in Hg, Hg/TOC and Hg/S. Hg/TOC ratios vary between ~5 ppb/% in some parts of the sulfidic intervals (as determined by März et al. 2008, outside the shaded bands in Fig. 7), and locally spike up to 15 ppb/% in the anoxic non-sulfidic intervals and directly above (shaded bands in Fig. 7). Both the carbonate content and the carbonate-free TOC are lowest in the non-sulfidic sediments. Although Hg and TOC only weakly correlate, the HI and OI are negatively and positively correlated to Hg and that leads to a correlation of HI and OI with Hg/TOC (Fig. 7,8D), suggesting organic-matter characteristics play an important role in shaping Hg and Hg/TOC. The negative correlation of Hg and Hg/TOC, marking Hg depletion relative to both (carbonate-free) Mo and TOC, are also observed here, similar to the Baltic Sea sites (Fig. 4E, 4F, 7E). The carbonate-corrected aluminum (Al) content is remarkably constant, suggesting stable Al accumulation rates throughout the analyzed interval. We find that Hg/Al follows the same pattern as Hg; a crucial observation that shows Hg burial was not constant and not driven primarily by a Hg associated with an increased influx of siliciclastic material. As the high Hg contents coincide with sediments containing evidence for ferruginous conditions, we surmise that a greater proportion of Hg may have been lost to overlying waters under euxinic conditions compared to ferruginous conditions.

3.3.2. Cenomanian, pre-OAE 2 level, Furlo, Italy

We here focus on organic-matter characteristics because paired trace-element records are not available for the selected samples, the bulk of the succession being represented by organic-lean white pelagic carbonates of the Scaglia Bianca (carbonate content 90–95%) and the remainder being represented by thin (centimeter-scale) black and green shales and black cherts, with variable but generally much lower carbonate content (0–80%). Overall, these sediments also show large differences in TOC and Hg content, and notably Hg/TOC (Fig. S5). The latter could be partly a consequence of TOC and Hg being often difficult to reliably measure in the carbonates (see also Supplementary text S2). In the more organic-rich facies, where such analytical issues do not play a role, Hg/TOC ranges from 17 to >400, compared to 30 to 350 obtained by Percival et al. (2018). The overall correlation between Hg and TOC in the shales and cherts is strong ($R^2 \sim 0.7$, Fig. S5D) while after normalizing Hg to TOC, only a weak correlation with HI remains, indicating that the type

and/or preservation state of organic matter here has no dominant influence on Hg/TOC (Fig. 8A).

3.3.3 Cenomanian–Turonian (OAE 2), S57 core, Tarfaya, Morocco

The TOC content of the S57 core samples from Tarfaya, Morocco, is consistently high (average 7%) and never drops below ~1% in the studied core interval (50–60 m core depth) (e.g., Tsikos et al., 2004; Percival et al., 2018). The TOC and Hg data used here are from Percival et al. (2018) and oxygenation for the sample levels is estimated based on Fe speciation and lipid biomarkers (Poulton et al., 2015). We here record high HI values, above 500 and average ~660, indicative of immature marine organic matter. Hg and TOC are well correlated across the entire analyzed interval (Percival et al., 2018). Hg/TOC values are generally low, averaging ~23 (min 9.5, max 88) and correlate moderately well ($R^2 \sim 0.4$) with the OI but only weakly with HI ($R^2 \sim 0.1$), suggesting that either preservation or a (small) refractory organic-matter pool plays a role in shaping Hg/TOC relationships. Across the ferruginous–euxinic cyclic variations, only small changes in Hg/TOC are observed, and correlation between Hg/TOC and OI in this interval is somewhat weaker than across the entire interval previously analyzed for Hg and TOC (Percival et al., 2018).

3.3.4 Cenomanian–Turonian (OAE 2), South Ferriby Black Band, UK

Hg contents across the South Ferriby Black Band range from 40 ppb in the pelagic white chalk to 350 ppb in the black-shale interval that is the hallmark of OAE 2. A correlation ($R^2 \sim 0.55$, Fig. S4B) with TOC is found, and correlations of Hg/TOC with HI and OI are significantly negative and positive, respectively (Fig. 8C). TOC in the pre-event carbonate-rich sediments is ~0.2%, reaching a maximum of 6–7% in the Black Band itself (Jenkyns et al., 2007). Hg/TOC ratios decrease from values above 200 ppb/wt % in the organic-lean carbonates below the Black Band to an average of ~45 ppb/wt % in the black shale. Minimum Hg/TOC coincides with the highest TOC contents and HI/OI indicates that the best-preserved (marine) organic matter shows lowest Hg/TOC (Fig. 8C).

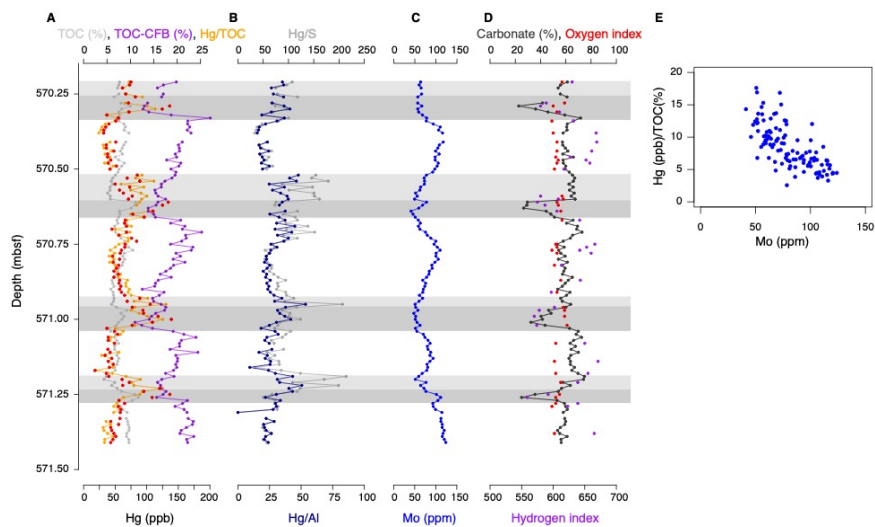


Figure 7. Coniacian–Santonian anoxic–euxinic cyclic succession analyzed from ODP Site 1261A. **A.** Hg, TOC, Hg/TOC and carbonate-free (CFB) TOC. **B.** Al and S-normalized Hg. **C.** Molybdenum (Mo) contents in ppm. **D.** Carbonate (%), HI and OI from Rock-Eval. Shaded bands indicate intervals where Hg/TOC is elevated, dark shading indicates where März et al., (2008) inferred anoxic non-sulfidic conditions. **E.** Hg/TOC vs Mo contents.

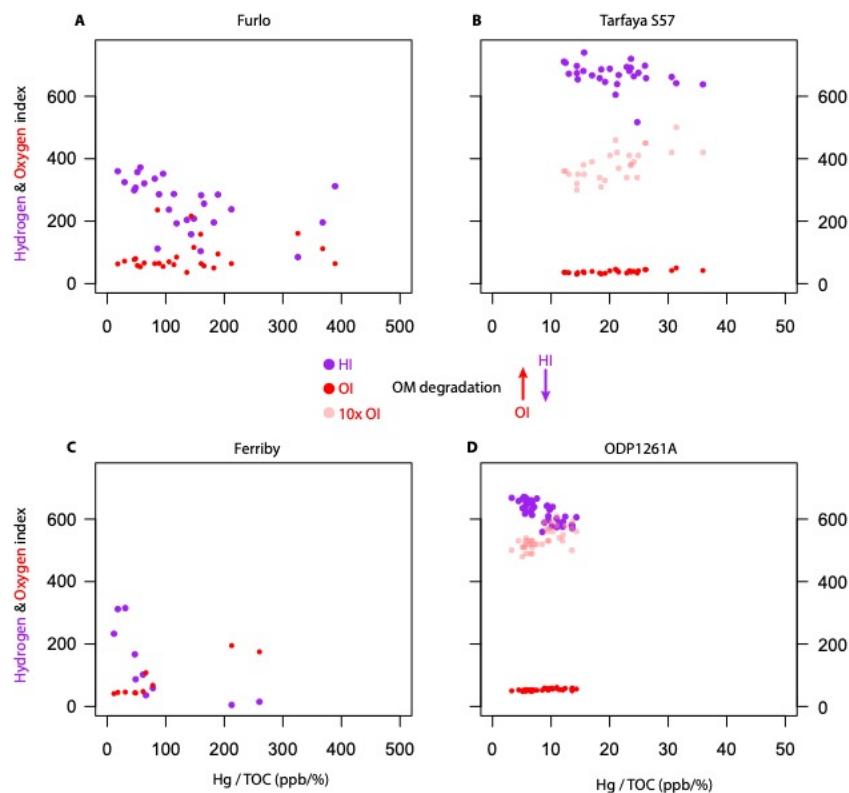


Figure 8. Hg/TOC plotted against hydrogen and oxygen indices, illustrating the influence of organic-matter preservation state. A.Furlo: HI and OI *vs* Hg/TOC, **B.** Same for Tarfaya S57, **C.** South Ferriby and **D.** ODP Site 1261A. Note the factor of 10 Hg/TOC scale difference between panels A, C and B, D and that for panels B and D, OI is also given inflated by a factor 10 to illustrate variability.

4. Discussion

4.1 Hg and Hg/TOC trends with (de)oxygenation

The Holocene Arabian Sea sediments provide insight into the effects of exposure to a range of oxygen concentrations and progressive OM breakdown on time-scales that cannot be (easily) observed in controlled environments (10s–1000s of years). We find only relatively minor differences in absolute Hg contents between the OMZ and more oxygenated sites (Fig. 3), especially below ~ 10 cm core depth. Intriguingly, the anoxic site (Station 1B, Fig. 3) has higher Hg contents at the top of the core but Hg contents stabilize at a much lower level in the lower part of the core. While this Hg trend appears to be similar to the widely documented anthropogenic contamination, the combination of the sediment age and chemical signatures of this and nearby sediment cores imply it is difficult to explain the signal with anthropogenic Hg loading (see section §3.1). Rather, we here consider the scenario that down-core Hg decrease at Station 1B hints at disproportionate Hg loss during sediment accumulation, decoupled from TOC.

For the anoxic Station 1B (Fig. 3A) we can assume that Hg and TOC arrived at the sea floor in a condition that is closely representative of the export particle flux from the anoxic waters below the photic zone, with only minor alteration due to very short (~ 1 year) residence time in oxidizing conditions (Lengger et al., 2014). This supposition is supported by TOC contents at the anoxic site (6.5–7.5 wt%) that do not appear to differ much from the organic-carbon fraction in the export particle flux (~ 8 wt%) (Honjo et al., 1999). Even if only a small fraction of OM appears to be broken down, this fraction seems to contain a large proportion of the

total Hg, perhaps implying a significant portion of Hg is only weakly bound at time of deposition and can be released without noticeable TOC loss.

The available primary and export productivity estimates across the region suggest all these stations started from a similar particle flux composition (Haake et al., 1993; Honjo et al., 1999; NASA Ocean Biology (OB.DAAC), 2014), and without oxidation should record similar TOC to what is observed in the particle flux and Station 1B (6.5–8%). Assuming these equal starting conditions, we calculate a significant fraction (80–90%) of organic carbon has been lost at Stations 6B and 10, which now average only 1.2 and 0.6 wt% TOC, respectively (Fig. 3C, E). The loss of organic carbon is, however, not clearly reflected in further decreasing Hg contents. The absolute Hg content at the intermediate water depth Station 6B (Fig. 3C) is approximately half that of the stratigraphically lowermost sediments at the anoxic Station 1B (Fig. 3A), while the deep-water, well-ventilated Station 10 (Fig. 3E) shows contents similar to those found at the anoxic Station 1B (Fig. 3). The stabilizing profiles of Hg and TOC suggest that the lower intervals (10–20 cm depth) of all three Arabian Sea cores represent signals that are potentially stored in the geological record.

Complementing the Arabian Sea sites, the Baltic Sea and Mediterranean sites allow us to test whether the observed trends hold for single localities experiencing different oxygenation regimes, which is situationally more similar to the geological record. These sites may also help reveal the potential influence of euxinic conditions and sulfate reduction in bottom and pore waters, which are generally considered to be negligible in the Arabian Sea (Kraal et al., 2012). In addition, the Mediterranean sapropel S1 records strong post-depositional OM oxidation (‘burn-down’) and influence of halted redox fronts, whereas the extremely high sediments and organic matter accumulation rates in the Baltic Sea sites largely prevent oxygen penetration into the sediments, stifling aerobic organic-matter breakdown even during relatively well-ventilated bottom water conditions.

Overall, the various Holocene and upper Pleistocene cores provide datasets comparable to those typically generated on core and outcrop material that records ancient (de)oxygenation events (e.g., Turgeon and Brumsack, 2006; Jenkyns, 2010). Here we generally find low to moderate (10–100 ppb) Hg contents, which are strongly correlated with TOC, suggesting that sedimentary Hg is predominantly TOC-bound. However, some caution is warranted because sedimentary sulfur is also strongly correlated with Hg and TOC and the presence of a considerable S-associated Hg fraction might only be revealed through Hg-speciation analyses.

When looking in more detail, we find that, despite the strong Hg-TOC and Hg-S correlations, the Hg increase in the anoxic and sulfidic intervals in the Baltic and Mediterranean Sea cores does not entirely match the TOC or S increases, resulting in lowered Hg/TOC at high TOC contents (Fig. 4, 5) and a similar effect can be seen in Hg/S (Supplementary Data). Published data from Holocene—upper Pleistocene oxic–anoxic marine localities, the Japan Sea and Peruvian Margin (Shen et al., 2020), show similarly lowered Hg/TOC in sediments deposited under anoxic and euxinic conditions. However, on the strongly sulfidic end of the spectrum, the Baltic Sea core material shows the Hg/TOC-Mo correlation becomes rather insensitive at high Mo contents (Fig. 4E,F), which suggests a breakdown of the relationship during the most sulfidic episodes. This feature of the geochemistry is consistent with the observation that, for strongly pyritized sediments (Shen et al., 2020), the relationship of Hg/TOC with low-oxygen and especially sulfidic conditions may be reversed, and may be marked by higher Hg sequestration, either as HgS or Hg inclusion in pyrite (Fig. 4,5), or a shift from TOC-bound to S-bound Hg deposition.

Furthermore, the Mediterranean sapropel record we generated confirms the occurrence of Hg focusing near paleo-redox fronts and shows, in specific cases, Hg/TOC, but notably also the Hg content itself to be elevated as a result of oxidation and/or immobilization at the oxic-anoxic boundary. This observation aligns with the findings of Mercone et al. (1999), who documented large Hg spikes associated with paleo-redox fronts in oxidized sapropels and turbidites, which were hypothesized to be associated with Fe-Mn (oxyhydr)oxide scavenging. The occurrence of an ash-layer at the top of sapropel S5 in some parts of the Eastern Mediterranean (a crypto tephra in core 64PE406-E1) may be argued to have added extraneous Hg in the analyzed interval. However, we consider a dominant volcanic source for this Hg spike unlikely or highly fortuitous: it remains extremely challenging to connect individual eruptions, and non-LIP activity in general, to Hg emissions (e.g.

Schuster et al., 2002; Guédron et al., 2019; Edwards et al., 2021). Perhaps more importantly, the placing of the S5 Hg spike coincides exactly with the position where burn-down stopped (paleo-redox front) in sapropel S1 (Fig. 5), akin to previously studied turbidites and S1 in other Mediterranean cores (Mercone et al. 1999) where tephras are not recorded. Collectively, these data support the findings of Mercone et al. (1999) who hypothesized Hg released during oxidation of OM and pyrite may be focused around halted redox fronts.

The low overall Hg/TOC values observed in the Holocene anoxic Baltic Sea (Fig. 4), Holocene–upper Pleistocene sapropels (Fig. 5), Peruvian Margin sediments (Shen et al., 2020), and the anoxic Arabian Sea site are noteworthy, especially considering various inter-site differences. The Holocene data presented here from the Baltic and Arabian Sea, with Holocene–upper Pleistocene sapropel data, in concert with published data from similar environments (Shen et al., 2020), show that shorter oxygen exposure can result in suppressed Hg/TOC, through preferentially enhanced preservation of organic matter and loss of Hg. Critically, we also find, based on our data from Mediterranean sapropels and published data (e.g. Mercone et al., 1999; Shen et al., 2020), that these relationships may reverse in (1) the most oxygen-depleted, strongly sulfidic conditions and (2) in cases where post-depositional oxidation affects sediments deposited in anoxic–sulfidic conditions, complicating the interpretation of deep-time Hg and Hg/TOC records, especially those for which no accurate, paired, oxygenation reconstructions exist.

The material from ODP Site 1261A recovered from Demerara Rise records clear cyclic variability in sedimentary geochemistry, including Hg, during the Coniacian–Santonian Ocean Anoxic Event 3. This variability confirms that the effects documented for soft sediments are also preserved in the geological record. With deposition alternating from euxinic to ferruginous (März et al., 2008), this sedimentary material was deposited under redox conditions somewhat similar to the Holocene Baltic Sea sites. Although the organic-matter content is very high throughout (5–15%; Fig. 7), the correlation between Hg and TOC is surprisingly weak, as is the correlation of Hg with S (both $R^2 \sim 0.05$). Both Hg and TOC show cyclicity, but these cycles are not aligned or in anti-phase.

When normalizing Hg to TOC, however, clearer trends with other geochemical proxies start to appear. Hg/S shows virtually identical trends to Hg/TOC (Fig. 7A, B) and the absence of a strong correlation with sedimentary S implies that it is unlikely that a large proportion of Hg is metal sulfide-bound or present as HgS inclusions. However, the negative correlation of Hg/TOC with HI might imply a mechanism whereby the OM preservation state, in this case the extent of oxidative degradation, controls the Hg/TOC. Counter-intuitively, the most carbonate-lean (“black” shale) intervals have the lowest HI and highest OI in this section, which may be explained by reduced accumulation rates. Together with the stable carbonate-free Al fraction, the low HI and high OI suggest lowered accumulation rates and, as a consequence, slow, protracted, breakdown of sedimentary OM during the deposition of the carbonate-poor intervals. The behavior of Hg relative to conservative detrital elements such as Al across the oxygenation cycles mimics that of Hg/TOC and Hg/S. This parallelism seems to provide further support for the notion that the highest Hg preservation efficiency and perhaps accumulation rates occurred during the ferruginous phases. Combined with the evidence for alteration of Hg and TOC signals in our Holocene core material, it seems likely that Hg and Hg/TOC signals were mostly fixed during early sedimentary diagenesis with a substantial influence of water-column and pore-water oxygenation, particularly through OM degradation in oxic settings and Hg loss in anoxic settings. The observation that TOC is lost relative to Hg aligns with observations on modern organic-rich substrates such as peats and varved lake sediments (e.g., Biester et al., 2003; Rydberg et al., 2008).

The effects of ambient redox conditions, as illustrated by OM matter preservation, also appear to be a common feature in all Cretaceous sites we studied. For example, when focusing on the Hg and TOC of the shale and chert levels at Furlo (Fig. S5), we find a positive correlation between Hg and TOC, but a weak negative correlation between Hg/TOC and HI (Fig. 8A). A negative correlation between Hg/TOC and HI and positive correlation between Hg/TOC and OI is seen at Tarfaya S57 (Fig. 8B), South Ferriby and ODP Hole 1261A (Fig. 8C,D). It is noteworthy that HI at both Furlo and South Ferriby is generally low compared to Tarfaya S57 and ODP Site 1261A (Fig. 8), and OI is generally higher, although both parameters show substantial variability, signaling a larger contribution of refractory organic matter and generally more

degraded TOC. In this light, the higher average and more variable Hg/TOC observed at Furlo and South Ferriby is in line with previous observations, indicating a primary control of OM preservation and type on Hg/TOC, at least within single stratigraphic records, but potentially also controlling differences between time-equivalent successions.

4.2 Origin and magnitude of biases in Hg, and Hg/TOC

Our new data reaffirms the observations on modern sediment observational data that Hg loss may occur during anoxic and (weakly) sulfidic conditions (see section 4.1) and, most importantly, that a signal of this process might be preserved in deep-time records (e.g. Fig. 7). Such a process is an important consideration for Hg studies that attempted to constrain volcanic activity during periods of extensive anoxia such as the Mesozoic OAEs (e.g., Percival et al., 2015; Scaife et al., 2017; Percival et al., 2021b), or similar Paleozoic events (e.g., Piszczowska et al., 2020; Rakociński et al., 2022), but also more regional or local deoxygenation as recognized during the Cenozoic (e.g., Jones et al., 2019; Cramwinckel et al., 2022). Although the Hg deficit is difficult to quantify properly without knowledge of the initial contents in the particle or burial flux, we perform a rough calculation for the Arabian Sea, assuming (1) a scenario in which Hg flux to the sediment–water interface is constant and (2) a scenario in which the upper part of the Station 1B sediments is representative of the original Hg/TOC (~ 20 ppb/%) ratio in the particle flux. Lower TOC ($\sim 8 > \sim 6\%$) in the upper part of the section at Station 1B suggests this part may have been deposited under slightly less reducing conditions or documents lower productivity compared to the lower part (Fig. 3). Even without correcting for better ventilation and lowered TOC (scenario 1), the difference in Hg contents from top to bottom is substantial (Hg decreasing by 50% from ~ 130 ppb near the sediment-water interface to 65 ppb below 10 cm depth, at Station 1B). However, assuming the Hg/TOC in the upper part is most representative of the particle flux (scenario 2), the initial Hg contents in the lower part of the Station 1B core might have been even higher (up to ca. 170 ppb). As a consequence, we speculate that an even larger proportion of Hg ($>60\%$) could have been removed during early diagenesis. While such Hg loss would not eliminate most Hg signals interpreted to result from LIP volcanism (see e.g. Grasby et al., 2019; Charbonnier et al., 2020 for a comparison of magnitudes), it appears likely that some pulses of LIP-derived Hg emitted during periods of anoxia are missed or systematically underestimated as a consequence.

Similarly, for the OAE 3 sediments, we can calculate Hg loss during the sulfidic episodes relative to the ferruginous phases. Assuming the highest Hg/TOC values represent the original signal, starting from peak values around ~ 120 ppb, Hg loss might have reached ~ 50 ppb or more. This calculation is more uncertain for the Baltic Sea sites because TOC and Al are much more variable. However, during the hypoxic periods, using the stable Hg/TOC from the less reducing (stable) background (Fig. 4A, C), the calculated relative Hg loss may range up to ~ 40 ppb, while only ~ 20 – 30 ppb is retained. Intriguingly, while starting from different Hg/TOC (6.4 at F80 *vs* 8.6 ppb/% at LL19, owing to the better ventilated nature of LL19), calculated Hg loss (in ppb) for both cores is identical.

Remarkably, despite age and other inter-site differences between the Holocene Arabian Sea and Baltic and the Cretaceous ODP Hole 1261A sediments, the calculated maximum Hg deficit is very similar and typically does not exceed 50–60%. The similarity in signals recovered from these materials reinforces our assertion that Hg is lost relative to TOC. Moreover, the maximum Hg loss of *ca.* 50–60% for anoxic-mildly euxinic deposition could imply that the processes involved in Hg loss cannot easily (re)mobilize the remaining Hg: perhaps for this fraction the Hg-species or (binding) location inhibits remobilization. We find a strong correlation of Hg evasion to Mo enrichment and other metals that are assumed to (co)precipitate with sulfides under anoxic conditions, including the Arabian Sea station where the concentration of sulfide is very low. This result seems to argue against a strong tendency to develop sulfide-enriched Hg or otherwise S-dominant Hg sequestration in anoxic to (mildly) sulfidic conditions. We find no indications that Hg is preferentially lost from or concentrated in sediments marked by continuous slightly hypoxic and oxic conditions.

The effects of oxygenation on Hg/TOC are even more pronounced compared to Hg. For the Arabian Sea sites, and other sediments deposited within and below OMZs in the ocean, the TOC contents alone may span orders of magnitude depending on the bottom and pore water oxygenation at the time of sediment deposition

(e.g., Müller and Suess, 1979; Hartnett et al., 1998). This signal subsequently modulates Hg/TOC. Order-of-magnitude changes, such as we find in the Arabian Sea sites, do not commonly occur in one single succession because most analyzed depositional settings will not have changed so dramatically, but both the Baltic Sea and ODP Site 1261 stratigraphic records clearly show changes to Hg and Hg/TOC related to redox changes (Fig. 4,6). Hence, extreme caution should be taken when analyzing successions across (de)oxygenation events, since signal amplification or suppression in Hg/TOC is likely to have occurred and can span at least an order of magnitude, on a par with many of the inferred volcanism-related Hg/TOC fluctuations in the geological record (Charbonnier et al., 2020). Likewise, the oxidation biases may have induced changes that exceed the commonly used limit for interpreting Hg enrichment factors (HgEF >2 Shen et al., 2019a, 2019b; Zhu et al., 2021). A more conservative approach is therefore warranted when interpreting Hg/TOC or otherwise normalized Hg records and perhaps even raw Hg data, and could, for example, utilize a series of criteria. The observations on the potential impact of ambient redox conditions on Hg and normalized Hg may warrant revisiting of Hg studies that are based on successions where substantial changes in ambient redox were recognized (e.g. Percival et al., 2018; Jones et al., 2019; Paschall et al., 2019; Rakociński et al., 2021; Bian et al., 2022; Zhao et al., 2022a). Critically, we find any anomalously elevated Hg/TOC data should at least be accompanied by substantially (at least >3 fold background) elevated Hg (as suggested previously; Percival et al., 2021) and, as such spikes might be associated with post-depositional oxidation of anoxic facies, evidence for stable redox conditions in the relevant stratigraphic interval that would support increased primary Hg loading.

4.3 Processes influencing Hg and Hg/TOC during early diagenesis

In our new data (Fig. 3-8) the TOC-normalized Hg (i.e., Hg/TOC) unambiguously increases with oxidation but this seems to result from multiple distinct processes affecting Hg and TOC separately. Specifically, there appears to be a distinction in Hg burial efficiency between oxygenated and anoxic to sulfidic conditions, whereby Hg appears to preferentially escape sediments under anoxic to sulfidic conditions while there is no measurable change in TOC content of the sediment (see section 4.1 & 4.2). Based on positive correlation (Supplementary data), Hg appears to be predominantly bound to TOC in many of the analyzed anoxic sample sets, implying this phenomenon could suggest either a substantially weaker binding of a part of the OM-bound Hg (Haitzer et al., 2002), or that a non-OM-bound Hg fraction is remobilized. Both options, however, require Hg remobilization and ultimately evasion (up to *ca.* 50-60%, see section 4.2) to the bottom waters.

We cannot confirm the occurrence of a specific process leading to Hg loss in anoxic to sulfidic environments, in which loss of organic matter would be minimal. There are, however, potential explanations for the slowly decreasing Hg contents in the intervals of Fe-reduction (and SO_4^{2-} reduction, see §2.1) in the anoxic Holocene sediments of the Arabian Sea (Fig. 3) and the lower Hg loading of TOC in the organic-rich, sulfidic, Holocene sediments of the Baltic Sea (Fig. 4). For example, it has been established that various sulfate- and Fe-reducing bacteria and archaea are able to methylate Hg to counteract its toxicity (Fleming et al., 2006; Gilmour et al., 2013). This distinct microbial behavior, also known from other biotoxic elements (Li et al., 2021), would increase Hg mobility. Intriguingly, marine organisms capable of Hg-methylation are widespread and seemingly diverse, including obligate anaerobes, but possibly also aerobic organisms (Villar et al., 2020). It might be that sulfate-reducing bacteria are more efficient compared to Fe-reducing bacteria (Fleming et al., 2006; Han et al., 2008). While it is impossible to confidently identify the process responsible for removal of Hg, our data are consistent with a mechanism whereby Hg methylation facilitates sedimentary Hg loss. Specifically, the negative correlation of Hg/TOC, and notably Hg/Al, with elevated Mo contents, which is used as evidence for sulfidic (pore-water) conditions at the time of deposition at ODP Site 1261, is interesting and mimics the trends observed in the Baltic Sea sites. As sulfide is an important modulator of Mo sequestration, the negative correlation between Mo and Hg/TOC tentatively supports a role for Hg methylation by sulfate reducers in Hg loss. Intriguingly, the negative correlations between Hg/TOC and Mo weaken at high Mo contents (>50 ppm in the Baltic Sea sites, Fig. 4E, F and >100 ppm for ODP Site 1261 Fig. 7D), which may be indicative of sulfide inhibition on Hg methylation by sulfate- and iron-reducing organisms, and may be accompanied with, or followed by, a switch to Hg sequestration by sulfide or metal sulfide complexes when

these species are readily available (Ullrich et al., 2001; Shen et al., 2020). Alternatively, working either in tandem or independently from Hg-methylation, an influence of temporary adsorption of Hg^{2+} with Fe or Mn (oxyhydr)oxide in Hg cycling cannot be ruled out. The mobility of Hg^{2+} would likely remain a limiting factor under these conditions, in the presence of efficient scavenging ligands such as free sulfide and organic matter.

At present, it is impossible to gauge whether and how these processes would influence deep-time records, but noticeable Hg loss under ferruginous–(mildly) euxinic conditions is consistent with the trends we find from the Holocene Baltic Sea sites, Pleistocene Mediterranean sapropel S5 and the Coniacian-Santonian OAE 3 sediments recovered at ODP Site 1261. Crucially, the observed Hg deficit – up to ~50% relative to stable Hg/TOC – occurs, in similar magnitude, both in deep-time and modern sediments, suggesting that this phenomenon might be a relatively common feature. Moreover, if Hg evasion is indeed a common feature of low-oxygen environments, questions are raised regarding the potential for redistribution and redeposition of Hg. The negative correlations of Hg and Hg/TOC with Mo and other redox-sensitive elements might be useful in identifying Hg loss. Regardless of the processes involved, both the geological imprint of Hg methylation and other mechanisms potentially leading to Hg loss from sediments warrant careful consideration when interpreting the geological Hg record.

Less surprisingly, we see progressive TOC loss with increased oxygen exposure, especially under oxic or mildly hypoxic conditions. However, Hg is not proportionally affected, resulting in progressively higher Hg/TOC with long-term oxidation, and occasionally Hg focusing (e.g., Fig. 5, Mercone et al. 1999). The early diagenetic changes examined here have echoed effects in situations where ancient sediments, initially deposited under anoxic conditions, have been subjected to surface weathering and oxidation in more recent time (Charbonnier et al., 2020). There are a couple of plausible mechanisms that would retain more Hg relative to TOC during oxidation. Firstly, if Hg were mobilized (as Hg^{2+}) during OM breakdown, it would most likely be immediately scavenged by other organic material, Fe/Mn (oxyhydr)oxides, pyrite and other sulfides, while dissolved inorganic carbon would be generally more mobile. Secondly, it is likely that a fraction of the sedimentary Hg would be associated with more refractory OM (e.g., Them et al. 2019), which could have had intrinsically higher Hg/TOC and was less easily mobilized (Them et al., 2019; Charbonnier et al., 2020). A relative increase in the refractory organic-matter fraction could hence cause a steeper Hg/TOC relationship during extensive TOC degradation, whereas a relative decrease in refractory organic-matter would result in flattening of the curves at higher TOC. Further detailed assessment of OM characteristics through, for example, maceral analyses or palynology, or Hg content data on specific types of OM, might help elucidate how preservation and OM sources interact to shape Hg/TOC patterns in ancient sediments. Even if some of those data types are available for some localities and periods, it is typically not paired with Hg (e.g., Harding et al., 2011; Kender et al., 2012; Jones et al., 2019; Kender et al., 2021), and these aspects are thus under-explored. Broad geochemical characteristics of OM (such as HI and OI, but also C/N ratios) might be used as first-order estimates of the preservation state (Fig. 8) as well as the relative contribution of refractory OM.

5. Conclusions

Differences in duration and intensity of sediment (de)oxygenation and, more broadly, changes in redox conditions, both between and within our Holocene–Pleistocene and Cretaceous sites resulted in markedly divergent Hg contents and Hg/TOC (Figs. 3-8). Importantly, we find that separate processes affect both the Hg and TOC, and contribute to the complexity and potential biases that may pose an additional challenge in the interpretation of Hg and Hg/TOC records. Through selecting sites with stable Hg loading throughout but with spatially or temporally variable ambient redox conditions and evolution, we isolate the effects of the redox conditions on the Hg and normalized-Hg records and how those effects might be stored in the geological record.

Results from the Holocene Arabian Sea cores show that order-of-magnitude differences in Hg/TOC can occur after oxidizing seemingly similar starting material. Under oxygen-depleted conditions, there is evidence that part of the Hg escapes the sediments during initial diagenesis, for example after methylation by Fe-oxide- and

sulfate-reducing bacteria and methanogens. If this phenomenon were a common factor during early diagenesis, it might be expected that Hg spikes would be suppressed in sediments deposited under such low-oxygen conditions. Such sediments are also commonly characterized by high burial efficiency of TOC, arguably further reducing the Hg/TOC ratio. Aerobic degradation, on the other hand, seems to predominantly affect sedimentary organic carbon, while Hg is mostly retained, thereby inflating Hg/TOC ratios. Stratigraphic focusing of Hg was found associated with the oxidized intervals of sediments that were deposited under anoxic–sulfidic conditions. Under such circumstances, Hg content spikes are observed around buried redox fronts, which are commonly observed associated with, but not unique to, turbidites (e.g., Mercone et al. 1999) and sapropels (Fig. 5). These type of settings, as a consequence, are particularly challenging targets for assessing paleo-volcanic activity.

For many key intervals in geological deep time that have been investigated for Hg and TOC, the potential influences of (de)oxygenation have far-reaching implications. Such complicating factors could be particularly important for periods associated with emplacement of subaerial LIPs that are also commonly associated with the most extreme carbon-cycle, climatic and environmental perturbations, including (transient) expansion of low-oxygen areas in the ocean, in extreme cases leading to ocean anoxic events. It is noteworthy that some overwhelmingly large Hg spikes occur during times of ocean anoxia, while our results show that deoxygenation generally has a higher probability of obscuring, rather than accentuating Hg/TOC spikes (e.g. Fig. 6). Indeed, it appears that under anoxic and (mildly) euxinic conditions Hg contents may be suppressed due to Hg evasion, likely as a result of methylation (Figs. 3,4,6,7). We cannot rule out that ocean anoxia, such as occurred during the Mesozoic Era, in combination with the nature of the LIP volcanism may have played an important role in reducing the perceived impact on the Hg cycle (e.g., Percival et al., 2018). On the other hand, high-amplitude oxygen fluctuations are likely to have led to increased variability in Hg and TOC and, in some cases, to Hg focusing resulting from oxidation of previously anoxic sediments. It also remains likely that S-driven Hg sequestration (within pyrite) occurs in extreme euxinic conditions, potentially amplifying Hg signals, but the sedimentary host phases and their potential for amplified Hg sequestration in geological samples will remain uncertain until a broad spectrum of dedicated Hg speciation data becomes available.

The magnitude of geochemical change from early diagenesis to both the Hg and TOC records is such that the resulting signals, without prior knowledge of the oxygenation history of a succession, could easily be misinterpreted as evidence for enhanced, suppressed, or intermittent volcanic activity. While the relative influence of oxygenation on any single record during high-amplitude environmental changes remains difficult to quantify, we calculate Hg loss on the order of ~50% in multiple records, while changes associated with Hg focusing around paleo-redox fronts is potentially of a similar magnitude (~a doubling). Critically, we also show that Hg/TOC might suffer order-of-magnitude alterations depending on the oxidative evolution of the host sediment. As such, we recommend paleo-oxygenation reconstructions through, for example, the use of (trace)-element analyses or, more indirectly, organic-matter characteristics, be employed as extensively as possible when interpreting Hg and (TOC-)normalized Hg signals.

Acknowledgments

We thank S. Wyatt and O. Green (University of Oxford), H. de Waard (Utrecht University) and S. Ossebaer (NIOZ) for analytical assistance. T.A.M. and J.F. acknowledge funding from ERC consolidator Grant (ERC-2018-COG-818717-V-ECHO). N.A.G.M.v.H. and C.P.S. acknowledge funding from ERC Synergy Grant 854088 (MARIX). G.-J.R. acknowledges funding from the Dutch Research Council (NWO) for the PASOM Cruise (2009) to the Arabian Sea. The Netherlands Earth System Science Centre (NESSC), financially supported by the Ministry of Education, Culture and Science (OCW) is acknowledged for funding the cruise that acquired the 64PE406 core.

Data availability statement

All newly generated data will be made available through a permanent online data repository upon publication.

Algeo T. J., Luo G. M., Song H. Y., Lyons T. W. and Canfield D. E. (2015) Reconstruction of secular variation in seawater sulfate concentrations. *Biogeosciences* **12**, 2131–2151.

Amos H. M., Jacob D. J., Streets D. G. and Sunderland E. M. (2013) Legacy impacts of all-time anthropogenic emissions on the global mercury cycle. *Global Biogeochem. Cycles* **27** , 410–421.

Amos H. M., Sonke J. E., Obrist D., Robins N., Hagan N., Horowitz H. M., Mason R. P., Witt M., Hedgcock I. M., Corbitt E. S. and Sunderland E. M. (2015) Observational and modeling constraints on global anthropogenic enrichment of mercury. *Environ. Sci. Technol.* **49** , 4036–4047.

Behar F., Beaumont V. and De B. Penteadó H. L. (2001) Rock-Eval 6 Technology: Performances and Developments. *Oil Gas Sci. Technol.* **56** , 111–134.

Benoit J. M., Gilmour C. C., Mason R. P. and Heyes A. (1999) Sulfide controls on mercury speciation and bioavailability to methylating bacteria in sediment pore waters. *Environ. Sci. Technol.* **33** , 951–957.

Berner R. A. (1989) Biogeochemical cycles of carbon and sulfur and their effect on atmospheric oxygen over Phanerozoic time. *Glob. Planet. Change* **1** , 97–122.

Berner R. A. and Raiswell R. (1983) Burial of organic carbon and pyrite sulfur in sediments over Phanerozoic time: a new theory. *Geochim. Cosmochim. Acta* **47** , 855–862.

Bian L., Chappaz A., Schovsbo N. H., Nielsen A. T. and Sanei H. (2022) High mercury enrichments in sediments from the Baltic continent across the late Cambrian: Controls and implications. *Chem. Geol.* **599** .

Biester H., Martínez-Cortizas A., Birkenstock S. and Kilian R. (2003) Effect of Peat Decomposition and Mass Loss on Historic Mercury Records in Peat Bogs from Patagonia. *Environ. Sci. Technol.* **37** , 32–39.

Biester H., Pérez-Rodríguez M., Gilfedder B.-S., Martínez Cortizas A. and Hermanns Y.-M. (2018) Solar irradiance and primary productivity controlled mercury accumulation in sediments of a remote lake in the Southern Hemisphere during the past 4000 years. *Limnol. Oceanogr.* **63** , 540–549.

Bowman K. L., Hammerschmidt C. R., Lamborg C. H. and Swarr G. (2015) Mercury in the North Atlantic Ocean: The U.S. GEOTRACES zonal and meridional sections. *Deep. Res. Part II Top. Stud. Oceanogr.* **116** , 251–261.

Bowman K. L., Hammerschmidt C. R., Lamborg C. H., Swarr G. J. and Agather A. M. (2016) Distribution of mercury species across a zonal section of the eastern tropical South Pacific Ocean (U.S. GEOTRACES GP16). *Mar. Chem.* **186** , 156–166.

Bravo A. G., Bouchet S., Tolu J., Björn E., Mateos-Rivera A. and Bertilsson S. (2017) Molecular composition of organic matter controls methylmercury formation in boreal lakes. *Nat. Commun.* **8** , 1–9.

Brumsack H. J. (2006) The trace metal content of recent organic carbon-rich sediments: Implications for Cretaceous black shale formation. *Palaeogeogr. Palaeoclimatol. Palaeoecol.* **232** , 344–361.

Calvert S. E. and Pedersen T. F. (1993) Geochemistry of Recent oxic and anoxic marine sediments: Implications for the geological record. *Mar. Geol.* **113** , 67–88.

Charbonnier G., Adate T., Föllmi K. B. and Suan G. (2020) Effect of Intense Weathering and Postdepositional Degradation of Organic Matter on Hg/TOC Proxy in Organic-rich Sediments and its Implications for Deep-Time Investigations. *Geochemistry, Geophys. Geosystems* **21** , 270.

Clarkson M. O., Hennekam R., Sweere T. C., Andersen M. B., Reichart G. J. and Vance D. (2021) Carbonate associated uranium isotopes as a novel local redox indicator in oxidatively disturbed reducing sediments. *Geochim. Cosmochim. Acta* **311** , 12–28.

Clarkson M. O., Stirling C. H., Jenkyns H. C., Dickson A. J., Porcelli D., Moy C. M., von Strandmann P. P. A. E., Cooke I. R. and Lenton T. M. (2018) Uranium isotope evidence for two episodes of deoxygenation during Oceanic Anoxic Event 2. *Proc. Natl. Acad. Sci. U. S. A.* **115** , 2918–2923.

Cohen A. S., Coe A. L., Harding S. M. and Schwark L. (2004) Osmium isotope evidence for the regulation of atmospheric CO₂ by continental weathering. *Geology* **32** , 157.

Compeau G. C. and Bartha R. (1985) Sulfate-Reducing Bacteria: Principal Methylators of Mercury in Anoxic Estuarine Sediment. *Appl. Environ. Microbiol.* **50** , 498–502.

Cooke C. A., Balcom P. H., Biester H. and Wolfe A. P. (2009) Over three millennia of mercury pollution in the Peruvian Andes. *Proc. Natl. Acad. Sci. U. S. A.* **106** , 8830–8834.

Cossa D., Knoery J., Bănaru D., Harmelin-Vivien M., Sonke J. E., Hedgecock I. M., Bravo A. G., Rosati G., Canu D., Horvat M., Sprovieri F., Pirrone N. and Heimbürger-Boavida L.-E. (2022) Mediterranean Mercury Assessment 2022: An Updated Budget, Health Consequences, and Research Perspectives. *Environ. Sci. Technol.* **56** , 3840–3862.

Covelli S., Faganeli J., Horvat M. and Brambati A. (2001) Mercury contamination of coastal sediments as the result of long-term cinnabar mining activity (Gulf of Trieste, northern Adriatic sea). *Appl. Geochemistry* **16** , 541–558.

Cramwinckel M. J., van der Ploeg R., van Helmond N. A. G. M., Waarlo N., Agnini C., Bijl P. K., van der Boon A., Brinkhuis H., Frieling J., Krijgsman W., Mather T. A., Middelburg J. J., Peterse F., Slomp C. P. and Sluijs A. (2022) Deoxygenation and organic carbon sequestration in the Tethyan realm associated with the Middle Eocene Climatic Optimum.

GSA Bull.

Dal Corso J., Mills B. J. W., Chu D., Newton R. J., Mather T. A., Shu W., Wu Y., Tong J. and Wignall P. B. (2020) Permo–Triassic boundary carbon and mercury cycling linked to terrestrial ecosystem collapse. *Nat. Commun.* **11** , 1–9.

Demaison G. J. and Moore G. T. (1980) Anoxic environments and oil source bed genesis. *Am. Assoc. Pet. Geol. Bull.* **64** , 1179–1209.

Edwards B. A., Kushner D. S., Outridge P. M. and Wang F. (2021) Fifty years of volcanic mercury emission research: Knowledge gaps and future directions. *Sci. Total Environ.* **757** , 1–17.

Emili A., Koron N., Covelli S., Faganeli J., Acquavita A., Predonzani S. and Vittor C. De (2011) Does anoxia affect mercury cycling at the sediment-water interface in the Gulf of Trieste (northern Adriatic Sea)? Incubation experiments using benthic flux chambers. *Appl. Geochemistry* **26** , 194–204.

Ernst R. E. and Youbi N. (2017) How Large Igneous Provinces affect global climate, sometimes cause mass extinctions, and represent natural markers in the geological record. *Palaeogeogr. Palaeoclimatol. Palaeoecol.* **478** , 30–52.

Fendley I. M., Mittal T., Sprain C. J., Marvin-DiPasquale M., Tobin T. S. and Renne P. R. (2019) Constraints on the volume and rate of Deccan Traps flood basalt eruptions using a combination of high-resolution terrestrial mercury records and geochemical box models. *Earth Planet. Sci. Lett.* **524** , 1–11.

Fitzgerald W. F., Lamborg C. H. and Hammerschmidt C. R. (2007) Marine biogeochemical cycling of mercury. *Chem. Rev.* **107** , 641–662.

Fleming E. J., Mack E. E., Green P. G. and Nelson D. C. (2006) Mercury methylation from unexpected sources: Molybdate-inhibited freshwater sediments and an iron-reducing bacterium. *Appl. Environ. Microbiol.* **72** , 457–464.

Gagnon C., Pelletier É. and Mucci A. (1997) Behaviour of anthropogenic mercury in coastal marine sediments. *Mar. Chem.* **59** , 159–176.

Gehrke G. E., Blum J. D. and Meyers P. A. (2009) The geochemical behavior and isotopic composition of Hg in a mid-Pleistocene western Mediterranean sapropel. *Geochim. Cosmochim. Acta* **73** , 1651–1665.

Gilmour C. C., Podar M., Bullock A. L., Graham A. M., Brown S. D., Somenahally A. C., Johs A., Hurt R. A., Bailey K. L. and Elias D. A. (2013) Mercury methylation by novel microorganisms from new environments.

Environ. Sci. Technol. **47** , 11810–11820.

Gobeil C. and Cossa D. (1993) Mercury in sediments and sediment pore water in the Laurentian Trough. *Can. J. Fish. Aquat. Sci.* **50** , 1794–1800.

Grasby S. E., Sanei H., Beauchamp B. and Chen Z. (2013) Mercury deposition through the Permo-Triassic Biotic Crisis. *Chem. Geol.* **351** , 209–216.

Grasby S. E., Them T. R., Chen Z., Yin R. and Ardakani O. H. (2019) Mercury as a proxy for volcanic emissions in the geologic record. *Earth-Science Rev.* **196** , 102880.

Gu B., Bian Y., Miller C. L., Dong W., Jiang X. and Liang L. (2011) Mercury reduction and complexation by natural organic matter in anoxic environments. *Proc. Natl. Acad. Sci. U. S. A.* **108** , 1479–1483.

Guédron S., Tolu J., Brisset E., Sabatier P., Perrot V., Bouchet S., Develle A. L., Bindler R., Cossa D., Fritz S. C. and Baker P. A. (2019) Late Holocene volcanic and anthropogenic mercury deposition in the western Central Andes (Lake Chungará Chile). *Sci. Total Environ.* **662** , 903–914.

Haake B., Ittekkot V., Rixen T., Ramaswamy V., Nair R. R. and Curry W. B. (1993) Seasonality and interannual variability of particle fluxes to the deep Arabian sea. *Deep. Res. Part I* **40** , 1323–1344.

Haitzer M., Aiken G. R. and Ryan J. N. (2002) Binding of Mercury(II) to Dissolved Organic Matter: The Role of the Mercury-to-DOM Concentration Ratio. *Environ. Sci. Technol.* **36** , 3564–3570.

Hammerschmidt C. R. and Fitzgerald W. F. (2004) Geochemical Controls on the Production and Distribution of Methylmercury in Near-Shore Marine Sediments. *Environ. Sci. Technol.* **38** , 1487–1495.

Han S., Obraztsova A., Pretto P., Deheyn D. D., Gieskes J. and Tebo B. M. (2008) Sulfide and iron control on mercury speciation in anoxic estuarine sediment slurries. *Mar. Chem.* **111** , 214–220.

Harding I. C., Charles A. J., Marshall J. E. A., Pälke H., Roberts A. P., Wilson P. A., Jarvis E., Thorne R., Morris E., Moremon R., Pearce R. B. and Akbari S. (2011) Sea-level and salinity fluctuations during the Paleocene–Eocene thermal maximum in Arctic Spitsbergen. *Earth Planet. Sci. Lett.* **303** , 97–107.

Hartnett H. E., Keil R. G., Hedges J. I. and Devol A. H. (1998) Influence of oxygen exposure time on organic carbon preservation in continental margin sediments. *Nature* **391** , 572–574.

Hazra B., Katz B. J., Pratap D. and Singh P. K. (2022) Impact of siderite on Rock-Eval S3 and oxygen index. *Mar. Pet. Geol.* **143** , 105804.

Hedges J. I., Hu F. S., Devol A. H., Hartnett H. E., Tsamakis E. and Keil R. G. (1999) Sedimentary organic matter preservation: A test for selective degradation under oxic conditions. *Am. J. Sci.* **299** , 529–555.

Hedges J. I. and Keil R. G. (1995) Sedimentary organic matter preservation: an assessment and speculative synthesis. *Mar. Chem.* **49** , 81–115.

Heimbürger L. E., Cossa D., Marty J. C., Migon C., Averty B., Dufour A. and Ras J. (2010) Methyl mercury distributions in relation to the presence of nano- and picophytoplankton in an oceanic water column (Ligurian Sea, North-western Mediterranean). *Geochim. Cosmochim. Acta* **74** , 5549–5559.

van Helmond N. A. G. M., Jilbert T. and Slomp C. P. (2018) Hypoxia in the Holocene Baltic Sea: Comparing modern versus past intervals using sedimentary trace metals. *Chem. Geol.* **493** , 478–490.

van Helmond N. A. G. M., Lougheed B. C., Vollebregt A., Peterse F., Fontorbe G., Conley D. J. and Slomp C. P. (2020) Recovery from multi-millennial natural coastal hypoxia in the Stockholm Archipelago, Baltic Sea, terminated by modern human activity. *Limnol. Oceanogr.* **65** , 3085–3097.

Helz G. R. and Vorlicek T. P. (2019) Precipitation of molybdenum from euxinic waters and the role of organic matter. *Chem. Geol.* **509** , 178–193.

- Hennekam R., van der Bolt B., van Nes E. H., de Lange G. J., Scheffer M. and Reichart G. J. (2020) Early-Warning Signals for Marine Anoxic Events. *Geophys. Res. Lett.* **47** .
- Higuera P., Oyarzun R., Biester H., Lillo J. and Lorenzo S. (2003) A first insight into mercury distribution and speciation in soils from the Almadén mining district, Spain. *J. Geochemical Explor.* **80** , 95–104.
- Honjo S., Dymond J., Prell W. and Ittekkot V. (1999) Monsoon-controlled export fluxes to the interior of the Arabian Sea. *Deep. Res. Part II Top. Stud. Oceanogr.* **46** , 1859–1902.
- Jenkyns H. C. (2010) Geochemistry of oceanic anoxic events. *Geochemistry, Geophys. Geosystems* **11** , 1–30.
- Jenkyns H. C., Matthews A., Tsikos H. and Erel Y. (2007) Nitrate reduction, sulfate reduction, and sedimentary iron isotope evolution during the Cenomanian-Turonian oceanic anoxic event. *Paleoceanography* **22** .
- Jiang T., Bravo A. G., Skjellberg U., Björn E., Wang D., Yan H. and Green N. W. (2018) Influence of dissolved organic matter (DOM) characteristics on dissolved mercury (Hg) species composition in sediment porewater of lakes from southwest China. *Water Res.* **146** , 146–158.
- Jilbert T. and Slomp C. P. (2013) Rapid high-amplitude variability in baltic sea hypoxia during the holocene. *Geology* **41** , 1183–1186.
- Jones M. T., Percival L. M. E. E., Stokke E. W., Frieling J., Mather T. A., Riber L., Schubert B. A., Schultz B., Tegner C., Planke S. and Svensen H. H. (2019) Mercury anomalies across the Palaeocene-Eocene Thermal Maximum. *Clim. Past* **15** , 217–236.
- Keller G., Mateo P., Monkenbusch J., Thibault N., Punekar J., Spangenberg J. E., Abramovich S., Ashckenazi-Polivoda S., Schoene B., Eddy M. P., Samperton K. M., Khadri S. F. R. and Adatte T. (2020) Mercury linked to Deccan Traps volcanism, climate change and the end-Cretaceous mass extinction. *Glob. Planet. Change* **194** , 103312.
- Keller G., Mateo P., Punekar J., Khozyem H., Gertsch B., Spangenberg J., Bitchong A. M. and Adatte T. (2018) Environmental changes during the Cretaceous-Paleogene mass extinction and Paleocene-Eocene Thermal Maximum: Implications for the Anthropocene. *Gondwana Res.* **56** , 69–89.
- Kender S., Bogus K., Pedersen G. K., Dybkjær K., Mather T. A., Mariani E., Ridgwell A., Riding J. B., Wagner T., Hesselbo S. P. and Leng M. J. (2021) Paleocene/Eocene carbon feedbacks triggered by volcanic activity. *Nat. Commun.* **12** , 1–10.
- Kender S., Stephenson M. H., Riding J. B., Leng M. J., Knox R. W. O. B., Peck V. L., Kendrick C. P., Ellis M. A., Vane C. H. and Jamieson R. (2012) Marine and terrestrial environmental changes in NW Europe preceding carbon release at the Paleocene-Eocene transition. *Earth Planet. Sci. Lett.* **353–354** , 108–120.
- Kim M., Han S., Gieskes J. and Deheyn D. D. (2011) Importance of organic matter lability for monomethylmercury production in sulfate-rich marine sediments. *Sci. Total Environ.* **409** , 778–784.
- Koho K. A., Nierop K. G. J., Moodley L., Middelburg J. J., Pozzato L., Soetaert K., Van Der Plicht J. and Reichart G. J. (2013) Microbial bioavailability regulates organic matter preservation in marine sediments. *Biogeosciences* **10** , 1131–1141.
- Kraal P., Slomp C. P., Reed D. C., Reichart G. J. and Poulton S. W. (2012) Sedimentary phosphorus and iron cycling in and below the oxygen minimum zone of the northern Arabian Sea. *Biogeosciences* **9** , 2603–2624.
- Lafargue E., Marquis F. and Pillot D. (1998) Rock-Eval 6 applications in hydrocarbon exploration, production, and soil contamination studies. *Rev. l'Institut Fr. du Pet.* **53** , 421–437.
- Leipe T., Moros M., Kotilainen A., Vallius H., Kabel K., Endler M. and Kowalski N. (2013) Mercury in Baltic Sea sediments-Natural background and anthropogenic impact. *Chemie der Erde* **73** , 249–259.

- Lengger S. K., Hopmans E. C., Sinninghe Damsté J. S. and Schouten S. (2014) Impact of sedimentary degradation and deep water column production on GDGT abundance and distribution in surface sediments in the Arabian Sea: Implications for the TEX86 paleothermometer. *Geochim. Cosmochim. Acta* **142** , 386–399.
- Li Y. P., Ben Fekih I., Chi Fru E., Moraleda-Munoz A., Li X., Rosen B. P., Yoshinaga M. and Rensing C. (2021) Antimicrobial Activity of Metals and Metalloids. *Annu. Rev. Microbiol.* **75** , 175–197.
- Lim D., Kim H., Kim J., Jeong D. and Kim D. (2020) Mercury proxy for hydrothermal and submarine volcanic activities in the sediment cores of Central Indian Ridge. *Mar. Pollut. Bull.* **159** , 1–8.
- Lowenstein T. K., Timofeeff M. N., Brennan S. T., Hardie L. A. and Demicco R. V (2001) Oscillations in Phanerozoic Seawater Chemistry: Evidence from Fluid Inclusions. *Science (80-.)*. **294** , 1086–1088.
- Lu X., Gu W., Zhao L., Ul Haque M. F., DiSpirito A. A., Semrau J. D. and Gu B. (2017) Methylmercury uptake and degradation by methanotrophs. *Sci. Adv.* **3** , 1–6.
- Lyons T. W., Anbar A. D., Severmann S., Scott C. and Gill B. C. (2009) Tracking Euxinia in the Ancient Ocean: A Multiproxy Perspective and Proterozoic Case Study. *Annu. Rev. Earth Planet. Sci.* **37** , 507–534.
- Machado W., Sanders C. J., Santos I. R., Sanders L. M., Silva-Filho E. V. and Luiz-Silva W. (2016) Mercury dilution by autochthonous organic matter in a fertilized mangrove wetland. *Environ. Pollut.* **213** , 30–35.
- Manceau A., Lemouchi C., Enescu M., Gaillot A. C., Lanson M., Magnin V., Glatzel P., Poulin B. A., Ryan J. N., Aiken G. R., Gautier-Luneau I. and Nagy K. L. (2015) Formation of Mercury Sulfide from Hg(II)-Thiolate Complexes in Natural Organic Matter. *Environ. Sci. Technol.* **49** , 9787–9796.
- März C., Poulton S. W., Beckmann B., Küster K., Wagner T. and Kasten S. (2008) Redox sensitivity of P cycling during marine black shale formation: Dynamics of sulfidic and anoxic, non-sulfidic bottom waters. *Geochim. Cosmochim. Acta* **72** , 3703–3717.
- Mason R. P., Choi A. L., Fitzgerald W. F., Hammerschmidt C. R., Lamborg C. H., Soerensen A. L. and Sunderland E. M. (2012) Mercury biogeochemical cycling in the ocean and policy implications. *Environ. Res.* **119** , 101–117.
- Mason R. P., Fitzgerald W. F. and Morel F. M. M. (1994) The biogeochemical cycling of elemental mercury: Anthropogenic influences. *Geochim. Cosmochim. Acta* **58** , 3191–3198.
- Mason R. P. and Sheu G. R. (2002) Role of the ocean in the global mercury cycle. *Global Biogeochem. Cycles* **16** , 40-1-40–14.
- Mercone D., Thomson J., Croudace I. . and Troelstra S. . (1999) A coupled natural immobilisation mechanism for mercury and selenium in deep-sea sediments. *Geochim. Cosmochim. Acta* **63** , 1481–1488.
- Merritt K. A. and Amirbahman A. (2009) Mercury methylation dynamics in estuarine and coastal marine environments - A critical review. *Earth-Science Rev.* **96** , 54–66.
- Mikac N., Niessen S., Ouddane B. and Wartel M. (1999) Speciation of mercury in sediments of the Seine estuary (France). *Appl. Organomet. Chem.* **13** , 715–725.
- Morel F. M. M., Kraepiel A. M. L. and Amyot M. (1998) The chemical cycle and bioaccumulation of mercury. *Annu. Rev. Ecol. Syst.* **29** , 543–566.
- Morse J. W. and Luther G. W. (1999) Chemical influences on trace metal-sulfide interactions in anoxic sediments. *Geochim. Cosmochim. Acta* **63** , 3373–3378.
- Müller P. J. and Suess E. (1979) Productivity, sedimentation rate, and sedimentary organic matter in the oceans—I. Organic carbon preservation. *Deep Sea Res. Part A. Oceanogr. Res. Pap.* **26** , 1347–1362.

NASA Ocean Biology (OB.DAAC) (2014) Mean annual sea surface chlorophyll-a concentration for the period 2009-2013 (composite dataset created by UNEP- WCMC).

Newton R. J., Reeves E. P., Kafousia N., Wignall P. B., Bottrell S. H. and Sha J. G. (2011) Low marine sulfate concentrations and the isolation of the European epicontinental sea during the Early Jurassic. *Geology* **39** , 7–10.

Nieuwenhuize J., Maas Y. E. M. and Middelburg J. J. (1994) Rapid analysis of organic carbon and nitrogen in particulate materials. *Mar. Chem.* **45** , 217–224.

Ogrinc N., Monperrus M., Kotnik J., Fajon V., Vidimova K., Amouroux D., Kocman D., Tessier E., Žižek S. and Horvat M. (2007) Distribution of mercury and methylmercury in deep-sea surficial sediments of the Mediterranean Sea. *Mar. Chem.* **107** , 31–48.

Outridge P. M., Sanei H., Stern G. A., Hamilton P. B. and Goodarzi F. (2007) Evidence for control of mercury accumulation rates in Canadian High Arctic Lake sediments by variations of aquatic primary productivity. *Environ. Sci. Technol.* **41** , 5259–5265.

Owens J. D., Lyons T. W., Hardisty D. S., Lowery C. M., Lu Z., Lee B. and Jenkyns H. C. (2017) Patterns of local and global redox variability during the Cenomanian–Turonian Boundary Event (Oceanic Anoxic Event 2) recorded in carbonates and shales from central Italy. *Sedimentology* **64** , 168–185.

Paschall O., Carmichael S. K., Königshof P., Waters J. A., Ta P. H., Komatsu T. and Dombrowski A. (2019) The Devonian-Carboniferous boundary in Vietnam: Sustained ocean anoxia with a volcanic trigger for the Hangenberg Crisis? *Glob. Planet. Change* **175** , 64–81.

Pedersen T. F. and Calvert S. E. (1990) Anoxia vs. productivity: what controls the formation of organic-carbon-rich sediments and sedimentary rocks? *Am. Assoc. Pet. Geol. Bull.* **74** , 454–466.

Percival Lawrence M. E., Bergquist B. A., Mather T. A. and Sanei H. (2021) Sedimentary Mercury Enrichments as a Tracer of Large Igneous Province Volcanism. In *Large Igneous Provinces: A Driver of Global Environmental and Biotic Changes* (eds. R. E. Ernst, A. J. Dickson, and A. Bekker). Geophysical Monograph Series, American Geophysical Union. pp. 247–262.

Percival L. M. E. E., Ruhl M., Hesselbo S. P., Jenkyns H. C., Mather T. A. and Whiteside J. H. (2017) Mercury evidence for pulsed volcanism during the end-Triassic mass extinction. *Proc. Natl. Acad. Sci. U. S. A.* **114** , 7929–7934.

Percival L. M. E. E., Witt M. L. I. I., Mather T. A., Hermoso M., Jenkyns H. C., Hesselbo S. P., Al-Suwaidi A. H., Storm M. S., Xu W. and Ruhl M. (2015) Globally enhanced mercury deposition during the end-Pliensbachian extinction and Toarcian OAE: A link to the Karoo-Ferrar Large Igneous Province. *Earth Planet. Sci. Lett.* **428** , 267–280.

Percival L. M. E., Jenkyns H. C., Mather T. A., Dickson A. J., Batenburg S. J., Ruhl M., Hesselbo S. P., Barclay R., Jarvis I., Robinson S. A. and Woelders L. (2018) Does large igneous province volcanism always perturb the mercury cycle? Comparing the records of Oceanic Anoxic Event 2 and the end-cretaceous to other Mesozoic events. *Am. J. Sci.* **318** , 799–860.

Percival L.M.E., Tedeschi L. R., Creaser R. A., Bottini C., Erba E., Giraud F., Svensen H., Savian J., Trindade R., Coccioni R., Frontalini F., Jovane L., Mather T. A. and Jenkyns H. C. (2021) Determining the style and provenance of magmatic activity during the Early Aptian Oceanic Anoxic Event (OAE 1a). *Glob. Planet. Change* **200** , 103461.

Pham A. L. T., Morris A., Zhang T., Ticknor J., Levard C. and Hsu-Kim H. (2014) Precipitation of nanoscale mercuric sulfides in the presence of natural organic matter: Structural properties, aggregation, and biotransformation. *Geochim. Cosmochim. Acta* **133** , 204–215.

Pirrone N., Cinnirella S., Feng X., Finkelman R. B., Friedli H. R., Leaner J., Mason R., Mukherjee A. B., Stracher G. B., Streets D. G. and Telmer K. (2010) Global mercury emissions to the atmosphere from anthropogenic and natural sources. *Atmos. Chem. Phys.* **10** , 5951–5964.

Pisarzowska A., Rakociński M., Marynowski L., Szczerba M., Thoby M., Paszkowski M., Perri M. C., Spalletta C., Schönlaub H.-P. P., Kowalik N. and Gereke M. (2020) Large environmental disturbances caused by magmatic activity during the Late Devonian Hangenberg Crisis. *Glob. Planet. Change* **190** , 103155.

Poulton S. W., Henkel S., März C., Urquhart H., Flögel S., Kasten S., Sinninghe Damsté J. S. and Wagner T. (2015) A continental-weathering control on orbitally driven redox-nutrient cycling during Cretaceous oceanic anoxic event 2. *Geology* **43** , 963–966.

Pyle D. M. and Mather T. A. (2003) The importance of volcanic emissions for the global atmospheric mercury cycle. *Atmos. Environ.* **37** , 5115–5124.

Racki G., Rakocinski M., Marynowski L. and Wignall P. B. (2018) Mercury enrichments and the Frasnian-Famennian biotic crisis: A volcanic trigger proved? *Geology* **46** , 543–546.

Rakociński M., Książak D., Pisarzowska A. and Marynowski L. (2022) Mercury evidence of intense submarine volcanism and hydrothermal activity during a mid-Tournaisian anoxic event in the Carnic Alps. *Gondwana Res.* **109** , 225–238.

Rakociński M., Marynowski L., Pisarzowska A., Beldowski J., Siedlewicz G., Zatoń M., Perri M. C., Spalletta C. and Schönlaub H. P. (2020) Volcanic related methylmercury poisoning as the possible driver of the end-Devonian Mass Extinction. *Sci. Rep.* **10** , 1–8.

Rakociński M., Pisarzowska A., Corradini C., Narkiewicz K., Dubicka Z. and Abdiyev N. (2021) Mercury spikes as evidence of extended arc-volcanism around the Devonian–Carboniferous boundary in the South Tian Shan (southern Uzbekistan). *Sci. Rep.* **11** , 1–15.

Ravichandran M. (2004) Interactions between mercury and dissolved organic matter - A review. *Chemosphere* **55** , 319–331.

Rohling E. J., Marino G. and Grant K. M. (2015) Mediterranean climate and oceanography, and the periodic development of anoxic events (sapropels). *Earth-Science Rev.* **143** , 62–97.

Rumayor M., Gallego J. R., Rodríguez-Valdés E. and Díaz-Somoano M. (2017) An assessment of the environmental fate of mercury species in highly polluted brownfields by means of thermal desorption. *J. Hazard. Mater.* **325** , 1–7.

Rydberg J., Gälman V., Renberg I., Bindler R., Lambertsson L. and Martínez-Cortizas A. (2008) Assessing the Stability of Mercury and Methylmercury in a Varved Lake Sediment Deposit. *Environ. Sci. Technol.* **42** , 4391–4396.

Sabatino N., Ferraro S., Coccioni R., Bonsignore M., Del Core M., Tancredi V. and Sprovieri M. (2018) Mercury anomalies in upper Aptian-lower Albian sediments from the Tethys realm. *Palaeogeogr. Palaeoclimatol. Palaeoecol.* **495** , 163–170.

Sanei H. and Goodarzi F. (2006) Relationship between organic matter and mercury in recent lake sediment: The physical-geochemical aspects. *Appl. Geochemistry* **21** , 1900–1912.

Sanei H., Grasby S. E. and Beauchamp B. (2012) Latest Permian mercury anomalies. *Geology* **40** , 63–66.

Van Santvoort P. J. M., De Lange G. J., Thomson J., Colley S., Meysman F. J. R. and Slomp C. P. (2002) Oxidation and origin of organic matter in surficial Eastern Mediterranean hemipelagic sediments. *Aquat. Geochemistry* **8** , 153–175.

Scaife J. D., Ruhl M., Dickson A. J., Mather T. A., Jenkyns H. C., Percival L. M. E., Hesselbo S. P., Cartwright J., Eldrett J. S., Bergman S. C. and Minisini D. (2017) Sedimentary Mercury Enrichments as a

Marker for Submarine Large Igneous Province Volcanism? Evidence From the Mid-Cenomanian Event and Oceanic Anoxic Event 2 (Late Cretaceous). *Geochemistry, Geophys. Geosystems* **18** , 4253–4275.

Schlanger S. O. and Jenkyns H. C. (1976) Cretaceous Oceanic Anoxic Events: Causes and Consequences. *Geol. en Mijnb.* **55** , 179–184.

Schuster P. F., Krabbenhoft D. P., Naftz D. L., Cecil L. D., Olson M. L., Dewild J. F., Susong D. D., Green J. R. and Abbott M. L. (2002) Atmospheric mercury deposition during the last 270 years: A glacial ice core record of natural and anthropogenic sources. *Environ. Sci. Technol.* **36** , 2303–2310.

Schütze M., Gatz P., Gilfedder B. and Biester H. (2021) Why productive lakes are larger mercury sedimentary sinks than oligotrophic brown water lakes. *Limnol. Oceanogr.* **66** , 1316–1332.

Shen J., Algeo T. J., Chen J., Planavsky N. J., Feng Q., Yu J. and Liu J. (2019a) Mercury in marine Ordovician/Silurian boundary sections of South China is sulfide-hosted and non-volcanic in origin. *Earth Planet. Sci. Lett.* **511** , 130–140.

Shen J., Algeo T. J., Planavsky N. J., Yu J., Feng Q., Song H. H., Song H. H., Rowe H., Zhou L. and Chen J. (2019b) Mercury enrichments provide evidence of Early Triassic volcanism following the end-Permian mass extinction. *Earth-Science Rev.* **195** , 191–212.

Shen J., Chen J., Algeo T. J., Yuan S., Feng Q., Yu J., Zhou L., O’Connell B. and Planavsky N. J. (2019c) Evidence for a prolonged Permian–Triassic extinction interval from global marine mercury records. *Nat. Commun.* **10** , 1–9.

Shen J., Feng Q., Algeo T. J., Liu Jinling, Zhou C., Wei W., Liu Jiangsi, Them T. R., Gill B. C. and Chen J. (2020) Sedimentary host phases of mercury (Hg) and implications for use of Hg as a volcanic proxy. *Earth Planet. Sci. Lett.* **543** , 116333.

Shipboard Scientific Party (2004) Site 1261. In *Proceedings of the Ocean Drilling Program, 207 Initial Reports* (eds. J. Erbacher, D. C. Mosher, and M. J. Malone). Ocean Drilling Program, College Station. pp. 1–103.

Snow L. J., Duncan R. A. and Bralower T. J. (2005) Trace element abundances in the Rock Canyon Anticline, Pueblo, Colorado, marine sedimentary section and their relationship to Caribbean plateau construction and oxygen anoxic event 2. *Paleoceanography* **20** , 1–14.

Sprain C. J., Renne P. R., Vanderkluyzen L., Pande K., Self S. and Mittal T. (2019) The eruptive tempo of Deccan volcanism in relation to the Cretaceous–Paleogene boundary. *Science (80-.)*. **363** , 866–870.

Strode S. A., Jaeglé L., Selin N. E., Jacob D. J., Park R. J., Yantosca R. M., Mason R. P. and Slemr F. (2007) Air-sea exchange in the global mercury cycle. *Global Biogeochem. Cycles* **21** , 1–12.

Sunderland E. M., Gobas F. A. P. C., Heyes A., Branfireun B. A., Bayer A. K., Cranston R. E. and Parsons M. B. (2004) Speciation and bioavailability of mercury in well-mixed estuarine sediments. *Mar. Chem.* **90** , 91–105.

Sweere T., Hennekam R., Vance D. and Reichart G. J. (2021) Molybdenum isotope constraints on the temporal development of sulfidic conditions during Mediterranean sapropel intervals. *Geochemical Perspect. Lett.* **17** , 16–20.

Takahashi T., Sutherland S. C., Sweeney C., Poisson A., Metzl N., Tilbrook B., Bates N., Wanninkhof R., Feely R. A., Sabine C., Olafsson J. and Nojiri Y. (2002) Global sea–air CO₂ flux based on climatological surface ocean pCO₂, and seasonal biological and temperature effects. *Deep Sea Res. Part II Top. Stud. Oceanogr.* **49** , 1601–1622.

Them T. R., Jagoe C. H., Caruthers A. H., Gill B. C., Grasby S. E., Gröcke D. R., Yin R. and Owens J. D. (2019) Terrestrial sources as the primary delivery mechanism of mercury to the oceans across the Toarcian Oceanic Anoxic Event (Early Jurassic). *Earth Planet. Sci. Lett.* **507** , 62–72.

Tremblin M., Khozyem H., Adatte T., Spangenberg J. E., Fillon C., Grauls A., Hunger T., Nowak A., Lauchli C., Lasseur E., Roig J.-Y., Serrano O., Calassou S., Guillocheau F. and Castellort S. (2022) Mercury enrichments of the Pyrenean foreland basins sediments support enhanced volcanism during the Paleocene-Eocene thermal maximum (PETM). *Glob. Planet. Change* **212** , 103794.

Tribovillard N., Algeo T. J., Lyons T. W. and Riboulleau A. (2006) Trace metals as paleoredox and paleo-productivity proxies: An update. *Chem. Geol.* **232** , 12–32.

Tsikos H., Jenkyns H. C., Walsworth-Bell B., Petrizzo M. R., Forster A., Kolonic S., Erba E., Premoli Silva I., Baas M., Wagner T. and Sinninghe Damste J. S. (2004) Carbon-isotope stratigraphy recorded by the Cenomanian-Turonian Oceanic Anoxic Event: Correlation and implications based on three key localities. *J. Geol. Soc. London.* **161** , 711–719.

Turgeon S. and Brumsack H. J. (2006) Anoxic vs dysoxic events reflected in sediment geochemistry during the Cenomanian-Turonian Boundary Event (Cretaceous) in the Umbria-Marche Basin of central Italy. *Chem. Geol.* **234** , 321–339.

Ullrich S. M., Tanton T. W. and Abdrashitova S. A. (2001) Mercury in the aquatic environment: A review of factors affecting methylation. *Crit. Rev. Environ. Sci. Technol.* **31** , 241–293.

Villar E., Cabrol L. and Heimburger-Boavida L. E. (2020) Widespread microbial mercury methylation genes in the global ocean. *Environ. Microbiol. Rep.* **12** , 277–287.

Du Vivier A. D. C., Selby D., Sageman B. B., Jarvis I., Grocke D. R. and Voigt S. (2014) Marine 187Os/188Os isotope stratigraphy reveals the interaction of volcanism and ocean circulation during Oceanic Anoxic Event 2. *Earth Planet. Sci. Lett.* **389** , 23–33.

Wallace G. T. (1982) The association of copper, mercury and lead with surface-active organic matter in coastal seawater. **11** , 379–394.

Wang K., Liu G. and Cai Y. (2021) Possible pathways for mercury methylation in oxic marine waters. *Crit. Rev. Environ. Sci. Technol.* , 1–19.

Wang Z., Tan J., Boyle R., Wang W., Kang X., Dick J. and Lyu Q. (2020) Mercury anomalies within the lower Cambrian (stage 2–3) in South China: Links between volcanic events and paleoecology. *Palaeogeogr. Palaeoclimatol. Palaeoecol.* **558** .

Wortmann U. G. and Chernyavsky B. M. (2007) Effect of evaporite deposition on Early Cretaceous carbon and sulphur cycling. *Nature* **446** , 654–656.

Xu W., Ruhl M., Jenkyns H. C., Leng M. J., Huggett J. M., Minisini D., Ullmann C. V., Riding J. B., Weijers J. W. H., Storm M. S., Percival L. M. E., Tosca N. J., Idiz E. F., Tegelaar E. W. and Hesselbo S. P. (2018) Evolution of the Toarcian (Early Jurassic) carbon-cycle and global climatic controls on local sedimentary processes (Cardigan Bay Basin, UK). *Earth Planet. Sci. Lett.* **484** , 396–411.

Zhao H., Grasby S. E., Wang X., Zhang L., Liu Y., Chen Z., Hu Z. and Huang Y. (2022a) Mercury enrichments during the Carnian Pluvial Event (Late Triassic) in South China. *GSA Bull.* , 1–12.

Zhao H., Shen J., Algeo T. J., Racki G., Chen J., Huang C., Song J., Qie W. and Gong Y. (2022b) Mercury isotope evidence for regional volcanism during the Frasnian-Famennian transition. *Earth Planet. Sci. Lett.* **581** , 117412.

Zhu G., Wang P., Li T., Zhao K., Yan H., Li J. and Zhou L. (2021) Nitrogen geochemistry and abnormal mercury enrichment of shales from the lowermost Cambrian Niutitang Formation in South China: Implications for the marine redox conditions and hydrothermal activity. *Glob. Planet. Change* **199** , 103449.

Hosted file

hg redox si text_rev.docx available at <https://authorea.com/users/521312/articles/594280-effects-of-redox-variability-and-early-diagenesis-on-marine-sedimentary-hg-records>

1 **Effects of redox variability and early diagenesis on marine sedimentary Hg records**

2 Frieling, J.^{1*}, Mather, T.A.¹, März, C.^{2#}, Jenkyns, H.C.¹, Hennekam, R.⁴, Reichart, G.-J.^{3,4}, Slomp,
3 C.P.^{3,5} and van Helmond, N.A.G.M.^{3,5}

4 1. *Department of Earth Sciences, University of Oxford, Oxford, United Kingdom*

5 2. *School of Earth and Environment, University of Leeds, Leeds, United Kingdom*

6 3. *Department of Earth Sciences, Utrecht University, Utrecht, the Netherlands*

7 4. *Royal Netherlands Institute for Sea Research (NIOZ), 't Horntje, Texel, the Netherlands*

8 5. *Radboud Institute for Biological and Environmental Sciences, Radboud University,*
9 *Nijmegen, the Netherlands*

10 # now at: *Institute for Geosciences, University of Bonn, Bonn, Germany*

11 *corresponding author: joost.frieling@earth.ox.ac.uk

12

13 Abstract

14 Volcanism is the dominant natural source of mercury (Hg) to the atmosphere, biosphere, ocean
15 and sediments. In recent years, sedimentary Hg contents have emerged as a tool to reconstruct
16 volcanic activity, and particularly activity of (subaerially emplaced) large igneous provinces (LIP)
17 in geological deep time. More specifically, Hg has shown potential as a useful proxy to illuminate
18 the previously elusive impact of such large-scale volcanism on marine and terrestrial paleo-
19 environments. While Hg is now widely applied as volcanism tracer, non-volcanic factors
20 controlling sedimentary Hg content are generally not well constrained. Part of this uncertainty
21 stems from our inability to directly observe a natural unperturbed “steady-state” environment as a
22 baseline, as the modern Hg cycle is heavily influenced by anthropogenic activity. Here we focus
23 on the effects of ambient redox conditions in the water column and shallow sediments (early
24 diagenesis), quantify their influence on the geological Hg record and thereby constrain their
25 potential impact on the use of Hg as a proxy for deep-time volcanic activity. Constraining these
26 factors is of critical importance for the application of Hg as a proxy. Many periods in the geological
27 past for which records have been generated, such as the Mesozoic Oceanic Anoxic Events, are
28 marked by a variety of high-amplitude environmental perturbations, including widespread
29 deoxygenation and deposition of organic-rich sediments. We estimate the impact of redox changes
30 and early diagenesis on the geological Hg record using a suite of (sub)recent–Pleistocene and
31 Upper Cretaceous sediments representing oxic to euxinic marine conditions. Our sample set
32 includes a transect through an oxygen minimum zone and cores that record transient shifts in
33 oxygenation state, as well as post-depositional effects – all unrelated to volcanism, to the best of
34 our knowledge. We find substantial alterations to the Hg record and the records of organic carbon
35 and total sulfur, which are typically assumed to be the most common carrier phases of Hg in marine
36 sediments. Moreover, these biases can lead to signal-alterations on a par with those interpreted to
37 result from volcanic activity. Geochemical modifications are ubiquitous and their potential
38 magnitude implies that the factors leading to biases in the geological record warrant careful
39 consideration before interpretation. Factors of particular concern to proxy application are (1) the
40 disproportionate loss of organic carbon and sulfur compounds relative to Hg during oxidation that
41 strongly modulates normalized Hg records, (2) the evasion of Hg in anoxic and mildly euxinic
42 sediments and (3) sharp focusing of Hg during post-depositional oxidation of organic matter. We
43 find paired analyses of additional redox-sensitive trace elements such as molybdenum, and
44 organic-matter characteristics, particularly the relative contributions of refractory and labile
45 organic matter, could provide first-order constraints on the role that redox and diagenetic changes
46 played in shaping the Hg record before attributing enrichments to volcanic activity.

47 1. Introduction

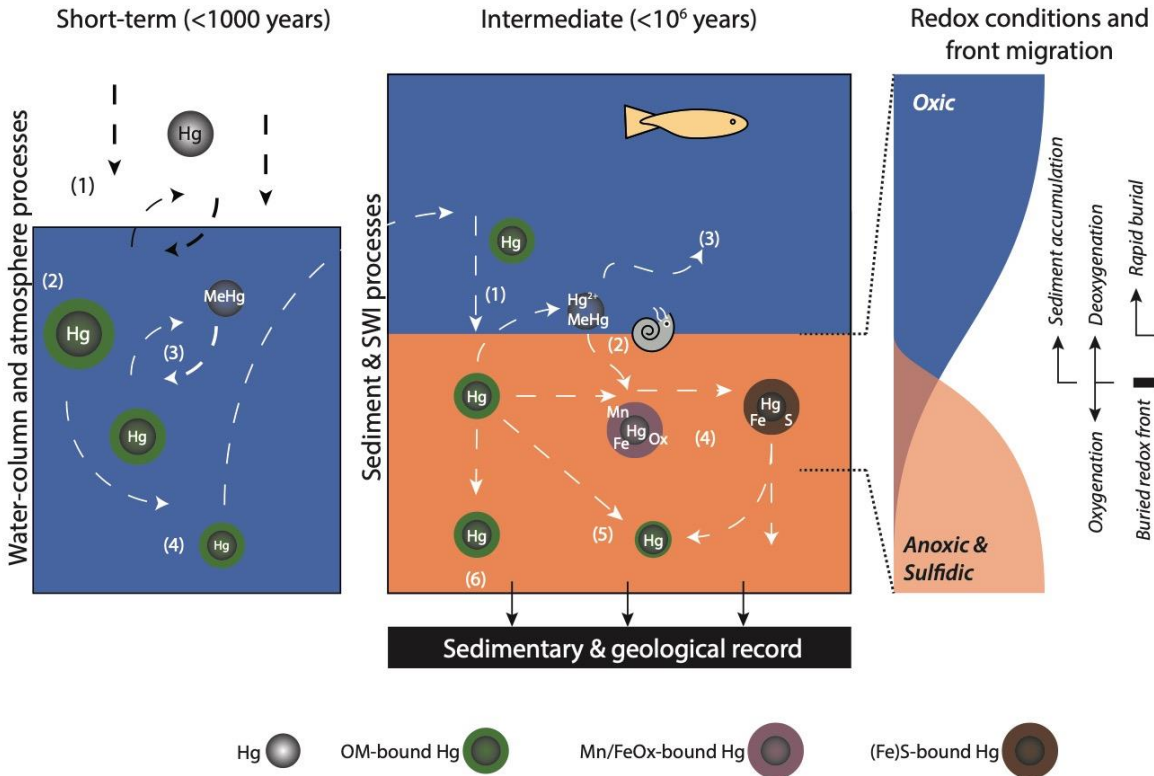
48 1.1 Hg in sedimentary records and its use as a proxy

49 In recent years, sedimentary mercury (Hg) has rapidly gained widespread attention due to its
50 proposed use as a proxy for volcanic activity, particularly the volcanism associated with (subaerial)
51 emplacement of large igneous provinces (LIPs) in the geological deep past ($\gg 10^6$ years) (e.g.
52 (Sanei et al., 2012; Grasby et al., 2013; Percival et al., 2017; Kender et al., 2021). This approach
53 is based on the predominance of volcanic-derived Hg prior to the emergence of anthropogenic
54 fluxes (Pyle and Mather, 2003; Fitzgerald et al., 2007; Pirrone et al., 2010). Particular attention
55 has been given to periods in geological time during which subaerial LIPs are thought to have been
56 highly active, based on other sedimentary proxies (such as Os isotopes and (trace) metal
57 enrichments; e.g., (Cohen et al., 2004; Snow et al., 2005; Du Vivier et al., 2014)) as well as direct
58 dating of volcanogenic deposits (e.g., Sprain et al., 2019). These periods of (subaerial) LIP activity
59 have also been studied for their high-amplitude environmental perturbations, including global
60 warming, increased weathering, loss of biodiversity, changes in terrestrial vegetation, soil erosion,
61 extensive water column anoxia–euxinia and ocean acidification.

62 To make accurate inferences about volcanic LIP activity from Hg enrichments in stratigraphic
63 records, the influence of other sedimentary changes on Hg and its carrier compounds needs to be
64 resolved in appropriate detail. For example, it is well established that particulate and dissolved
65 organic matter (OM) concentration is an important factor in governing the Hg levels in seawater
66 (Wallace, 1982) and sediments (Fitzgerald et al., 2007; Gehrke et al., 2009). This relationship is
67 due to the very high affinity of Hg^{2+} for OM, which commonly leads to strong correlations between
68 total organic carbon (TOC) and Hg (Outridge et al., 2007; Gehrke et al., 2009). While there are
69 some indications that, under extremely high productivity regimes, dilution of Hg by organic matter
70 might play a role (Machado et al., 2016), this appears to be uncommon in modern aquatic and
71 sedimentary environments where Hg concentrations and Hg sequestration are positively correlated
72 to (algal) OM abundance (profiles), although this relation is not necessarily linear (Wallace, 1982;
73 Sanei and Goodarzi, 2006; Fitzgerald et al., 2007; Outridge et al., 2007; Bowman et al., 2016;
74 Biester et al., 2018; Schütze et al., 2021; Cossa et al., 2022). To eliminate variation induced by
75 changes in OM content, normalizing Hg contents against TOC in sedimentary records has become
76 common practice in deep-time literature (e.g. Percival et al., 2015; Percival et al., 2017; Grasby et
77 al., 2019; Jones et al., 2019; Shen et al., 2019b; Kender et al., 2021; Tremblin et al., 2022; Zhao et
78 al., 2022a). The basis for this approach lies in that Hg in the sedimentary record is primarily bound
79 to OM and only secondarily to other potential scavenging compounds (e.g., sulfides, forming
80 compounds such as mercury sulfide (HgS) or Hg inclusion in pyrite, or adsorption to clays),
81 especially in the presence of abundant OM (e.g., Fitzgerald et al., 2007 and references therein). In
82 the absence of large Hg-cycle perturbations, the positive correlation between Hg and TOC, both
83 at single sample localities (e.g., Percival et al., 2015; Shen et al., 2020) and at broader scales (e.g.,
84 Grasby et al., 2019) in the geological record, provides support for this generalization. However,
85 the relation between Hg and TOC is in many instances not straightforward and since normalized

86 Hg is not stable across all environments, the assumption that Hg/TOC (or otherwise normalized
87 Hg) remains stable (in the absence of large-scale volcanic emissions) does not hold true for many
88 deep-time records analyzed to date. Moreover, it has been established that, for example, other
89 sedimentary Hg carrier phases such as sulfur (S) and pyrite can play an important role, especially
90 in strongly euxinic conditions (Shen et al., 2019a, 2020; Wang et al., 2020). Through association
91 with TOC, clays and S, Hg might appear to behave in a similar way to bio-essential, redox-
92 sensitive and/or sulfide-forming trace metals (such as, for example, Mo, V, Ni, Cd, Zn), that may
93 change phase associations following their deposition at the seafloor (e.g., Tribovillard et al., 2006;
94 Brumsack, 2006).

95



97

98 **Fig. 1. Simplified diagram illustrating a selection of pathways that influence aquatic (marine) sedimentary**
 99 **mercury (Hg) and/or organic-matter cycling (green circles).** Blue and brown/orange colors in middle panel indicate
 100 water and sediment, respectively.

101 **Left-hand panel: atmospheric deposition and aquatic processes** – (1) influx from rivers and atmosphere, (2) gas
 102 exchange in the surface layer (Mason and Sheu, 2002; Strode et al., 2007; Mason et al., 2012), (3) remineralization in
 103 the upper water column and methyl-mercury (MeHg) formation (Heimbürger et al., 2010), (4) progressive OM and
 104 Hg cycling and remineralization in the lower water column. Note that ageing deep water accumulates both C and Hg
 105 (Takahashi et al., 2002; Bowman et al., 2015, 2016).

106 **Middle panel – processes potentially influenced by ambient oxygenation:** (1) deposition of OM-bound Hg from
 107 the water column (Wallace, 1982) (2) bioturbation, diffusion and biologically driven cycling of OM and Hg near the
 108 sediment–water interface, (3) potentially resulting in Hg evasion (with MeHg or Mn/Fe (oxyhydr)oxides as
 109 intermediate phases) (Gagnon et al., 1997; Mikac et al., 1999; Hammerschmidt and Fitzgerald, 2004), (4) (temporary)
 110 binding to Mn/Fe (oxyhydr)oxides and sulfide minerals (Gagnon et al., 1997; Shen et al., 2020), (5) recalcitrant OM
 111 and Hg remaining after oxidation, (6) unaltered recording of Hg scavenged from the water column.

112 **Right-hand panel - simplified reduction-oxidation (redox) front – controlling the position and intensity of**
 113 **processes depicted in the middle panel.** The redox front, here illustrated from the sediment-water interface down,
 114 migrates upwards with sediment accumulation and deoxygenation, downwards with (re)ventilation and may be buried
 115 and fixed, for example when a mass-transport deposit such as a turbidite rapidly covers the sediment–water interface.
 116 The position of the redox front influences many (trace-) element records and, combined with processes shown in the
 117 middle panel, such as Hg binding to Mn/Fe (oxyhydr)oxides, sulfides and methylation, conceivably also shapes the
 118 sedimentary Hg record.

119 To date, variability in pre-industrial marine sediments, and particularly in deep-time records,
120 related to the processes controlling coupled TOC, S and Hg burial remains poorly understood.
121 These processes can be roughly divided into three categories. In the first category are processes
122 that influence Hg and/or TOC before they enter the sedimentary record, such as the riverine flux
123 of Hg and terrestrial OM, ocean–atmosphere exchange, and water-column processes (abundance
124 of marine OM, remineralization, scavenging efficiency). The second category includes processes
125 that take place during or shortly after the sedimentary record is formed, particularly early
126 diagenetic and soft-sediment processes: redox behavior, remineralization and remobilization. The
127 cycling of Hg, the position of the redox front and its migration ultimately determine the signal
128 preserved in the sedimentary record (Fig. 1). Third, signal deterioration may occur in samples that
129 have been exposed for long periods on the Earth’s surface (Charbonnier et al., 2020). The potential
130 for weathering to alter Hg records is high in arid regions that provide seemingly excellent outcrop
131 material for less reactive compounds such as clays and carbonates (Keller et al., 2018, 2020; Racki
132 et al., 2018; Sabatino et al., 2018).

133 Whereas unaltered material may be recovered given the right circumstances or through deep
134 drilling, the short-term processes that lead to the original Hg deposition in the marine realm, as
135 well as early diagenesis, potentially influence any geological record of Hg and OM. Therefore,
136 these processes warrant careful consideration in terms of what their effects might be and how they
137 might be recognized. Because Hg, TOC and other Hg-binding ligands are unlikely to be uniformly
138 influenced by early diagenesis, and particularly by oxidation, TOC- or S-normalized records will
139 be especially sensitive to these poorly constrained confounding factors. We here focus on the short-
140 term post-depositional diagenetic alteration of Hg and its carrier phases and how such alteration
141 might have influenced the sedimentary record.

142 *1.2 Behavior of major Hg carriers: sedimentary TOC & S*

143 The preservation of OM in sediments is a function of several factors, most notably plankton
144 productivity, export carbon flux, ventilation of the overlying water and influx rate and type of
145 siliciclastic material (Demaison and Moore, 1980; Pedersen and Calvert, 1990). Overall, less
146 exposure to oxidants is expected to yield higher preservation potential of OM, including relatively
147 labile compounds (Hedges and Keil, 1995; Hedges et al., 1999). At the same time, redox-sensitive
148 elements are scavenged, released or remobilized at various depths in the water column and
149 sediment (Calvert and Pedersen, 1993; Tribovillard et al., 2006).

150 In typical marine sediments since the Mesozoic Era, S has been deposited under non-sulfidic
151 water-column conditions in a fairly constant ratio with organic carbon (C/S) of around ~3–4
152 (Bernier and Raiswell, 1983; Bernier, 1989). However, in sulfidic settings, a larger proportion of
153 sedimentary S might be present as sulfide minerals. Increased S sequestration is relevant as Hg,
154 like many divalent metals (Morse and Luther, 1999), may be sequestered directly as a sulfide
155 mineral (HgS) or as an inclusion in, for example, pyrite (Hg-FeS₂)(Shen et al., 2020; Wang et al.,
156 2020). Moreover, during times of much lower (μ M-levels rather than mM) marine sulfate

157 concentration than in the present-day ocean, the occurrence of widespread sulfidic conditions may
158 have been limited (e.g. Lowenstein et al., 2001; Wortmann and Chernyavsky, 2007; Newton et al.,
159 2011; Xu et al., 2018), and it is conceivable that, in some intervals during the Phanerozoic, the rate
160 of pyrite burial was also temporarily limited (Wortmann and Chernyavsky, 2007; Algeo et al.,
161 2015).

162 Overall, the preservation of both TOC and S is likely to be significantly controlled by the intensity
163 and duration of bottom- and pore-water oxygenation. Under euxinic conditions, sedimentary S
164 might show further enrichment relative to TOC, as S is also sequestered through formation of
165 various metal sulfides. The trends that sedimentary TOC and S follow with changing ambient
166 redox conditions are relatively well established and thereby provide useful simplifications until
167 more detailed data become available. But it should be noted that Hg may not exclusively follow
168 the classic OM- or S-bound path, as has been shown, for example, by Mo (Helz and Vorlicek,
169 2019).

170 *1.3 Behavior of Hg in sediments – (de)oxygenation*

171 Unlike many other divalent metals, Hg is not usually associated with any sulfate mineral (cf. Ba
172 in barite), and it does not serve as an essential micro-nutrient (as do, for example, Fe, Cu, Mo, Ni),
173 which could lead to direct metal-OM associations. Many other predominantly divalent heavy
174 metals that are also associated with OM may bind to sulfide and are traditionally used as redox
175 proxies themselves (e.g., Mo, Cd: Brumsack, 2006; Lyons et al., 2009; Tribovillard et al., 2006).
176 Binding to sulfide minerals implies that these elements can be efficiently trapped in sulfidic (pore)
177 waters. By contrast, it might be expected that sulfate-depleted anoxic conditions (see section 1.2)
178 could lead to lower HgS and pyrite-associated Hg burial, relying on other carrier phases to
179 sequester Hg. Although Hg speciation and element mapping data are very scarce for Pleistocene
180 and older sediment samples (Shen et al., 2019a, 2020; Wang et al., 2020), the limited evidence
181 suggests that Hg-S associations (specifically pyrite) are rarely dominant and perhaps less common
182 than expected. Most deep-time studies that have argued for S-bound Hg inferred this association
183 from stronger statistical correlation of Hg and S compared to other tested parameters (e.g., Sanei
184 et al., 2012; Shen et al., 2020; Zhao et al., 2022b). However, using statistical correlations to derive
185 the (dominant) sedimentary host phase of Hg can be especially challenging as Hg carriers (TOC,
186 S and clays) tend to be coupled or co-varying. For TOC and S, this covariation might primarily
187 result from Hg binding to organic-S compounds such as thiols (Haitzer et al., 2002; Ravichandran,
188 2004), and HgS formation in sulfide-enriched (micro-) environments during OM remineralization
189 (Pham et al., 2014; Manceau et al., 2015).

190 Moreover, some groups of micro-organisms, i.e., Fe- and sulfate-reducing and methanogenic
191 bacteria and archaea, are capable of methylating Hg to avoid its toxic effects (Benoit et al., 1999;
192 Fleming et al., 2006; Gilmour et al., 2013), while some methanotrophic bacteria can demethylate
193 Hg (e.g., Lu et al., 2017). The mono- and di-methylated Hg (hereafter referred to collectively as
194 MeHg) have been extensively studied because these Hg species are particularly toxic to higher

195 organisms and subject to bio-accumulation in food webs (e.g., Morel et al., 1998; Fitzgerald et al.,
196 2007; Merritt and Amirbahman, 2009; Cossa et al., 2022). Although some studies have hinted at
197 MeHg presence in ancient rock archives (Rakociński et al., 2020), it seems unlikely many deep-
198 time samples would retain ancient MeHg given the lability of this Hg species (Rydberg et al.,
199 2008).

200 Compared to the rapidly scavenged dissolved Hg^{2+} , MeHg is considered more mobile in pore and
201 bottom waters, which may result in significant Hg evasion from sediments (Hammerschmidt and
202 Fitzgerald, 2004; Emili et al., 2011). The impact of Hg remobilization through MeHg formation
203 on the geological record is worth exploring as methylation appears to be generally higher under
204 oxygen-depleted conditions (Compeau and Bartha, 1985; Merritt and Amirbahman, 2009; Gu et
205 al., 2011; Wang et al., 2021). MeHg formation also increases with abundant labile algal organic
206 matter in the water column and sediment (Kim et al., 2011; Bravo et al., 2017; Jiang et al., 2018),
207 factors that are often considered intimately coupled with low-oxygen conditions. If Hg-
208 methylation is indeed a (more) common process in anoxic environments, sediments subjected to
209 ferruginous or (mildly) sulfidic conditions may be expected to have comparatively low
210 preservation potential for Hg, in apparent contrast to the more common assumption for deep-time
211 studies that sulfidic waters may lead to Hg spikes (Grasby et al., 2019; Shen et al., 2020). While
212 MeHg is usually not a large proportion of total Hg in modern (surface) sediments (~0.1-1%, e.g.,
213 Hammerschmidt and Fitzgerald, 2004; Fitzgerald et al., 2007), it can be argued that through net
214 loss of MeHg to overlying waters, methylation of Hg can ultimately modulate total sedimentary
215 Hg even if methylation is a slow process (Ogrinc et al., 2007; Emili et al., 2011).

216 It might be argued from these observations on Hg-methylation that the paradoxical scarcity of
217 apparent Hg-sulfide complexes in the geological record could in part be a consequence of Hg
218 methylation by sulfate reducers. HgS formation and pyrite inclusions could potentially be limited
219 to (pore-water) environments where high concentrations of dissolved sulfide inhibit for Hg
220 methylation by sulfate- and Fe-reducers (Compeau and Bartha, 1985; Merritt and Amirbahman,
221 2009). However, given that the vast majority of deep-time sedimentary Hg associations are
222 inferred from statistical correlations, it is conceivable that even if sedimentary Hg was associated
223 with S in sulfidic settings, this would remain obscured by the covariance of S with other host
224 phases. Unfortunately, Hg speciation data, while fairly common for modern soil and sediment
225 samples (e.g., Higuera et al., 2003; Sunderland et al., 2004; Cooke et al., 2009; Rumayor et al.,
226 2017; Lim et al., 2020 and many others), is virtually absent for the deep-time rock record with a
227 few notable exceptions (Shen et al., 2020; Wang et al., 2020). Whether Hg-S associations are truly
228 scarce in the deep-time sediment records or remain systematically underappreciated may only be
229 resolved when further dedicated Hg-speciation data become available for a range of geological
230 samples.

231 Soft-sediment Hg redox studies, focusing on the mobility of Hg in polluted settings, also showed
232 that, around active redox fronts, sedimentary Hg can be associated with Fe (oxyhydr)oxides
233 through adsorption which, in turn, could imply that Hg mobility is affected by Fe and potentially

234 Mn reduction and oxidation (Gobeil and Cossa, 1993; Mikac et al., 1999; Tribovillard et al., 2006).
235 Data from post-depositionally oxidized turbidite sediments show Hg spikes at or around the buried
236 oxidation fronts, which supports a degree of Hg adsorption to, and subsequent release from, Mn
237 or Fe (oxyhydr)oxides (Mercone et al., 1999). Preserved Mn- and Fe-Hg associations in the
238 geological record appear to be rare. (Shen et al., 2020; Zhao et al., 2022b). Similar to Hg-S
239 associations, the complication arises that with the currently available data these associations are
240 generally only inferred via statistical correlation of Hg with Mn or Fe. Unlike Hg-S associations,
241 scarce geological occurrence of Mn/Fe (oxyhydr)oxide-bound Hg (Shen et al., 2020) would align
242 the notion that Hg adsorption to Mn/Fe (oxyhydr)oxides is an intermediate phase, whose
243 preservation may be limited to buried redox fronts.

244 In summary, despite the somewhat uncertain long-term (10s to >1000s of years) and perhaps
245 limited redox cycling of Hg^{2+} , we can expect some smoothing and alterations to the Hg signal
246 relative to the burial flux with changing ambient redox conditions due to, for example, the mobility
247 of MeHg and increased efficiency of Hg sequestration in sulfidic pore waters. Changes in ambient
248 redox conditions have been recognized for many deep-time geological records, such as the
249 Mesozoic Ocean Anoxic Events, several of which are also recognized as periods of LIP activity,
250 both submarine and subaerial. Moreover, the progressive loss of TOC and S with oxidation
251 (section 1.2) implies that normalization to TOC or S could introduce further uncertainty.

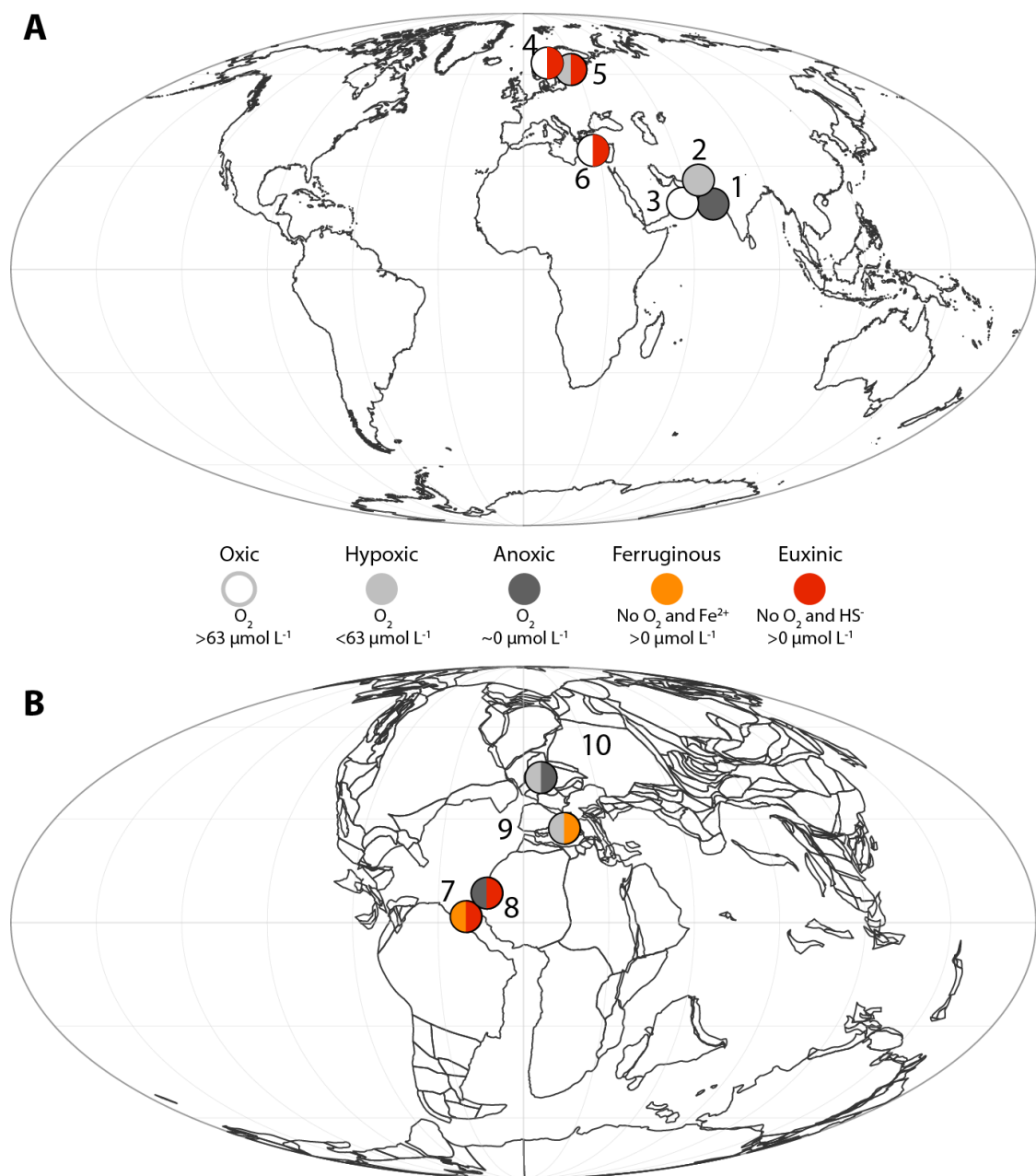
252 *1.4 Aim and approach*

253 Before applying the knowledge of Hg redox behavior in modern systems to the geological record,
254 it is critical to recognize that this is based on recent and often polluted (soft) sediments (e.g.,
255 Fitzgerald et al., 2007; Gagnon et al., 1997). These sediments do not only have temporally and
256 spatially highly variable and uncertain Hg influxes (e.g., Covelli et al., 2001; Leipe et al., 2013;
257 Mason et al., 1994), but, even if not heavily polluted, are also subject to ongoing oxidation and
258 redox-front migration. As these modern environments are continuously being geochemically
259 modified, also on time-scales beyond those that can be observed in controlled environments (10s
260 to >1000s of years), the findings obtained from them cannot be directly applied to signals that are
261 recorded in ancient sedimentary Hg records. Moreover, as discussed above, syn-sedimentary
262 oxidation leads to progressive loss of sedimentary OM and, after oxygen-depletion, increased
263 sedimentary reduced S from sulfide minerals. As TOC and S are considered the most common Hg
264 carriers these processes add a second layer of complexity to TOC- and S-normalized Hg records.
265 Constraining the behavior of Hg and its relationship to the most common carrier phases (TOC, S)
266 under variable redox conditions and understanding how these signals are recorded in sediments is
267 fundamental for the use of (normalized) sedimentary Hg as a direct proxy for Hg-cycle
268 perturbations and volcanic activity.

269 Understanding the role of chemical changes associated with early diagenesis and (an)oxic
270 degradation is particularly important because many of the key intervals in geological deep time for
271 which enhanced volcanic activity is discussed were also marked by high-amplitude variations in

272 primary productivity, (local) oxygenation and TOC contents in accumulating sediment (Schlanger
273 and Jenkyns, 1976; Jenkyns, 2010; Ernst and Youbi, 2017). Some soft-sediment studies show that
274 Hg could have been enriched at, or actively moved away from, (extinct) redox fronts, and microbial
275 Hg methylation could have resulted in active evasion from sediments (Mercione et al., 1999; Mikac
276 et al., 1999; Fitzgerald et al., 2007, Fig. 1). Consequently, we here consider resolving the paired
277 geochemical behavior of Hg itself, and of its potential carrier phases, during early diagenesis. This
278 knowledge is fundamental for the reliable use of Hg and normalized Hg as proxies for enhanced
279 volcanism in geological deep time. Moreover, global, regional and local biogeochemical models
280 that include or focus on the long-term (sedimentary) Hg cycle (e.g., Amos et al., 2013; Amos et
281 al., 2015; Fendley et al., 2019; Dal Corso et al., 2020) benefit greatly from further data-driven
282 constraints on how Hg is sequestered on geological timescales. Ultimately, well-constrained
283 models might facilitate inverse modelling of Hg fluxes and hence volcanic (Hg) emissions.

284 We designed our study to elucidate various influences of changing redox conditions on Hg, TOC
285 and S (and hence the most widely reported host phases of Hg records in the natural environment).
286 To bridge the gap between soft-sediment processes and signals recorded in geological deep time,
287 we generated new Hg and TOC data for a total of 10 depositional settings, 6 (sub)recent-
288 Pleistocene and 4 Late Cretaceous ones (Fig. 2), representing a wide range of (paleo-)redox
289 conditions and depositional environments (Fig. 2, Table 1). We relate these measurements to
290 published major- and trace-element chemistry and associated inferred redox conditions. We seek
291 to eliminate major influences on the Hg flux other than locally produced marine OM, changes in
292 local oxygenation and inherited effects. To do so, we focus on geological intervals without known
293 substantial subaerial LIP activity or nearby submarine LIP activity that may influence Hg records
294 (Percival et al., 2018), and localities without substantial or variable input of terrestrial higher plant
295 material that may have influenced Hg records (Them et al., 2019; Dal Corso et al., 2020). The
296 main objectives of this study are to (1) establish whether variable oxidation leads to alteration in
297 Hg and normalized Hg, (2) subsequently quantify any observed biases resulting from variable
298 oxidation, and (3) resolve the origins of these biases



299

300 **Fig. 2. Maps of site locations. A.** Holocene–upper Pleistocene sites: (1, 2 and 3 Stations 1B, 6B and 10, Arabian Sea,
 301 (4 and 5) LL19, F80, Baltic Sea, (6) 64PE406-E1, Eastern Mediterranean Sea. **B.** Plate reconstruction for 90 Million
 302 years ago (Ma) with Cretaceous sites (7) ODP1261A Coniacian–Santonian Oceanic Anoxic Event (OAE3; ~86 Ma)
 303 3, (8) Cenomanian–Turonian (OAE2; ~94 Ma) Tarfaya Basin core S57, Morocco, (9) Late Cenomanian, Furlo, Italy
 304 and (10) Cenomanian–Turonian (OAE2) South Ferriby, United Kingdom. Colored symbols depict reconstructed
 305 bottom-water oxygenation from oxic (white), hypoxic (light grey – lowered oxygen conditions; $[O_2]_{aq} < 63 \mu\text{mol L}^{-1}$),
 306 anoxic (dark grey – oxygen-depleted conditions $\sim 0 \mu\text{mol L}^{-1}$), ferruginous (orange – no oxygen and Fe^{2+}) to euxinic
 307 (red – no oxygen and free HS^-). Differently colored semi-circles for a single site illustrate the approximate range of
 308 oxidation regimes within the analyzed sequence.

309

310 2. Materials & Methods

311 Materials – site descriptions

312 2.1 Site selection

313 We first study the influence of natural long-term (10s to 1000s of years; Lengger et al., 2014)
314 oxidation in a multi-core depth transect through the Arabian Sea oxygen minimum zone (OMZ)
315 where it intersects the sea floor (Kraal et al., 2012). The three short (0-25 cm depth) cores (Stations
316 1B, 6B and 10; see also Kraal et al. (2012)) represent anoxic, hypoxic and oxic conditions
317 respectively, and with the exception of Station 1B, where OM breakdown results from anaerobic
318 processes, the uppermost sediments are subject to continued aerobic degradation. The observed
319 differences between these sites can be attributed to oxidation in the water column and sediment
320 and make the Arabian Sea OMZ an ideal testing ground for oxidation-induced sedimentary signals,
321 including those in Hg and its carrier phases (see e.g., Kraal et al., 2012; Koho et al., 2013; Lengger
322 et al., 2014 and Supplementary material 1.1).

323 Compared to the Arabian Sea multi-core data, the Baltic and Mediterranean Sea sediments cover
324 transient redox variability, similar to those reconstructed for many deep-time Hg records, and
325 allow us to test how these changes in oxygenation shape the geological record of Hg and Hg
326 carriers. To this end, we analyzed gravity core material from the Baltic Sea, representing a time-
327 series of the past 8 kyr (Supplementary material 1.2) (Jilbert and Slomp, 2013). These two cores,
328 from the Fårö Deep (core F80) and Northern Gotland Basin (LL19), record oxic to euxinic bottom-
329 water conditions and several transitions from oxic to euxinic conditions and *vice versa*, within the
330 same core (e.g., Jilbert and Slomp, 2013; van Helmond et al., 2018). The Baltic Sea cores thus
331 provide insight as to how transitions in oxygenation might influence single sedimentary Hg records
332 and to what extent such signals are preserved in the geological record. In addition, a multi- and
333 piston-core composite site 64PE406E-1 in the Mediterranean Sea (Supplementary material 1.3),
334 containing several sapropels (sapropel S1 and S5 are used here, see e.g., Rohling et al., (2015) for
335 a review of the Mediterranean sapropel records), is studied to further assess the influence of
336 deoxygenation, post-depositional oxidation of organic-rich sediments and paleo-redox fronts
337 (Mercone et al., 1999; Hennekam & van der Bolt et al., 2020; Sweere et al., 2021).

338 Lastly, we analyze four Upper Cretaceous successions to test whether the signals found in the oxic
339 to sulfidic unconsolidated sediment are transferred to the rock record – on which sedimentary Hg
340 studies targeting deep-time volcanic activity are based. For this purpose, we selected one
341 Coniacian–Santonian black shale record from Ocean Drilling Program (ODP) Hole 1261A (März
342 et al., 2008) (Supplementary material 1.4) recording cyclic alternations from ferruginous to sulfidic
343 bottom-water conditions, and three upper Cenomanian to lowest Turonian successions (Furlo,
344 Italy, South Ferriby, UK and Tarfaya core S57, Morocco) marked by high-amplitude variations in
345 oxygenation (e.g., Poulton et al., 2015; Owens et al., 2017; Clarkson et al., 2018 and
346 Supplementary material 1.5-1.7). The Cenomanian–Turonian successions might have been

347 affected by contemporaneous LIP activity, but because the LIPs in question are thought to have
 348 been largely subaqueously emplaced and at substantial distance to the studied sites, the Hg-cycle
 349 perturbation is thought to be geographically confined even during periods of intense volcanism
 350 (Scaife et al., 2017; Percival et al., 2018).

Site	Core/Locality	No. on map	Period	Environmental setting	Oxygenation regime(s)	Sediment accumulation rate	Data from literature (paired data only)	Key references	Data generated for this study	Study aim	Isolated factors	Expected processes
Murray Ridge, Arabian Sea	Station 1B	1	Holocene	Open marine, upwelling zone (~900m water depth)	Anoxic	Moderate (1-10 cm/kyr)			Hg	Resolve Hg & TOC accumulation in permanent strongly oxygen-depleted to oxic conditions, and relation to oxygenation in other sites with similar export flux (St. 1B, 6B and 10). Excludes temporal & spatial variability as a factor in shaping Hg records		Hg sequestration with organic matter and/or sulfur, Hg evasion through methylation(?)
	Station 6B	2	Holocene	Open marine, upwelling zone (~1500m water depth)	Hypoxic	Moderate (1-10 cm/kyr)	TOC, trace elements (part), pore-water chemistry, Fe-speciation	Kraal et al. (2012), Lengger et al. (2014)	Hg		Oxygenation	Hg sequestration with organic matter, subsequent slow break-down of organic matter and impact on Hg/TOC
	Station 10	3	Holocene	Open marine, upwelling zone (~3000m water depth)	Oxic	Moderate (1-10 cm/kyr)			Hg			Hg sequestration with organic matter, subsequent break-down of organic matter and impact on Hg/TOC
Northern Gotland Basin, Baltic Sea	LL19	4	(Anthropocene)-Holocene	Restricted, marginal sea (~170m water depth)	Oxic/hypoxic to euxinic	Very high (>50 cm/kyr)	TOC, trace elements	Jilbert & Slomp (2011), van Helmond et al. (2018)	Hg	Resolve Hg & TOC accumulation during transitions from oxic/dynamic to euxinic conditions and vice versa, includes temporal variability. LL19 and F80 together provide control on potential spatial variability.	Transient variability in oxygenation	Hg sequestration with organic matter and sulfur, Hg focusing with sulfides, Hg evasion through methylation
Fårö Deep, Baltic Sea	F80	5	(Anthropocene)-Holocene	Restricted, marginal sea (~190m water depth)	Oxic/hypoxic to euxinic	Very high (>50 cm/kyr)			Hg			Hg sequestration with organic matter and sulfur, Hg focusing with sulfides, Hg evasion through methylation
Eastern Mediterranean	64PE406E-1	6	Holocene-late Pleistocene	Open marine (~1760m water depth)	Oxic to euxinic	Moderate (1-10 cm/kyr)	TOC (part), trace elements	Rush et al. (2019), Hennekam & van der Bilt et al. (2020), Sweere et al. (2021)	Hg, TOC (part)	Resolve Hg & TOC accumulation during transitions from oxic/dynamic to euxinic conditions, includes temporal variability and post-depositional oxidation including buried redox fronts.	Post-depositional oxidation	Hg sequestration with organic matter and sulfur, Hg focusing with sulfides, Hg evasion through methylation, Hg focusing during post-depositional oxidation or redox front fixation
Demarara Rise, Equatorial Atlantic	ODP1261A	7	Cenozoic-Santonian	Open marine (semi-restricted)	Ferruginous to euxinic	Low-moderate (~1 cm/kyr)	TOC, trace elements	Marz et al. (2008)	Hg, TOC (part)			
Morocco	Tarfaya 557	8	OAE2 interval	Open marine, upwelling zone(?)	Ferruginous to euxinic	Low-moderate (~1 cm/kyr)		Talbot et al. (2004), Poulton et al. (2015)	Hg, TOC			Test if geological deep time sedimentary successions record similar effects as seen in Holocene-Pleistocene records and if those effects can be traced to individual processes
Italy	Furlo	9	Cenomanian (pre-OAE2)	Open marine	Hypoxic to euxinic	Very low-low (<1 cm/kyr)		Jenkins et al. (2007), Owens et al. (2017)	Hg, TOC			
United Kingdom	South Ferraby	10	OAE2 interval	Marginal sea	Oxic to hypoxic/anoxic	Very low (<1 cm/kyr)		Jenkins et al. (2007), Pogge von Strandmann et al. (2013)	Hg, TOC			

351
 352 **Table 1. Overview of studied localities.** For a more detailed description of each record we refer
 353 to section 1 of the supplementary text.

354 2.2 Methods

355 2.2.1 Hg analyses

356 Mercury (Hg) analyses were conducted with a Lumex 915+ device, attached to a pyrolysis unit
 357 (PYRO-915) at the University of Oxford. For each sample, approximately 50–200 mg of
 358 homogenized powdered sediment was pyrolyzed at 700 °C and ~60% of samples were analyzed in
 359 duplicate to assess reproducibility. Calibration of the Lumex 915+ unit was performed using a
 360 paint-contaminated soil standard (NIST2587), which contains 290 ppb (ng/g) Hg. Reproducibility,
 361 estimated through both standard and replicate sample measurements, was generally better than
 362 10%, falling to approximately 5% at higher Hg contents. A few samples with very low Hg contents
 363 (<5 ppb), around and below the detection limit, have analytical uncertainty >10%. With the
 364 exception of the Mediterranean core (64PE406E-1) all Hg was analyzed on sample powders that
 365 have also been analyzed for TOC, S and trace elements. For 64PE406E-1, we utilize a combination
 366 of calibrated Mo concentrations from XRF scanning (Hennekam et al., 2020) and new and existing
 367 dedicated TOC measurements on the same powders that were analyzed for Hg.

368 2.2.2 Determination of organic and inorganic carbon

369 For black shales and samples expected to be relatively rich in organic carbon, total organic carbon
 370 (TOC), hydrocarbon yield of the organic matter and inorganic carbon were assessed with a Rock-

371 Eval 6 device (Lafargue et al., 1998; Behar et al., 2001) at the University of Oxford. For every 10
372 samples, at least one in-house standard of homogenized sediment with pre-determined values was
373 analyzed to assess reproducibility. The reproducibility of parameters of interest (TOC, T_{max} ,
374 Hydrogen Index (HI), Oxygen Index (OI), mineral carbon) was always better than 10% and
375 typically better than 5% of the measured value, based on repeated measurements of the in-house
376 standard. The hydrogen index (HI) and oxygen index (OI) are used as in, e.g., Behar et al., (2001);
377 briefly, the mass of released hydrocarbons (“S2”) and CO₂ (“S3”) during standard pyrolysis in mg
378 is multiplied by 100 and divided by TOC to obtain HI and OI, respectively. Analyses of a
379 decarbonated standard (~48% carbonate) suggest that TOC, S2, S3 and consequently HI and OI
380 were not significantly impacted by low-temperature decomposition of carbonates (Hazra et al.,
381 2022). As all tested samples are dominated by marine organic matter (see Supplementary materials
382 (S1.2-1.7)), we interpret HI and OI primarily as indicator of organic matter degradation. For the
383 samples that were previously analyzed for TOC after an acid-washing procedure (März et al.,
384 2008) and here analyzed with RockEval (ODP1261A), average TOC is slightly higher ($8.2 \pm 1.4\%$)
385 for acid-washed than for bulk RockEval analysis ($7.5 \pm 1.3\%$), confirming there is minimal
386 influence of methodology on the measured TOC content (Nieuwenhuize et al., 1994).

387 Organic-lean carbonates from the Furlo section were analyzed on a Strohlein Coulomat 702 at the
388 University of Oxford. Total carbon of the bulk sediment was determined by analyzing 20–40 mg
389 of untreated homogenized powdered material, while a second 20–40 mg aliquot was heated to 450
390 °C in a combustion furnace overnight to remove organic carbon. The difference between the two
391 measurements indicates the TOC, whereas the heated aliquot represents the total inorganic carbon
392 fraction (TIC). Long-term analytical reproducibility based on an in-house pure carbonate standard
393 was determined to be ~0.1% C.

394 A subset of samples (25) from the 64PE406-E1 multi- and piston core were analyzed for TOC at
395 Royal Netherlands Institute for Sea Research (NIOZ). Samples were dried, homogenized,
396 decarbonated with 2M HCl and subsequently dried and homogenized again, followed by
397 measurement on a Thermo-Interscience Flash EA1112 Series Elemental Analyzer. Based on
398 replicate analyses of standard materials the accuracy is ~0.3% for TOC, with a detection limit of
399 ~0.1%.

400 2.2.3 Determination of Pb and Zn

401 For a small subset of samples from the Arabian Sea, sedimentary lead (Pb) and zinc (Zn) content
402 were determined by analyzing the 1M HCl total digestion extracts of Kraal et al. (2012) on an
403 Inductively Coupled Plasma Mass Spectrometer (Thermo Fisher Scientific XSERIES 2 ICP-MS)
404 at Utrecht University. The accuracy (recovery), based on QCs, was 99% for both Pb and Zn.
405 Average analytical uncertainty based on sample replicates was 1.4% for Pb and 3.6% for Zn.

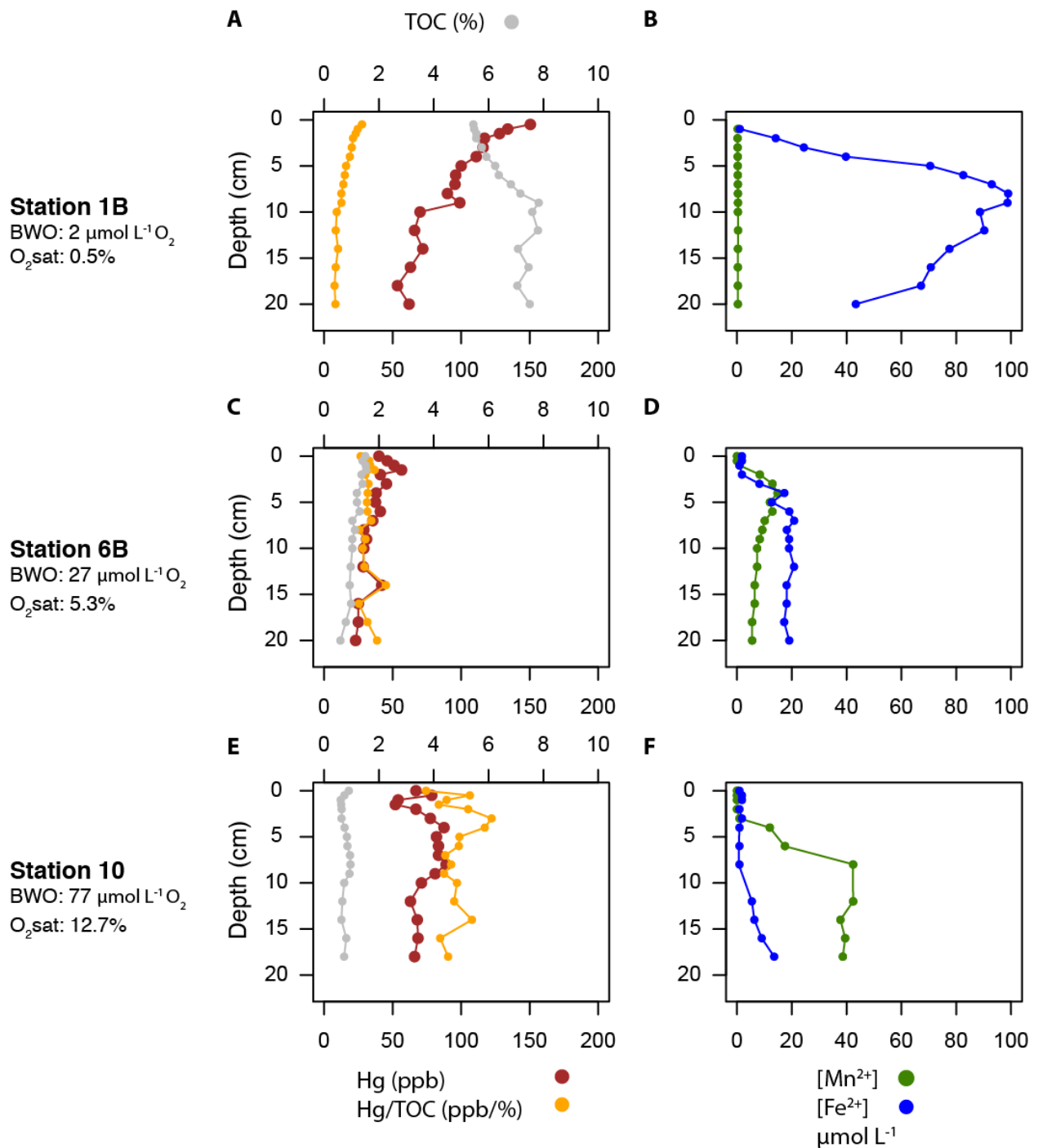
406 3. Results

407 3.1 Natural long-term oxidation – Arabian Sea

408 At the three Arabian Sea stations, Hg contents are highest at the top of Station 1B (the shallowest
409 water station), with a maximum of 150 ppb, and lowest (23 ppb) for the lowermost sample of the
410 Station 6B core (Fig. 3). Station 10 (greatest water depth) shows rather stable Hg contents (50–90
411 ppb). The elevated Hg contents at the top (<10 cm) of the anoxic station (1B) seem to suggest
412 some influence of anthropogenic pollution. There are, however, several reasons why we consider
413 anthropogenic contamination unlikely even at the top of the Station 1B core. For example, the
414 elevated Hg does not appear in similar fashion at the other locations, the average accumulation
415 rates (~5–10 cm kyr⁻¹) would imply significant Hg perturbation prior to the industrial revolution
416 (Koho et al., 2013) and there is a complete absence of anomalous values in other commonly Hg
417 pollution-associated heavy metals such as Pb, Zn (Supplementary data). Lastly, there is no clear
418 evidence for a trend break in Hg or Hg/TOC similar to the youngest part of the Baltic Sea cores
419 (Fig. 3A, C); in the Arabian Sea Station 1B and 6B Hg content gradually decreases with depth. Hg
420 overall correlates positively with TOC when all data from the three stations are combined ($R^2 \sim 0.3$;
421 Supplementary Fig. 1A), and the strength of the correlation increases when the two deeper water
422 stations are considered individually ($R^2 \sim 0.7$ for the intermediate site (6B) and $R^2 \sim 0.45$ for the
423 deep-water site (10)). Remarkably, a negative correlation ($R^2 \sim 0.7$) with TOC is found at the
424 shallowest water Station 1B.

425 Mercury and Hg/TOC for the shallowest water station (1B) show a strong decreasing trend with
426 depth, as Hg decreases from 150 to 60 ppb while TOC increases from ~5.5% to 7.5% (Fig. 3A).
427 Mercury at the intermediate station (6B) shows a similar, albeit much shallower, trend (Fig. 3C)
428 but clear depth-dependent trends in Hg/TOC are not recorded here or at Station 10 (Fig. 3C, E).
429 At Station 1B, the absence of dissolved Mn (assumed to be Mn²⁺) and presence of dissolved Fe
430 (assumed to be Fe²⁺) shows that reduction of Fe-oxides is presumably the primary pathway for the
431 (microbial) degradation of organic matter throughout the studied interval (Fig. 3B) (Kraal et al.,
432 2012). Kraal et al. (2012) also determined that Mn-oxide reduction is more prevalent at Station 6B
433 and becomes the dominant anaerobic pathway for (microbial) degradation of organic matter at
434 Station 10 (Fig. 3D, F).

435 Across the site transect, average Hg/TOC increases markedly with oxygenation; we find Hg/TOC
436 of 15 ± 6 ppb/% (mean, standard deviation) at the shallowest (anoxic) site (Station 1B) (Fig. 3A),
437 rising to 32 ± 5 at the intermediate (6B) (Fig. 3C) and 96 ± 12 at the deepest, most oxic site (10)
438 (Fig. 3E). Arguably, the lowermost (i.e., greatest core depth) recovered sediments, where trends
439 with depth are minimal in Hg and TOC, are most representative of the burial signal. Focusing on
440 the lowermost 10 cm of each core, we find a further decrease in Hg/TOC in the anoxic site to 8.7
441 ± 0.9 , whereas Hg/TOC at the other sites remains virtually unchanged from top to bottom of the
442 analyzed interval.



443

444 **Figure 3. Hg, TOC and sediment and pore-water chemistry for the Holocene (~0-4 ka) Arabian Sea stations. A,**
 445 **C, E.** Hg, TOC and Hg/TOC for Station 1B, 6B and 10 respectively. **B, D, F.** Mn²⁺ and Fe²⁺ concentrations in pore-
 446 waters. Bottom-water oxygen concentration (BWO) and saturation (O_2sat) for each station (Koho et al., 2013). TOC
 447 and pore-water data were published in Kraal et al. (2012).

448 **3.2 Influence of transient changes in oxygenation: Baltic Sea soft sediments**

449 The Holocene sediment cores F80 and LL19 from the Baltic Sea (See Table 1, see Supplementary
450 text 1.2 for details on age-depth models and previous studies using F80, LL19) show identical
451 trends in TOC-normalized Hg and Hg content throughout. In the pre-industrial (<1750 calendar
452 years common era (CE)); based on the detailed age model of Jilbert and Slomp, 2013), sedimentary
453 Hg content did not exceed 40 ppb, whereas it reached a maximum well above 200 ppb around
454 ~1980 CE. Core F80 seems to record a subtle increase in Hg and Hg/TOC from about 1100-1200
455 CE, suggesting that, for example, small-scale early industrial activity or deforestation around the
456 Baltic Sea may have influenced Hg influx at our sites, as is also supported by the Pb record in the
457 study by van Helmond et al. (2020). The pre-industrial Holocene Hg and TOC contents in our
458 cores are very similar to those obtained during earlier work in the Baltic Sea that focused mainly
459 on the recent centuries and effects of modern anthropogenic Hg pollution (Leipe et al., 2013).

460 Before the main period of anthropogenic Hg emissions (<1750 CE), Hg loading in the oxic–anoxic
461 sediments, based on correlation with TOC, appears to be almost completely controlled by their
462 TOC contents (Supplementary Fig. 2A, C). In some anoxic–sulfidic intervals, TOC spikes above
463 10%, whereas the more oxic intervals generally have 1–2% TOC (Jilbert and Slomp, 2013).
464 Hg/TOC averages ~3.8–5.5 ppb/% in the anoxic to sulfidic intervals and averages 6.4 (F80) to 8.6
465 (LL19) in the more oxic intervals (Fig. 4, 6B, C). The non-sulfidic intervals at F80 show elevated
466 Mo and lower Hg/TOC compared to the same intervals in LL19 (Fig. 4). This pattern may signal
467 continued oxygen deficiency at F80 even during the most oxic phases, which is supported by
468 sedimentary Re content data (van Helmond et al., 2018). Prior to the emergence of overwhelming
469 Hg pollution (1750 CE), negative correlations between both Hg and Hg/TOC and redox-sensitive
470 elements (Mo, U, Cd etc.) are ubiquitous. This illustrates such redox-sensitive elements are usually
471 also enriched or proportional with the TOC increase, whereas the rise in Hg is smaller than that in
472 TOC (Fig. 4). This relationship implies that the correlation of other TOC-bound elements with Hg
473 is generally positive and that the correlation of these elements with Hg/TOC is negative, as also
474 indicated by the decreasing Hg/TOC with TOC. The negative correlation between sulfide-bound
475 elements (Mo) and Hg/TOC weakens with increasing Mo, which suggests a non-linear connection
476 between anoxic and especially sulfide-enriched (pore) waters and decrease in Hg/TOC (Fig. 4E,
477 F).

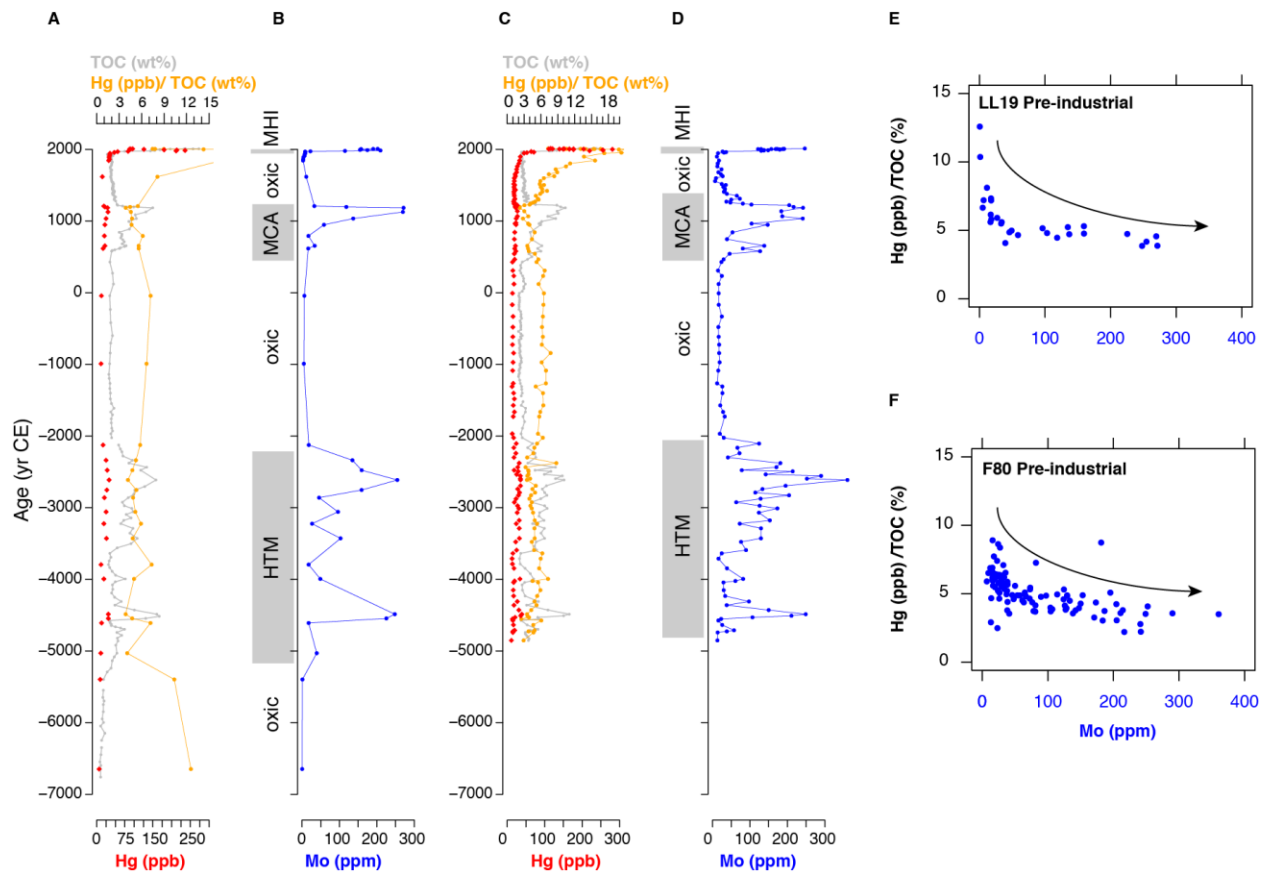
478 **3.3 Influence of post-depositional oxidation: Mediterranean Sea soft sediments**

479 The sapropels S1 and S5 in sediments from the Eastern Mediterranean Sea show increased Hg
480 contents (Fig. 5). However, (slightly) subdued or stable Hg/TOC values appear in the anoxic
481 intervals (high Mo, high Ba; for details on oxygenation during sapropel deposition see, e.g.,
482 Hennekam et al., 2020; Clarkson et al., 2021; Sweere et al., 2021), similar to the Arabian and
483 Baltic Sea records. Background Hg contents in the oxygenated (low Mo, low Ba) sediments are
484 ~10 ppb, increasing to relatively stable values around ~50 ppb (S1) and ~100 ppb (S5) within the
485 sapropel layers. The profiles also show second-order variability both below and above the sapropel
486 layers. For example, the top of both S1 and S5 is marked by a clear spike in Hg contents (up to
487 ~100 ppb in S1 and 250 ppb in S5), approximately double the Hg contents observed in the lower

488 part of the sapropels. These spikes are not paralleled by a further increase in TOC, which remains
 489 stable around the average of the sapropel interval (values around ~2% in S1 and ~5-6% in S5),
 490 above background values of ~0.5-1%. In general, the preserved Hg/TOC ratios are more variable
 491 (Fig. 5C, 6D) during deposition of background sediments than during sapropel deposition.
 492 Whether Hg/TOC during background deposition are higher compared to sapropel deposition, as
 493 suggested by the trends across the onset of sapropel S5, cannot be confidently determined with the
 494 available data.

495 Intriguingly, Hg/TOC for S1 is higher (~25 ppb/%) than for S5 (~17 ppb / %), which may be linked
 496 to more intense deoxygenation during S5 (Sweere et al., 2021). In the oxidized part of S1, where
 497 high Ba is considered to follow the original extent and intensity of the sapropel (e.g. van Santvoort
 498 et al., 2002) (*ca.* 28 – 23.5 cm depth, 8.3 – 6.5 ka), Hg spikes and Hg/TOC remain at a relatively
 499 elevated level. This pattern contrasts with TOC, of which a substantial part has been removed
 500 during post-depositional oxidation: the oxidized part of S1 records 0.8% TOC, whereas the
 501 unoxidized part records 2%. A similar effect appears to occur at the upper 3–4 cm of S5 (*ca.* 122
 502 ka).

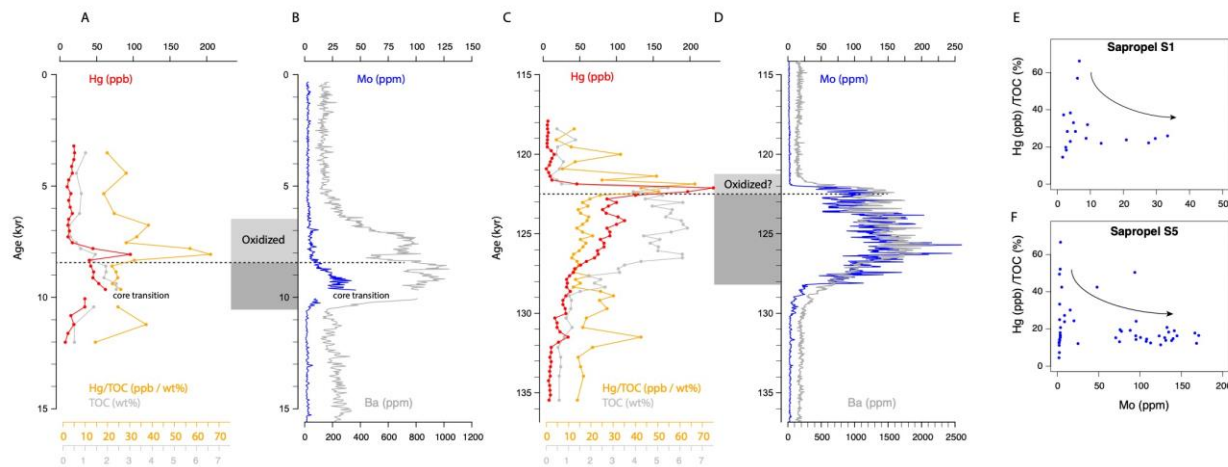
503



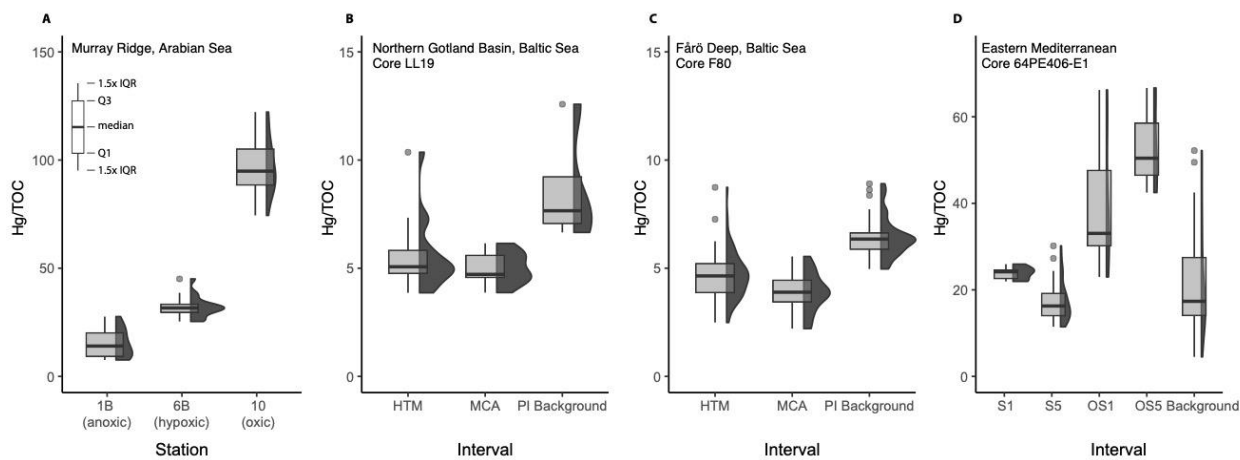
504

505 **Figure 4. Hg, TOC, and trace-element records for Baltic Sea cores LL19 and F80 for the Holocene (~0-8 ka).**
 506 **A.** Hg, TOC and Hg/TOC for core LL19, North Gotland Basin. **B.** Molybdenum (Mo) contents for LL19 (data from

507 van Helmond et al. 2018). **C.** Hg, TOC and Hg/TOC for core F80, Fårö Deep. **D.** Mo contents for F80 (data from van
 508 Helmond et al. 2018). Abbreviations – MHI: Modern hypoxic interval, MCA: Medieval Climate Anomaly, HTM:
 509 Holocene Thermal Maximum, CE: Common Era. **E.** Pre-industrial (<1750CE) Hg/TOC vs Mo for core LL19, **F.** Same
 510 as panel E, for core F80.



511
 512 **Figure 5. Hg, TOC and trace-element records for 64PE406-E1 through intervals encompassing Sapropel S1**
 513 **(deposited ca. 10.5-6.1 ka) and S5 (deposited ca. 128.3-121.5 ka). A.** Hg, TOC and Hg/TOC for sapropel S1. **B.**
 514 Molybdenum (Mo) and barium (Ba) contents in ppm from calibrated high-resolution XRF scanning (data published
 515 in Hennekam & van der Bolt, et al. 2020). **C.** Hg, TOC and Hg/TOC for sapropel S5. **D.** Mo and Ba in ppm
 516 from calibrated high-resolution XRF scanning (data published in Hennekam & van der Bolt et al., 2020). Dark shaded boxes
 517 show the extent of the existing sapropel and light shading shows the extent of post-depositional oxidation. **E.** Hg/TOC
 518 vs Mo for the sapropel S1 interval. **F.** Same as panel E, but for sapropel S5.



519
 520 **Figure 6. Summary of observed Recent to upper Pleistocene Hg/TOC in the Baltic, Arabian and Mediterranean**
 521 **Sea cores. A.** Hg/TOC for the Arabian Sea stations, going from anoxic (1B) to oxic (10). **B.** Hg/TOC for the Holocene
 522 Thermal Maximum (HTM) and Medieval Climate Anomaly (MCA) euxinic and pre-industrial (PI) oxic background
 523 intervals for core LL19. **C.** As panel B but for core F80. **D.** Hg/TOC for Site 64PE406-E1, Eastern Mediterranean,
 524 split by oxidation regimes: sapropels “S1”, “S5”, their oxidized tops, “OS1” and “OS5”, and background.

525 **3.3 Influence of transient oxygen variability: the deep-time sedimentary record**

526 **3.3.1 Coniacian–Santonian, Ocean Drilling Program (ODP) Site 1261A**

527 The Coniacian–Santonian sediments at Demarara Rise ODP Leg 207 Site 1261 Hole A (Shipboard
528 Scientific Party, 2004) (Fig. 7) show generally high to very high TOC (4-12%) and moderate Hg
529 content (20–140 ppb), compared to geological averages (~60 ppb for shales, ~30 ppb for
530 limestones, Grasby et al., 2019). We find no obvious correlation between Hg and TOC or Hg and
531 S (Supplementary Fig. 3), and see a pronounced cyclicity in Hg, Hg/TOC and Hg/S. Hg/TOC
532 ratios vary between ~5 ppb/% in some parts of the sulfidic intervals (as determined by März et al.
533 2008, outside the shaded bands in Fig. 7), and locally spike up to 15 ppb/% in the anoxic non-
534 sulfidic intervals and directly above (shaded bands in Fig. 7). Both the carbonate content and the
535 carbonate-free TOC are lowest in the non-sulfidic sediments. Although Hg and TOC only weakly
536 correlate, the HI and OI are negatively and positively correlated to Hg and that leads to a
537 correlation of HI and OI with Hg/TOC (Fig. 7,8D), suggesting organic-matter characteristics play
538 an important role in shaping Hg and Hg/TOC. The negative correlation of Hg and Hg/TOC,
539 marking Hg depletion relative to both (carbonate-free) Mo and TOC, are also observed here,
540 similar to the Baltic Sea sites (Fig. 4E, 4F, 7E). The carbonate-corrected aluminum (Al) content is
541 remarkably constant, suggesting stable Al accumulation rates throughout the analyzed interval.
542 We find that Hg/Al follows the same pattern as Hg; a crucial observation that shows Hg burial was
543 not constant and not driven primarily by a Hg associated with an increased influx of siliciclastic
544 material. As the high Hg contents coincide with sediments containing evidence for ferruginous
545 conditions, we surmise that a greater proportion of Hg may have been lost to overlying waters
546 under euxinic conditions compared to ferruginous conditions.

547 **3.3.2. Cenomanian, pre-OAE 2 level, Furlo, Italy**

548 We here focus on organic-matter characteristics because paired trace-element records are not
549 available for the selected samples, the bulk of the succession being represented by organic-lean
550 white pelagic carbonates of the Scaglia Bianca (carbonate content 90-95%) and the remainder
551 being represented by thin (centimeter-scale) black and green shales and black cherts, with variable
552 but generally much lower carbonate content (0-80%). Overall, these sediments also show large
553 differences in TOC and Hg content, and notably Hg/TOC (Fig. S5). The latter could be partly a
554 consequence of TOC and Hg being often difficult to reliably measure in the carbonates (see also
555 Supplementary text S2). In the more organic-rich facies, where such analytical issues do not play
556 a role, Hg/TOC ranges from 17 to >400, compared to 30 to 350 obtained by Percival et al. (2018).
557 The overall correlation between Hg and TOC in the shales and cherts is strong ($R^2 \sim 0.7$, Fig. S5D)
558 while after normalizing Hg to TOC, only a weak correlation with HI remains, indicating that the
559 type and/or preservation state of organic matter here has no dominant influence on Hg/TOC (Fig.
560 8A).

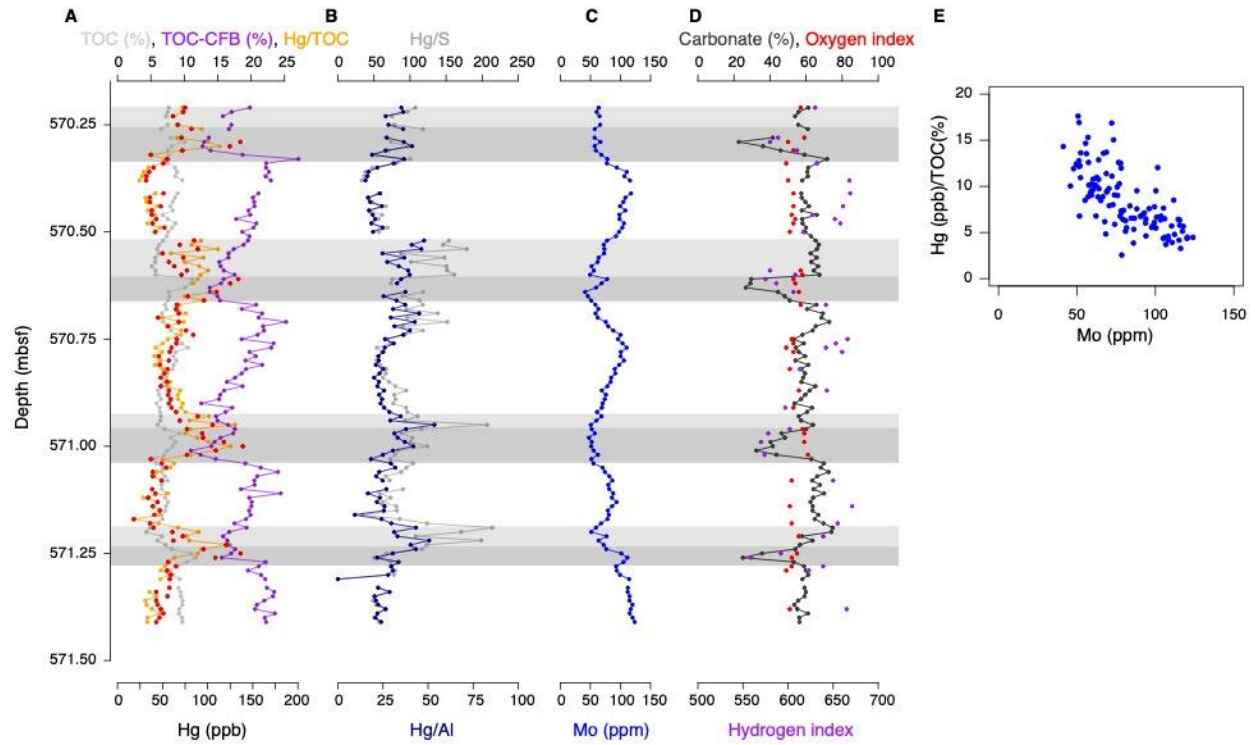
561 **3.3.3 Cenomanian–Turonian (OAE 2), S57 core, Tarfaya, Morocco**

562 The TOC content of the S57 core samples from Tarfaya, Morocco, is consistently high (average
563 7%) and never drops below ~1% in the studied core interval (50–60 m core depth) (e.g., Tsikos et
564 al., 2004; Percival et al., 2018). The TOC and Hg data used here are from Percival et al. (2018)
565 and oxygenation for the sample levels is estimated based on Fe speciation and lipid biomarkers
566 (Poulton et al., 2015). We here record high HI values, above 500 and average ~660, indicative of
567 immature marine organic matter. Hg and TOC are well correlated across the entire analyzed
568 interval (Percival et al., 2018). Hg/TOC values are generally low, averaging ~23 (min 9.5, max
569 88) and correlate moderately well ($R^2 \sim 0.4$) with the OI but only weakly with HI ($R^2 \sim 0.1$),
570 suggesting that either preservation or a (small) refractory organic-matter pool plays a role in
571 shaping Hg/TOC relationships. Across the ferruginous–euxinic cyclic variations, only small
572 changes in Hg/TOC are observed, and correlation between Hg/TOC and OI in this interval is
573 somewhat weaker than across the entire interval previously analyzed for Hg and TOC (Percival et
574 al., 2018).

575 **3.3.4 Cenomanian–Turonian (OAE 2), South Ferriby Black Band, UK**

576 Hg contents across the South Ferriby Black Band range from 40 ppb in the pelagic white chalk to
577 350 ppb in the black-shale interval that is the hallmark of OAE 2. A correlation ($R^2 \sim 0.55$, Fig.
578 S4B) with TOC is found, and correlations of Hg/TOC with HI and OI are significantly negative
579 and positive, respectively (Fig. 8C). TOC in the pre-event carbonate-rich sediments is ~0.2%,
580 reaching a maximum of 6–7% in the Black Band itself (Jenkyns et al., 2007). Hg/TOC ratios
581 decrease from values above 200 ppb/wt % in the organic-lean carbonates below the Black Band to
582 an average of ~45 ppb/wt % in the black shale. Minimum Hg/TOC coincides with the highest TOC
583 contents and HI/OI indicates that the best-preserved (marine) organic matter shows lowest
584 Hg/TOC (Fig. 8C).

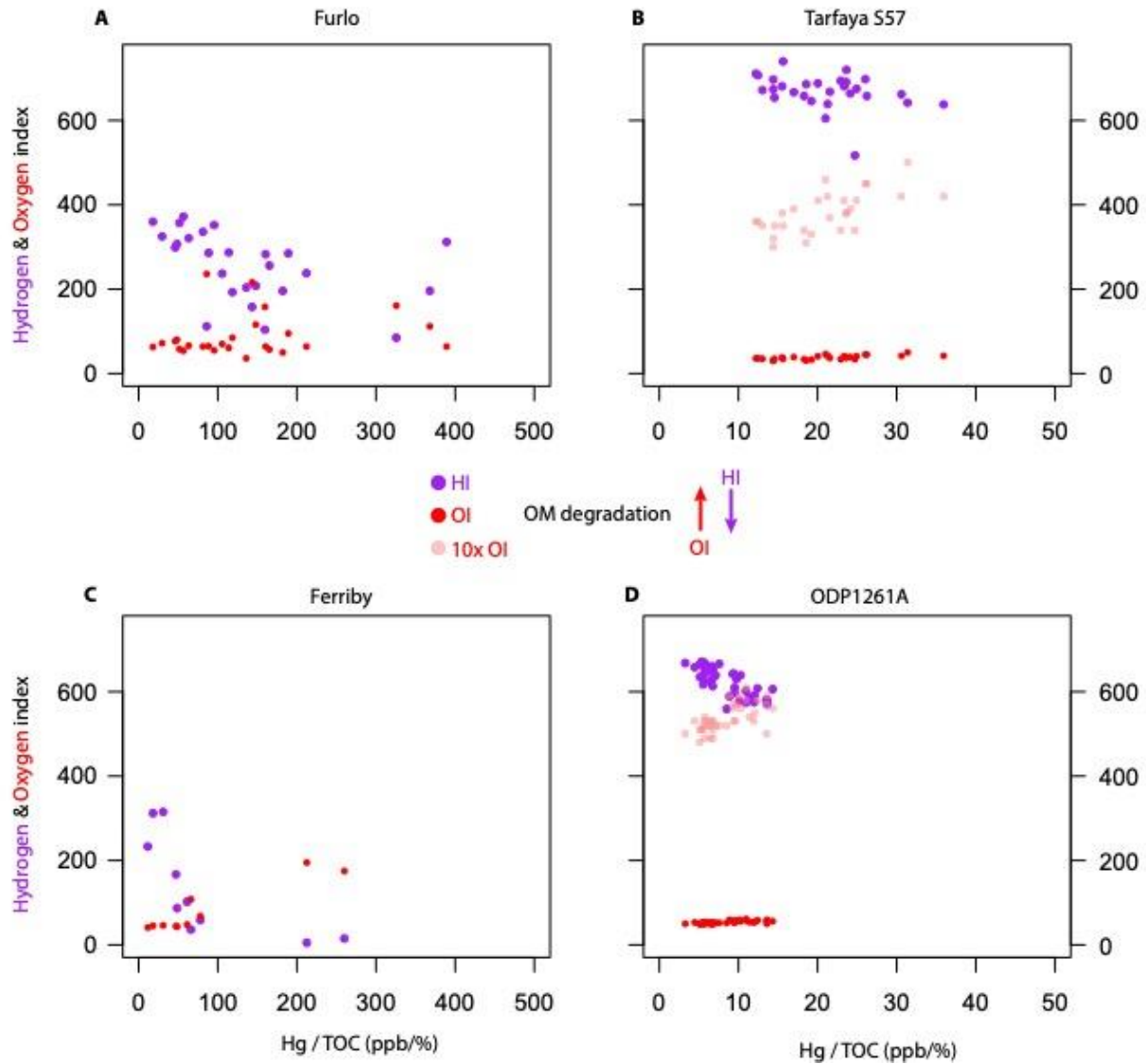
585



586

587 **Figure 7. Coniacian–Santonian anoxic–euxinic cyclic succession analyzed from ODP Site 1261A. A.** Hg, TOC,
 588 Hg/TOC and carbonate-free (CFB) TOC. **B.** Al and S-normalized Hg. **C.** Molybdenum (Mo) contents in ppm. **D.**
 589 Carbonate (%), HI and OI from Rock-Eval. Shaded bands indicate intervals where Hg/TOC is elevated, dark shading
 590 indicates where März et al., (2008) inferred anoxic non-sulfidic conditions. **E.** Hg/TOC vs Mo contents.

591



592

593 **Figure 8. Hg/TOC plotted against hydrogen and oxygen indices, illustrating the influence of organic-matter**
 594 **preservation state. A. Furlo: HI and OI vs Hg/TOC, B. Same for Tarfaya S57, C. South Ferriby and D. ODP Site**
 595 **1261A. Note the factor of 10 Hg/TOC scale difference between panels A, C and B, D and that for panels B and D, OI**
 596 **is also given inflated by a factor 10 to illustrate variability.**

597

598 4. Discussion

599 4.1 Hg and Hg/TOC trends with (de)oxygenation

600 The Holocene Arabian Sea sediments provide insight into the effects of exposure to a range of
601 oxygen concentrations and progressive OM breakdown on time-scales that cannot be (easily)
602 observed in controlled environments (10s–1000s of years). We find only relatively minor
603 differences in absolute Hg contents between the OMZ and more oxygenated sites (Fig. 3),
604 especially below ~10 cm core depth. Intriguingly, the anoxic site (Station 1B, Fig. 3) has higher
605 Hg contents at the top of the core but Hg contents stabilize at a much lower level in the lower part
606 of the core. While this Hg trend appears to be similar to the widely documented anthropogenic
607 contamination, the combination of the sediment age and chemical signatures of this and nearby
608 sediment cores imply it is difficult to explain the signal with anthropogenic Hg loading (see section
609 §3.1). Rather, we here consider the scenario that down-core Hg decrease at Station 1B hints at
610 disproportionate Hg loss during sediment accumulation, decoupled from TOC.

611 For the anoxic Station 1B (Fig. 3A) we can assume that Hg and TOC arrived at the sea floor in a
612 condition that is closely representative of the export particle flux from the anoxic waters below the
613 photic zone, with only minor alteration due to very short (~1 year) residence time in oxidizing
614 conditions (Lengger et al., 2014). This supposition is supported by TOC contents at the anoxic site
615 (6.5–7.5 wt%) that do not appear to differ much from the organic-carbon fraction in the export
616 particle flux (~8 wt%) (Honjo et al., 1999). Even if only a small fraction of OM appears to be
617 broken down, this fraction seems to contain a large proportion of the total Hg, perhaps implying a
618 significant portion of Hg is only weakly bound at time of deposition and can be released without
619 noticeable TOC loss.

620 The available primary and export productivity estimates across the region suggest all these stations
621 started from a similar particle flux composition (Haake et al., 1993; Honjo et al., 1999; NASA
622 Ocean Biology (OB.DAAC), 2014), and without oxidation should record similar TOC to what is
623 observed in the particle flux and Station 1B (6.5–8%). Assuming these equal starting conditions,
624 we calculate a significant fraction (80–90%) of organic carbon has been lost at Stations 6B and 10,
625 which now average only 1.2 and 0.6 wt% TOC, respectively (Fig. 3C, E). The loss of organic
626 carbon is, however, not clearly reflected in further decreasing Hg contents. The absolute Hg
627 content at the intermediate water depth Station 6B (Fig. 3C) is approximately half that of the
628 stratigraphically lowermost sediments at the anoxic Station 1B (Fig. 3A), while the deep-water,
629 well-ventilated Station 10 (Fig. 3E) shows contents similar to those found at the anoxic Station 1B
630 (Fig. 3). The stabilizing profiles of Hg and TOC suggest that the lower intervals (10–20 cm depth)
631 of all three Arabian Sea cores represent signals that are potentially stored in the geological record.

632 Complementing the Arabian Sea sites, the Baltic Sea and Mediterranean sites allow us to test
633 whether the observed trends hold for single localities experiencing different oxygenation regimes,
634 which is situationally more similar to the geological record. These sites may also help reveal the

635 potential influence of euxinic conditions and sulfate reduction in bottom and pore waters, which
636 are generally considered to be negligible in the Arabian Sea (Kraal et al., 2012). In addition, the
637 Mediterranean sapropel S1 records strong post-depositional OM oxidation ('burn-down') and
638 influence of halted redox fronts, whereas the extremely high sediments and organic matter
639 accumulation rates in the Baltic Sea sites largely prevent oxygen penetration into the sediments,
640 stifling aerobic organic-matter breakdown even during relatively well-ventilated bottom water
641 conditions.

642 Overall, the various Holocene and upper Pleistocene cores provide datasets comparable to those
643 typically generated on core and outcrop material that records ancient (de)oxygenation events (e.g.,
644 Turgeon and Brumsack, 2006; Jenkyns, 2010). Here we generally find low to moderate (10–100
645 ppb) Hg contents, which are strongly correlated with TOC, suggesting that sedimentary Hg is
646 predominantly TOC-bound. However, some caution is warranted because sedimentary sulfur is
647 also strongly correlated with Hg and TOC and the presence of a considerable S-associated Hg
648 fraction might only be revealed through Hg-speciation analyses.

649 When looking in more detail, we find that, despite the strong Hg-TOC and Hg-S correlations, the
650 Hg increase in the anoxic and sulfidic intervals in the Baltic and Mediterranean Sea cores does not
651 entirely match the TOC or S increases, resulting in lowered Hg/TOC at high TOC contents (Fig.
652 4, 5) and a similar effect can be seen in Hg/S (Supplementary Data). Published data from
653 Holocene–upper Pleistocene oxic–anoxic marine localities, the Japan Sea and Peruvian Margin
654 (Shen et al., 2020), show similarly lowered Hg/TOC in sediments deposited under anoxic and
655 euxinic conditions. However, on the strongly sulfidic end of the spectrum, the Baltic Sea core
656 material shows the Hg/TOC-Mo correlation becomes rather insensitive at high Mo contents (Fig.
657 4E,F), which suggests a breakdown of the relationship during the most sulfidic episodes. This
658 feature of the geochemistry is consistent with the observation that, for strongly pyritized sediments
659 (Shen et al., 2020), the relationship of Hg/TOC with low-oxygen and especially sulfidic conditions
660 may be reversed, and may be marked by higher Hg sequestration, either as HgS or Hg inclusion in
661 pyrite (Fig. 4,5), or a shift from TOC-bound to S-bound Hg deposition.

662 Furthermore, the Mediterranean sapropel record we generated confirms the occurrence of Hg
663 focusing near paleo-redox fronts and shows, in specific cases, Hg/TOC, but notably also the Hg
664 content itself to be elevated as a result of oxidation and/or immobilization at the oxic-anoxic
665 boundary. This observation aligns with the findings of Mercone et al. (1999), who documented
666 large Hg spikes associated with paleo-redox fronts in oxidized sapropels and turbidites, which
667 were hypothesized to be associated with Fe-Mn (oxyhydr)oxide scavenging. The occurrence of an
668 ash-layer at the top of sapropel S5 in some parts of the Eastern Mediterranean (a crypto tephra in
669 core 64PE406-E1) may be argued to have added extraneous Hg in the analyzed interval. However,
670 we consider a dominant volcanic source for this Hg spike unlikely or highly fortuitous: it remains
671 extremely challenging to connect individual eruptions, and non-LIP activity in general, to Hg
672 emissions (e.g. Schuster et al., 2002; Guédron et al., 2019; Edwards et al., 2021). Perhaps more
673 importantly, the placing of the S5 Hg spike coincides exactly with the position where burn-down

674 stopped (paleo-redox front) in sapropel S1 (Fig. 5), akin to previously studied turbidites and S1 in
675 other Mediterranean cores (Mercone et al. 1999) where tephras are not recorded. Collectively,
676 these data support the findings of Mercone et al. (1999) who hypothesized Hg released during
677 oxidation of OM and pyrite may be focused around halted redox fronts.

678 The low overall Hg/TOC values observed in the Holocene anoxic Baltic Sea (Fig. 4), Holocene–
679 upper Pleistocene sapropels (Fig. 5), Peruvian Margin sediments (Shen et al., 2020), and the anoxic
680 Arabian Sea site are noteworthy, especially considering various inter-site differences. The
681 Holocene data presented here from the Baltic and Arabian Sea, with Holocene-upper Pleistocene
682 sapropel data, in concert with published data from similar environments (Shen et al., 2020), show
683 that shorter oxygen exposure can result in suppressed Hg/TOC, through preferentially enhanced
684 preservation of organic matter and loss of Hg. Critically, we also find, based on our data from
685 Mediterranean sapropels and published data (e.g. Mercone et al., 1999; Shen et al., 2020), that
686 these relationships may reverse in (1) the most oxygen-depleted, strongly sulfidic conditions and
687 (2) in cases where post-depositional oxidation affects sediments deposited in anoxic–sulfidic
688 conditions, complicating the interpretation of deep-time Hg and Hg/TOC records, especially those
689 for which no accurate, paired, oxygenation reconstructions exist.

690 The material from ODP Site 1261A recovered from Demerara Rise records clear cyclic variability
691 in sedimentary geochemistry, including Hg, during the Coniacian–Santonian Ocean Anoxic Event
692 3. This variability confirms that the effects documented for soft sediments are also preserved in
693 the geological record. With deposition alternating from euxinic to ferruginous (März et al., 2008),
694 this sedimentary material was deposited under redox conditions somewhat similar to the Holocene
695 Baltic Sea sites. Although the organic-matter content is very high throughout (5–15%; Fig. 7), the
696 correlation between Hg and TOC is surprisingly weak, as is the correlation of Hg with S (both R^2
697 ~ 0.05). Both Hg and TOC show cyclicity, but these cycles are not aligned or in anti-phase.

698 When normalizing Hg to TOC, however, clearer trends with other geochemical proxies start to
699 appear. Hg/S shows virtually identical trends to Hg/TOC (Fig. 7A, B) and the absence of a strong
700 correlation with sedimentary S implies that it is unlikely that a large proportion of Hg is metal
701 sulfide-bound or present as HgS inclusions. However, the negative correlation of Hg/TOC with
702 HI might imply a mechanism whereby the OM preservation state, in this case the extent of
703 oxidative degradation, controls the Hg/TOC. Counter-intuitively, the most carbonate-lean (“black”
704 shale) intervals have the lowest HI and highest OI in this section, which may be explained by
705 reduced accumulation rates. Together with the stable carbonate-free Al fraction, the low HI and
706 high OI suggest lowered accumulation rates and, as a consequence, slow, protracted, breakdown
707 of sedimentary OM during the deposition of the carbonate-poor intervals. The behavior of Hg
708 relative to conservative detrital elements such as Al across the oxygenation cycles mimics that of
709 Hg/TOC and Hg/S. This parallelism seems to provide further support for the notion that the highest
710 Hg preservation efficiency and perhaps accumulation rates occurred during the ferruginous phases.
711 Combined with the evidence for alteration of Hg and TOC signals in our Holocene core material,
712 it seems likely that Hg and Hg/TOC signals were mostly fixed during early sedimentary diagenesis

713 with a substantial influence of water-column and pore-water oxygenation, particularly through OM
714 degradation in oxic settings and Hg loss in anoxic settings. The observation that TOC is lost
715 relative to Hg aligns with observations on modern organic-rich substrates such as peats and varved
716 lake sediments (e.g., Biester et al., 2003; Rydberg et al., 2008).

717 The effects of ambient redox conditions, as illustrated by OM matter preservation, also appear to
718 be a common feature in all Cretaceous sites we studied. For example, when focusing on the Hg
719 and TOC of the shale and chert levels at Furlo (Fig. S5), we find a positive correlation between
720 Hg and TOC, but a weak negative correlation between Hg/TOC and HI (Fig. 8A). A negative
721 correlation between Hg/TOC and HI and positive correlation between Hg/TOC and OI is seen at
722 Tarfaya S57 (Fig. 8B), South Ferriby and ODP Hole 1261A (Fig. 8C,D). It is noteworthy that HI
723 at both Furlo and South Ferriby is generally low compared to Tarfaya S57 and ODP Site 1261A
724 (Fig. 8), and OI is generally higher, although both parameters show substantial variability,
725 signaling a larger contribution of refractory organic matter and generally more degraded TOC. In
726 this light, the higher average and more variable Hg/TOC observed at Furlo and South Ferriby is in
727 line with previous observations, indicating a primary control of OM preservation and type on
728 Hg/TOC, at least within single stratigraphic records, but potentially also controlling differences
729 between time-equivalent successions.

730 **4.2 Origin and magnitude of biases in Hg, and Hg/TOC**

731 Our new data reaffirms the observations on modern sediment observational data that Hg loss may
732 occur during anoxic and (weakly) sulfidic conditions (see section 4.1) and, most importantly, that
733 a signal of this process might be preserved in deep-time records (e.g. Fig. 7). Such a process is an
734 important consideration for Hg studies that attempted to constrain volcanic activity during periods
735 of extensive anoxia such as the Mesozoic OAEs (e.g., Percival et al., 2015; Scaife et al., 2017;
736 Percival et al., 2021b), or similar Paleozoic events (e.g., Piszczowska et al., 2020; Rakociński et
737 al., 2022), but also more regional or local deoxygenation as recognized during the Cenozoic (e.g.,
738 Jones et al., 2019; Cramwinckel et al., 2022). Although the Hg deficit is difficult to quantify
739 properly without knowledge of the initial contents in the particle or burial flux, we perform a rough
740 calculation for the Arabian Sea, assuming (1) a scenario in which Hg flux to the sediment–water
741 interface is constant and (2) a scenario in which the upper part of the Station 1B sediments is
742 representative of the original Hg/TOC (~20 ppb/%) ratio in the particle flux. Lower TOC (~8 >
743 ~6%) in the upper part of the section at Station 1B suggests this part may have been deposited
744 under slightly less reducing conditions or documents lower productivity compared to the lower
745 part (Fig. 3). Even without correcting for better ventilation and lowered TOC (scenario 1), the
746 difference in Hg contents from top to bottom is substantial (Hg decreasing by 50% from ~130 ppb
747 near the sediment-water interface to 65 ppb below 10 cm depth, at Station 1B). However, assuming
748 the Hg/TOC in the upper part is most representative of the particle flux (scenario 2), the initial Hg
749 contents in the lower part of the Station 1B core might have been even higher (up to ca. 170 ppb).
750 As a consequence, we speculate that an even larger proportion of Hg (>60%) could have been
751 removed during early diagenesis. While such Hg loss would not eliminate most Hg signals

752 interpreted to result from LIP volcanism (see e.g. Grasby et al., 2019; Charbonnier et al., 2020 for
753 a comparison of magnitudes), it appears likely that some pulses of LIP-derived Hg emitted during
754 periods of anoxia are missed or systematically underestimated as a consequence.

755 Similarly, for the OAE 3 sediments, we can calculate Hg loss during the sulfidic episodes relative
756 to the ferruginous phases. Assuming the highest Hg/TOC values represent the original signal,
757 starting from peak values around ~120 ppb, Hg loss might have reached ~50 ppb or more. This
758 calculation is more uncertain for the Baltic Sea sites because TOC and Al are much more variable.
759 However, during the hypoxic periods, using the stable Hg/TOC from the less reducing (stable)
760 background (Fig. 4A, C), the calculated relative Hg loss may range up to ~40 ppb, while only ~20–
761 30 ppb is retained. Intriguingly, while starting from different Hg/TOC (6.4 at F80 vs 8.6 ppb/% at
762 LL19, owing to the better ventilated nature of LL19), calculated Hg loss (in ppb) for both cores is
763 identical.

764 Remarkably, despite age and other inter-site differences between the Holocene Arabian Sea and
765 Baltic and the Cretaceous ODP Hole 1261A sediments, the calculated maximum Hg deficit is very
766 similar and typically does not exceed 50-60%. The similarity in signals recovered from these
767 materials reinforces our assertion that Hg is lost relative to TOC. Moreover, the maximum Hg loss
768 of *ca.* 50-60% for anoxic-mildly euxinic deposition could imply that the processes involved in Hg
769 loss cannot easily (re)mobilize the remaining Hg: perhaps for this fraction the Hg-species or
770 (binding) location inhibits remobilization. We find a strong correlation of Hg evasion to Mo
771 enrichment and other metals that are assumed to (co)precipitate with sulfides under anoxic
772 conditions, including the Arabian Sea station where the concentration of sulfide is very low. This
773 result seems to argue against a strong tendency to develop sulfide-enriched Hg or otherwise S-
774 dominant Hg sequestration in anoxic to (mildly) sulfidic conditions. We find no indications that
775 Hg is preferentially lost from or concentrated in sediments marked by continuous slightly hypoxic
776 and oxic conditions.

777 The effects of oxygenation on Hg/TOC are even more pronounced compared to Hg. For the
778 Arabian Sea sites, and other sediments deposited within and below OMZs in the ocean, the TOC
779 contents alone may span orders of magnitude depending on the bottom and pore water oxygenation
780 at the time of sediment deposition (e.g., Müller and Suess, 1979; Hartnett et al., 1998). This signal
781 subsequently modulates Hg/TOC. Order-of-magnitude changes, such as we find in the Arabian
782 Sea sites, do not commonly occur in one single succession because most analyzed depositional
783 settings will not have changed so dramatically, but both the Baltic Sea and ODP Site 1261
784 stratigraphic records clearly show changes to Hg and Hg/TOC related to redox changes (Fig. 4,6).
785 Hence, extreme caution should be taken when analyzing successions across (de)oxygenation
786 events, since signal amplification or suppression in Hg/TOC is likely to have occurred and can
787 span at least an order of magnitude, on a par with many of the inferred volcanism-related Hg/TOC
788 fluctuations in the geological record (Charbonnier et al., 2020). Likewise, the oxidation biases may
789 have induced changes that exceed the commonly used limit for interpreting Hg enrichment factors
790 ($HgEF > 2$ Shen et al., 2019a, 2019b; Zhu et al., 2021). A more conservative approach is therefore

791 warranted when interpreting Hg/TOC or otherwise normalized Hg records and perhaps even raw
792 Hg data, and could, for example, utilize a series of criteria. The observations on the potential
793 impact of ambient redox conditions on Hg and normalized Hg may warrant revisiting of Hg studies
794 that are based on successions where substantial changes in ambient redox were recognized (e.g.
795 Percival et al., 2018; Jones et al., 2019; Paschall et al., 2019; Rakociński et al., 2021; Bian et al.,
796 2022; Zhao et al., 2022a). Critically, we find any anomalously elevated Hg/TOC data should at
797 least be accompanied by substantially (at least >3 fold background) elevated Hg (as suggested
798 previously; Percival et al., 2021) and, as such spikes might be associated with post-depositional
799 oxidation of anoxic facies, evidence for stable redox conditions in the relevant stratigraphic
800 interval that would support increased primary Hg loading.

801 **4.3 Processes influencing Hg and Hg/TOC during early diagenesis**

802 In our new data (Fig. 3-8) the TOC-normalized Hg (i.e., Hg/TOC) unambiguously increases with
803 oxidation but this seems to result from multiple distinct processes affecting Hg and TOC
804 separately. Specifically, there appears to be a distinction in Hg burial efficiency between
805 oxygenated and anoxic to sulfidic conditions, whereby Hg appears to preferentially escape
806 sediments under anoxic to sulfidic conditions while there is no measurable change in TOC content
807 of the sediment (see section 4.1 & 4.2). Based on positive correlation (Supplementary data), Hg
808 appears to be predominantly bound to TOC in many of the analyzed anoxic sample sets, implying
809 this phenomenon could suggest either a substantially weaker binding of a part of the OM-bound
810 Hg (Haitzer et al., 2002), or that a non-OM-bound Hg fraction is remobilized. Both options,
811 however, require Hg remobilization and ultimately evasion (up to *ca.* 50-60%, see section 4.2) to
812 the bottom waters.

813 We cannot confirm the occurrence of a specific process leading to Hg loss in anoxic to sulfidic
814 environments, in which loss of organic matter would be minimal. There are, however, potential
815 explanations for the slowly decreasing Hg contents in the intervals of Fe-reduction (and SO_4^{2-}
816 reduction, see §2.1) in the anoxic Holocene sediments of the Arabian Sea (Fig. 3) and the lower
817 Hg loading of TOC in the organic-rich, sulfidic, Holocene sediments of the Baltic Sea (Fig. 4). For
818 example, it has been established that various sulfate- and Fe-reducing bacteria and archaea are able
819 to methylate Hg to counteract its toxicity (Fleming et al., 2006; Gilmour et al., 2013). This distinct
820 microbial behavior, also known from other biotoxic elements (Li et al., 2021), would increase Hg
821 mobility. Intriguingly, marine organisms capable of Hg-methylation are widespread and seemingly
822 diverse, including obligate anaerobes, but possibly also aerobic organisms (Villar et al., 2020). It
823 might be that sulfate-reducing bacteria are more efficient compared to Fe-reducing bacteria
824 (Fleming et al., 2006; Han et al., 2008). While it is impossible to confidently identify the process
825 responsible for removal of Hg, our data are consistent with a mechanism whereby Hg methylation
826 facilitates sedimentary Hg loss. Specifically, the negative correlation of Hg/TOC, and notably
827 Hg/Al, with elevated Mo contents, which is used as evidence for sulfidic (pore-water) conditions
828 at the time of deposition at ODP Site 1261, is interesting and mimics the trends observed in the
829 Baltic Sea sites. As sulfide is an important modulator of Mo sequestration, the negative correlation

830 between Mo and Hg/TOC tentatively supports a role for Hg methylation by sulfate reducers in Hg
831 loss. Intriguingly, the negative correlations between Hg/TOC and Mo weaken at high Mo contents
832 (>50 ppm in the Baltic Sea sites, Fig. 4E, F and >100 ppm for ODP Site 1261 Fig. 7D), which may
833 be indicative of sulfide inhibition on Hg methylation by sulfate- and iron-reducing organisms, and
834 may be accompanied with, or followed by, a switch to Hg sequestration by sulfide or metal sulfide
835 complexes when these species are readily available (Ullrich et al., 2001; Shen et al., 2020).
836 Alternatively, working either in tandem or independently from Hg-methylation, an influence of
837 temporary adsorption of Hg²⁺ with Fe or Mn (oxyhydr)oxide in Hg cycling cannot be ruled out.
838 The mobility of Hg²⁺ would likely remain a limiting factor under these conditions, in the presence
839 of efficient scavenging ligands such as free sulfide and organic matter.

840 At present, it is impossible to gauge whether and how these processes would influence deep-time
841 records, but noticeable Hg loss under ferruginous–(mildly) euxinic conditions is consistent with
842 the trends we find from the Holocene Baltic Sea sites, Pleistocene Mediterranean sapropel S5 and
843 the Coniacian-Santonian OAE 3 sediments recovered at ODP Site 1261. Crucially, the observed
844 Hg deficit – up to ~50% relative to stable Hg/TOC – occurs, in similar magnitude, both in deep-
845 time and modern sediments, suggesting that this phenomenon might be a relatively common
846 feature. Moreover, if Hg evasion is indeed a common feature of low-oxygen environments,
847 questions are raised regarding the potential for redistribution and redeposition of Hg. The negative
848 correlations of Hg and Hg/TOC with Mo and other redox-sensitive elements might be useful in
849 identifying Hg loss. Regardless of the processes involved, both the geological imprint of Hg
850 methylation and other mechanisms potentially leading to Hg loss from sediments warrant careful
851 consideration when interpreting the geological Hg record.

852 Less surprisingly, we see progressive TOC loss with increased oxygen exposure, especially under
853 oxic or mildly hypoxic conditions. However, Hg is not proportionally affected, resulting in
854 progressively higher Hg/TOC with long-term oxidation, and occasionally Hg focusing (e.g., Fig.
855 5, Mercone et al. 1999). The early diagenetic changes examined here have echoed effects in
856 situations where ancient sediments, initially deposited under anoxic conditions, have been
857 subjected to surface weathering and oxidation in more recent time (Charbonnier et al., 2020). There
858 are a couple of plausible mechanisms that would retain more Hg relative to TOC during oxidation.
859 Firstly, if Hg were mobilized (as Hg²⁺) during OM breakdown, it would most likely be
860 immediately scavenged by other organic material, Fe/Mn (oxyhydr)oxides, pyrite and other
861 sulfides, while dissolved inorganic carbon would be generally more mobile. Secondly, it is likely
862 that a fraction of the sedimentary Hg would be associated with more refractory OM (e.g., Them et
863 al. 2019), which could have had intrinsically higher Hg/TOC and was less easily mobilized (Them
864 et al., 2019; Charbonnier et al., 2020). A relative increase in the refractory organic-matter fraction
865 could hence cause a steeper Hg/TOC relationship during extensive TOC degradation, whereas a
866 relative decrease in refractory organic-matter would result in flattening of the curves at higher
867 TOC. Further detailed assessment of OM characteristics through, for example, maceral analyses
868 or palynology, or Hg content data on specific types of OM, might help elucidate how preservation

869 and OM sources interact to shape Hg/TOC patterns in ancient sediments. Even if some of those
870 data types are available for some localities and periods, it is typically not paired with Hg (e.g.,
871 Harding et al., 2011; Kender et al., 2012; Jones et al., 2019; Kender et al., 2021), and these aspects
872 are thus under-explored. Broad geochemical characteristics of OM (such as HI and OI, but also
873 C/N ratios) might be used as first-order estimates of the preservation state (Fig. 8) as well as the
874 relative contribution of refractory OM.

875 **5. Conclusions**

876 Differences in duration and intensity of sediment (de)oxygenation and, more broadly, changes in
877 redox conditions, both between and within our Holocene–Pleistocene and Cretaceous sites resulted
878 in markedly divergent Hg contents and Hg/TOC (Figs. 3-8). Importantly, we find that separate
879 processes affect both the Hg and TOC, and contribute to the complexity and potential biases that
880 may pose an additional challenge in the interpretation of Hg and Hg/TOC records. Through
881 selecting sites with stable Hg loading throughout but with spatially or temporally variable ambient
882 redox conditions and evolution, we isolate the effects of the redox conditions on the Hg and
883 normalized-Hg records and how those effects might be stored in the geological record.

884 Results from the Holocene Arabian Sea cores show that order-of-magnitude differences in
885 Hg/TOC can occur after oxidizing seemingly similar starting material. Under oxygen-depleted
886 conditions, there is evidence that part of the Hg escapes the sediments during initial diagenesis,
887 for example after methylation by Fe-oxide- and sulfate-reducing bacteria and methanogens. If this
888 phenomenon were a common factor during early diagenesis, it might be expected that Hg spikes
889 would be suppressed in sediments deposited under such low-oxygen conditions. Such sediments
890 are also commonly characterized by high burial efficiency of TOC, arguably further reducing the
891 Hg/TOC ratio. Aerobic degradation, on the other hand, seems to predominantly affect sedimentary
892 organic carbon, while Hg is mostly retained, thereby inflating Hg/TOC ratios. Stratigraphic
893 focusing of Hg was found associated with the oxidized intervals of sediments that were deposited
894 under anoxic–sulfidic conditions. Under such circumstances, Hg content spikes are observed
895 around buried redox fronts, which are commonly observed associated with, but not unique to,
896 turbidites (e.g., Mercone et al. 1999) and sapropels (Fig. 5). These type of settings, as a
897 consequence, are particularly challenging targets for assessing paleo-volcanic activity.

898 For many key intervals in geological deep time that have been investigated for Hg and TOC, the
899 potential influences of (de)oxygenation have far-reaching implications. Such complicating factors
900 could be particularly important for periods associated with emplacement of subaerial LIPs that are
901 also commonly associated with the most extreme carbon-cycle, climatic and environmental
902 perturbations, including (transient) expansion of low-oxygen areas in the ocean, in extreme cases
903 leading to ocean anoxic events. It is noteworthy that some overwhelmingly large Hg spikes occur
904 during times of ocean anoxia, while our results show that deoxygenation generally has a higher
905 probability of obscuring, rather than accentuating Hg/TOC spikes (e.g. Fig. 6). Indeed, it appears
906 that under anoxic and (mildly) euxinic conditions Hg contents may be suppressed due to Hg

907 evasion, likely as a result of methylation (Figs. 3,4,6,7). We cannot rule out that ocean anoxia,
908 such as occurred during the Mesozoic Era, in combination with the nature of the LIP volcanism
909 may have played an important role in reducing the perceived impact on the Hg cycle (e.g., Percival
910 et al., 2018). On the other hand, high-amplitude oxygen fluctuations are likely to have led to
911 increased variability in Hg and TOC and, in some cases, to Hg focusing resulting from oxidation
912 of previously anoxic sediments. It also remains likely that S-driven Hg sequestration (within
913 pyrite) occurs in extreme euxinic conditions, potentially amplifying Hg signals, but the
914 sedimentary host phases and their potential for amplified Hg sequestration in geological samples
915 will remain uncertain until a broad spectrum of dedicated Hg speciation data becomes available.

916 The magnitude of geochemical change from early diagenesis to both the Hg and TOC records is
917 such that the resulting signals, without prior knowledge of the oxygenation history of a succession,
918 could easily be misinterpreted as evidence for enhanced, suppressed, or intermittent volcanic
919 activity. While the relative influence of oxygenation on any single record during high-amplitude
920 environmental changes remains difficult to quantify, we calculate Hg loss on the order of ~50% in
921 multiple records, while changes associated with Hg focusing around paleo-redox fronts is
922 potentially of a similar magnitude (~a doubling). Critically, we also show that Hg/TOC might
923 suffer order-of-magnitude alterations depending on the oxidative evolution of the host sediment.
924 As such, we recommend paleo-oxygenation reconstructions through, for example, the use of
925 (trace)-element analyses or, more indirectly, organic-matter characteristics, be employed as
926 extensively as possible when interpreting Hg and (TOC-)normalized Hg signals.

927

928 **Acknowledgments**

929 We thank S. Wyatt and O. Green (University of Oxford), H. de Waard (Utrecht University) and S.
930 Ossebaar (NIOZ) for analytical assistance. T.A.M. and J.F. acknowledge funding from ERC
931 consolidator Grant (ERC-2018-COG-818717-V-ECHO). N.A.G.M.v.H. and C.P.S. acknowledge
932 funding from ERC Synergy Grant 854088 (MARIX). G.-J.R. acknowledges funding from the
933 Dutch Research Council (NWO) for the PASOM Cruise (2009) to the Arabian Sea. The
934 Netherlands Earth System Science Centre (NESSC), financially supported by the Ministry of
935 Education, Culture and Science (OCW) is acknowledged for funding the cruise that acquired the
936 64PE406 core.

937 **Data availability statement**

938 All newly generated data will be made available through a permanent online data repository upon
939 publication.

940

- 941 Algeo T. J., Luo G. M., Song H. Y., Lyons T. W. and Canfield D. E. (2015) Reconstruction of secular variation in
942 seawater sulfate concentrations. *Biogeosciences* **12**, 2131–2151.
- 943 Amos H. M., Jacob D. J., Streets D. G. and Sunderland E. M. (2013) Legacy impacts of all-time anthropogenic
944 emissions on the global mercury cycle. *Global Biogeochem. Cycles* **27**, 410–421.
- 945 Amos H. M., Sonke J. E., Obrist D., Robins N., Hagan N., Horowitz H. M., Mason R. P., Witt M., Hedgecock I. M.,
946 Corbitt E. S. and Sunderland E. M. (2015) Observational and modeling constraints on global anthropogenic
947 enrichment of mercury. *Environ. Sci. Technol.* **49**, 4036–4047.
- 948 Behar F., Beaumont V. and De B. Penteado H. L. (2001) Rock-Eval 6 Technology: Performances and
949 Developments. *Oil Gas Sci. Technol.* **56**, 111–134.
- 950 Benoit J. M., Gilmour C. C., Mason R. P. and Heyes A. (1999) Sulfide controls on mercury speciation and
951 bioavailability to methylating bacteria in sediment pore waters. *Environ. Sci. Technol.* **33**, 951–957.
- 952 Berner R. A. (1989) Biogeochemical cycles of carbon and sulfur and their effect on atmospheric oxygen over
953 Phanerozoic time. *Glob. Planet. Change* **1**, 97–122.
- 954 Berner R. A. and Raiswell R. (1983) Burial of organic carbon and pyrite sulfur in sediments over Phanerozoic time:
955 a new theory. *Geochim. Cosmochim. Acta* **47**, 855–862.
- 956 Bian L., Chappaz A., Schovsbo N. H., Nielsen A. T. and Sanei H. (2022) High mercury enrichments in sediments
957 from the Baltic continent across the late Cambrian: Controls and implications. *Chem. Geol.* **599**.
- 958 Biester H., Martinez-Cortizas A., Birkenstock S. and Kilian R. (2003) Effect of Peat Decomposition and Mass Loss
959 on Historic Mercury Records in Peat Bogs from Patagonia. *Environ. Sci. Technol.* **37**, 32–39.
- 960 Biester H., Pérez-Rodríguez M., Gilfedder B.-S., Martínez Cortizas A. and Hermanns Y.-M. (2018) Solar irradiance
961 and primary productivity controlled mercury accumulation in sediments of a remote lake in the Southern
962 Hemisphere during the past 4000 years. *Limnol. Oceanogr.* **63**, 540–549.
- 963 Bowman K. L., Hammerschmidt C. R., Lamborg C. H. and Swarr G. (2015) Mercury in the North Atlantic Ocean:
964 The U.S. GEOTRACES zonal and meridional sections. *Deep. Res. Part II Top. Stud. Oceanogr.* **116**, 251–
965 261.
- 966 Bowman K. L., Hammerschmidt C. R., Lamborg C. H., Swarr G. J. and Agather A. M. (2016) Distribution of
967 mercury species across a zonal section of the eastern tropical South Pacific Ocean (U.S. GEOTRACES GP16).
968 *Mar. Chem.* **186**, 156–166.
- 969 Bravo A. G., Bouchet S., Tolu J., Björn E., Mateos-Rivera A. and Bertilsson S. (2017) Molecular composition of
970 organic matter controls methylmercury formation in boreal lakes. *Nat. Commun.* **8**, 1–9.
- 971 Brumsack H. J. (2006) The trace metal content of recent organic carbon-rich sediments: Implications for Cretaceous
972 black shale formation. *Palaeogeogr. Palaeoclimatol. Palaeoecol.* **232**, 344–361.
- 973 Calvert S. E. and Pedersen T. F. (1993) Geochemistry of Recent oxic and anoxic marine sediments: Implications for
974 the geological record. *Mar. Geol.* **113**, 67–88.
- 975 Charbonnier G., Adatte T., Föllmi K. B. and Suan G. (2020) Effect of Intense Weathering and Postdepositional
976 Degradation of Organic Matter on Hg/TOC Proxy in Organic- rich Sediments and its Implications for Deep-
977 Time Investigations. *Geochemistry, Geophys. Geosystems* **21**, 270.
- 978 Clarkson M. O., Hennekam R., Sweere T. C., Andersen M. B., Reichart G. J. and Vance D. (2021) Carbonate
979 associated uranium isotopes as a novel local redox indicator in oxidatively disturbed reducing sediments.
980 *Geochim. Cosmochim. Acta* **311**, 12–28.
- 981 Clarkson M. O., Stirling C. H., Jenkyns H. C., Dickson A. J., Porcelli D., Moy C. M., von Strandmann P. P. A. E.,

- 982 Cooke I. R. and Lenton T. M. (2018) Uranium isotope evidence for two episodes of deoxygenation during
983 Oceanic Anoxic Event 2. *Proc. Natl. Acad. Sci. U. S. A.* **115**, 2918–2923.
- 984 Cohen A. S., Coe A. L., Harding S. M. and Schwark L. (2004) Osmium isotope evidence for the regulation of
985 atmospheric CO₂ by continental weathering. *Geology* **32**, 157.
- 986 Compeau G. C. and Bartha R. (1985) Sulfate-Reducing Bacteria: Principal Methylators of Mercury in Anoxic
987 Estuarine Sediment. *Appl. Environ. Microbiol.* **50**, 498–502.
- 988 Cooke C. A., Balcom P. H., Biester H. and Wolfe A. P. (2009) Over three millennia of mercury pollution in the
989 Peruvian Andes. *Proc. Natl. Acad. Sci. U. S. A.* **106**, 8830–8834.
- 990 Cossa D., Knoery J., Bănaru D., Harmelin-Vivien M., Sonke J. E., Hedgecock I. M., Bravo A. G., Rosati G., Canu
991 D., Horvat M., Sprovieri F., Pirrone N. and Heimbürger-Boavida L.-E. (2022) Mediterranean Mercury
992 Assessment 2022: An Updated Budget, Health Consequences, and Research Perspectives. *Environ. Sci.*
993 *Technol.* **56**, 3840–3862.
- 994 Covelli S., Faganeli J., Horvat M. and Brambati A. (2001) Mercury contamination of coastal sediments as the result
995 of long-term cinnabar mining activity (Gulf of Trieste, northern Adriatic sea). *Appl. Geochemistry* **16**, 541–
996 558.
- 997 Cramwinckel M. J., van der Ploeg R., van Helmond N. A. G. M., Waarlo N., Agnini C., Bijl P. K., van der Boon A.,
998 Brinkhuis H., Frieling J., Krijgsman W., Mather T. A., Middelburg J. J., Peterse F., Slomp C. P. and Sluijs A.
999 (2022) Deoxygenation and organic carbon sequestration in the Tethyan realm associated with the Middle
1000 Eocene Climatic Optimum. *GSA Bull.*
- 1001 Dal Corso J., Mills B. J. W., Chu D., Newton R. J., Mather T. A., Shu W., Wu Y., Tong J. and Wignall P. B. (2020)
1002 Permo–Triassic boundary carbon and mercury cycling linked to terrestrial ecosystem collapse. *Nat. Commun.*
1003 **11**, 1–9.
- 1004 Demaison G. J. and Moore G. T. (1980) Anoxic environments and oil source bed genesis. *Am. Assoc. Pet. Geol.*
1005 *Bull.* **64**, 1179–1209.
- 1006 Edwards B. A., Kushner D. S., Outridge P. M. and Wang F. (2021) Fifty years of volcanic mercury emission
1007 research: Knowledge gaps and future directions. *Sci. Total Environ.* **757**, 1–17.
- 1008 Emili A., Koron N., Covelli S., Faganeli J., Acquavita A., Predonzani S. and Vittor C. De (2011) Does anoxia affect
1009 mercury cycling at the sediment-water interface in the Gulf of Trieste (northern Adriatic Sea)? Incubation
1010 experiments using benthic flux chambers. *Appl. Geochemistry* **26**, 194–204.
- 1011 Ernst R. E. and Youbi N. (2017) How Large Igneous Provinces affect global climate, sometimes cause mass
1012 extinctions, and represent natural markers in the geological record. *Palaeogeogr. Palaeoclimatol. Palaeoecol.*
1013 **478**, 30–52.
- 1014 Fendley I. M., Mittal T., Sprain C. J., Marvin-DiPasquale M., Tobin T. S. and Renne P. R. (2019) Constraints on the
1015 volume and rate of Deccan Traps flood basalt eruptions using a combination of high-resolution terrestrial
1016 mercury records and geochemical box models. *Earth Planet. Sci. Lett.* **524**, 1–11.
- 1017 Fitzgerald W. F., Lamborg C. H. and Hammerschmidt C. R. (2007) Marine biogeochemical cycling of mercury.
1018 *Chem. Rev.* **107**, 641–662.
- 1019 Fleming E. J., Mack E. E., Green P. G. and Nelson D. C. (2006) Mercury methylation from unexpected sources:
1020 Molybdate-inhibited freshwater sediments and an iron-reducing bacterium. *Appl. Environ. Microbiol.* **72**, 457–
1021 464.
- 1022 Gagnon C., Pelletier É. and Mucci A. (1997) Behaviour of anthropogenic mercury in coastal marine sediments. *Mar.*
1023 *Chem.* **59**, 159–176.

- 1024 Gehrke G. E., Blum J. D. and Meyers P. A. (2009) The geochemical behavior and isotopic composition of Hg in a
1025 mid-Pleistocene western Mediterranean sapropel. *Geochim. Cosmochim. Acta* **73**, 1651–1665.
- 1026 Gilmour C. C., Podar M., Bullock A. L., Graham A. M., Brown S. D., Somenahally A. C., Johs A., Hurt R. A.,
1027 Bailey K. L. and Elias D. A. (2013) Mercury methylation by novel microorganisms from new environments.
1028 *Environ. Sci. Technol.* **47**, 11810–11820.
- 1029 Gobeil C. and Cossa D. (1993) Mercury in sediments and sediment pore water in the Laurentian Trough. *Can. J.*
1030 *Fish. Aquat. Sci.* **50**, 1794–1800.
- 1031 Grasby S. E., Sanei H., Beauchamp B. and Chen Z. (2013) Mercury deposition through the Permo-Triassic Biotic
1032 Crisis. *Chem. Geol.* **351**, 209–216.
- 1033 Grasby S. E., Them T. R., Chen Z., Yin R. and Ardakani O. H. (2019) Mercury as a proxy for volcanic emissions in
1034 the geologic record. *Earth-Science Rev.* **196**, 102880.
- 1035 Gu B., Bian Y., Miller C. L., Dong W., Jiang X. and Liang L. (2011) Mercury reduction and complexation by
1036 natural organic matter in anoxic environments. *Proc. Natl. Acad. Sci. U. S. A.* **108**, 1479–1483.
- 1037 Guédron S., Tolu J., Brisset E., Sabatier P., Perrot V., Bouchet S., Develle A. L., Bindler R., Cossa D., Fritz S. C.
1038 and Baker P. A. (2019) Late Holocene volcanic and anthropogenic mercury deposition in the western Central
1039 Andes (Lake Chungará Chile). *Sci. Total Environ.* **662**, 903–914.
- 1040 Haake B., Ittekkot V., Rixen T., Ramaswamy V., Nair R. R. and Curry W. B. (1993) Seasonality and interannual
1041 variability of particle fluxes to the deep Arabian sea. *Deep. Res. Part I* **40**, 1323–1344.
- 1042 Haitzer M., Aiken G. R. and Ryan J. N. (2002) Binding of Mercury(II) to Dissolved Organic Matter: The Role of the
1043 Mercury-to-DOM Concentration Ratio. *Environ. Sci. Technol.* **36**, 3564–3570.
- 1044 Hammerschmidt C. R. and Fitzgerald W. F. (2004) Geochemical Controls on the Production and Distribution of
1045 Methylmercury in Near-Shore Marine Sediments. *Environ. Sci. Technol.* **38**, 1487–1495.
- 1046 Han S., Obraztsova A., Pretto P., Deheyn D. D., Gieskes J. and Tebo B. M. (2008) Sulfide and iron control on
1047 mercury speciation in anoxic estuarine sediment slurries. *Mar. Chem.* **111**, 214–220.
- 1048 Harding I. C., Charles A. J., Marshall J. E. A., Pälke H., Roberts A. P., Wilson P. A., Jarvis E., Thorne R., Morris
1049 E., Moremon R., Pearce R. B. and Akbari S. (2011) Sea-level and salinity fluctuations during the Paleocene–
1050 Eocene thermal maximum in Arctic Spitsbergen. *Earth Planet. Sci. Lett.* **303**, 97–107.
- 1051 Hartnett H. E., Keil R. G., Hedges J. I. and Devol A. H. (1998) Influence of oxygen exposure time on organic carbon
1052 preservation in continental margin sediments. *Nature* **391**, 572–574.
- 1053 Hazra B., Katz B. J., Pratap D. and Singh P. K. (2022) Impact of siderite on Rock-Eval S3 and oxygen index. *Mar.*
1054 *Pet. Geol.* **143**, 105804.
- 1055 Hedges J. I., Hu F. S., Devol A. H., Hartnett H. E., Tsamakis E. and Keil R. G. (1999) Sedimentary organic matter
1056 preservation: A test for selective degradation under oxic conditions. *Am. J. Sci.* **299**, 529–555.
- 1057 Hedges J. I. and Keil R. G. (1995) Sedimentary organic matter preservation: an assessment and speculative
1058 synthesis. *Mar. Chem.* **49**, 81–115.
- 1059 Heimbürger L. E., Cossa D., Marty J. C., Migon C., Averty B., Dufour A. and Ras J. (2010) Methyl mercury
1060 distributions in relation to the presence of nano- and picophytoplankton in an oceanic water column (Ligurian
1061 Sea, North-western Mediterranean). *Geochim. Cosmochim. Acta* **74**, 5549–5559.
- 1062 van Helmond N. A. G. M., Jilbert T. and Slomp C. P. (2018) Hypoxia in the Holocene Baltic Sea: Comparing
1063 modern versus past intervals using sedimentary trace metals. *Chem. Geol.* **493**, 478–490.

- 1064 van Helmond N. A. G. M., Lougheed B. C., Vollebregt A., Peterse F., Fontorbe G., Conley D. J. and Slomp C. P.
1065 (2020) Recovery from multi-millennial natural coastal hypoxia in the Stockholm Archipelago, Baltic Sea,
1066 terminated by modern human activity. *Limnol. Oceanogr.* **65**, 3085–3097.
- 1067 Helz G. R. and Vorlicek T. P. (2019) Precipitation of molybdenum from euxinic waters and the role of organic
1068 matter. *Chem. Geol.* **509**, 178–193.
- 1069 Hennekam R., van der Bolt B., van Nes E. H., de Lange G. J., Scheffer M. and Reichart G. J. (2020) Early-Warning
1070 Signals for Marine Anoxic Events. *Geophys. Res. Lett.* **47**.
- 1071 Higuera P., Oyarzun R., Biester H., Lillo J. and Lorenzo S. (2003) A first insight into mercury distribution and
1072 speciation in soils from the Almadén mining district, Spain. *J. Geochemical Explor.* **80**, 95–104.
- 1073 Honjo S., Dymond J., Prell W. and Ittekkot V. (1999) Monsoon-controlled export fluxes to the interior of the
1074 Arabian Sea. *Deep. Res. Part II Top. Stud. Oceanogr.* **46**, 1859–1902.
- 1075 Jenkyns H. C. (2010) Geochemistry of oceanic anoxic events. *Geochemistry, Geophys. Geosystems* **11**, 1–30.
- 1076 Jenkyns H. C., Matthews A., Tsikos H. and Erel Y. (2007) Nitrate reduction, sulfate reduction, and sedimentary iron
1077 isotope evolution during the Cenomanian-Turonian oceanic anoxic event. *Paleoceanography* **22**.
- 1078 Jiang T., Bravo A. G., Skjellberg U., Björn E., Wang D., Yan H. and Green N. W. (2018) Influence of dissolved
1079 organic matter (DOM) characteristics on dissolved mercury (Hg) species composition in sediment porewater
1080 of lakes from southwest China. *Water Res.* **146**, 146–158.
- 1081 Jilbert T. and Slomp C. P. (2013) Rapid high-amplitude variability in baltic sea hypoxia during the holocene.
1082 *Geology* **41**, 1183–1186.
- 1083 Jones M. T., Percival L. M. E. E., Stokke E. W., Frieling J., Mather T. A., Riber L., Schubert B. A., Schultz B.,
1084 Tegner C., Planke S. and Svensen H. H. (2019) Mercury anomalies across the Palaeocene-Eocene Thermal
1085 Maximum. *Clim. Past* **15**, 217–236.
- 1086 Keller G., Mateo P., Monkenbusch J., Thibault N., Puneekar J., Spangenberg J. E., Abramovich S., Ashckenazi-
1087 Polivoda S., Schoene B., Eddy M. P., Samperton K. M., Khadri S. F. R. and Adatte T. (2020) Mercury linked
1088 to Deccan Traps volcanism, climate change and the end-Cretaceous mass extinction. *Glob. Planet. Change*
1089 **194**, 103312.
- 1090 Keller G., Mateo P., Puneekar J., Khozyem H., Gertsch B., Spangenberg J., Bitchong A. M. and Adatte T. (2018)
1091 Environmental changes during the Cretaceous-Paleogene mass extinction and Paleocene-Eocene Thermal
1092 Maximum: Implications for the Anthropocene. *Gondwana Res.* **56**, 69–89.
- 1093 Kender S., Bogus K., Pedersen G. K., Dybkjær K., Mather T. A., Mariani E., Ridgwell A., Riding J. B., Wagner T.,
1094 Hesselbo S. P. and Leng M. J. (2021) Paleocene/Eocene carbon feedbacks triggered by volcanic activity. *Nat.*
1095 *Commun.* **12**, 1–10.
- 1096 Kender S., Stephenson M. H., Riding J. B., Leng M. J., Knox R. W. O. B., Peck V. L., Kendrick C. P., Ellis M. A.,
1097 Vane C. H. and Jamieson R. (2012) Marine and terrestrial environmental changes in NW Europe preceding
1098 carbon release at the Paleocene-Eocene transition. *Earth Planet. Sci. Lett.* **353–354**, 108–120.
- 1099 Kim M., Han S., Gieskes J. and Dehey D. D. (2011) Importance of organic matter lability for monomethylmercury
1100 production in sulfate-rich marine sediments. *Sci. Total Environ.* **409**, 778–784.
- 1101 Koho K. A., Nierop K. G. J., Moodley L., Middelburg J. J., Pozzato L., Soetaert K., Van Der Plicht J. and Reichart
1102 G. J. (2013) Microbial bioavailability regulates organic matter preservation in marine sediments.
1103 *Biogeosciences* **10**, 1131–1141.
- 1104 Kraal P., Slomp C. P., Reed D. C., Reichart G. J. and Poulton S. W. (2012) Sedimentary phosphorus and iron
1105 cycling in and below the oxygen minimum zone of the northern Arabian Sea. *Biogeosciences* **9**, 2603–2624.

- 1106 Lafargue E., Marquis F. and Pillot D. (1998) Rock-Eval 6 applications in hydrocarbon exploration, production, and
1107 soil contamination studies. *Rev. l'Institut Fr. du Pet.* **53**, 421–437.
- 1108 Leipe T., Moros M., Kotilainen A., Vallius H., Kabel K., Endler M. and Kowalski N. (2013) Mercury in Baltic Sea
1109 sediments-Natural background and anthropogenic impact. *Chemie der Erde* **73**, 249–259.
- 1110 Lengger S. K., Hopmans E. C., Sinninghe Damsté J. S. and Schouten S. (2014) Impact of sedimentary degradation
1111 and deep water column production on GDGT abundance and distribution in surface sediments in the Arabian
1112 Sea: Implications for the TEX86 paleothermometer. *Geochim. Cosmochim. Acta* **142**, 386–399.
- 1113 Li Y. P., Ben Fekih I., Chi Fru E., Moraleda-Munoz A., Li X., Rosen B. P., Yoshinaga M. and Rensing C. (2021)
1114 Antimicrobial Activity of Metals and Metalloids. *Annu. Rev. Microbiol.* **75**, 175–197.
- 1115 Lim D., Kim H., Kim J., Jeong D. and Kim D. (2020) Mercury proxy for hydrothermal and submarine volcanic
1116 activities in the sediment cores of Central Indian Ridge. *Mar. Pollut. Bull.* **159**, 1–8.
- 1117 Lowenstein T. K., Timofeeff M. N., Brennan S. T., Hardie L. A. and Demicco R. V (2001) Oscillations in
1118 Phanerozoic Seawater Chemistry: Evidence from Fluid Inclusions. *Science (80-.)*. **294**, 1086–1088.
- 1119 Lu X., Gu W., Zhao L., Ul Haque M. F., DiSpirito A. A., Semrau J. D. and Gu B. (2017) Methylmercury uptake and
1120 degradation by methanotrophs. *Sci. Adv.* **3**, 1–6.
- 1121 Lyons T. W., Anbar A. D., Severmann S., Scott C. and Gill B. C. (2009) Tracking Euxinia in the Ancient Ocean: A
1122 Multiproxy Perspective and Proterozoic Case Study. *Annu. Rev. Earth Planet. Sci.* **37**, 507–534.
- 1123 Machado W., Sanders C. J., Santos I. R., Sanders L. M., Silva-Filho E. V. and Luiz-Silva W. (2016) Mercury
1124 dilution by autochthonous organic matter in a fertilized mangrove wetland. *Environ. Pollut.* **213**, 30–35.
- 1125 Manceau A., Lemouchi C., Enescu M., Gaillot A. C., Lanson M., Magnin V., Glatzel P., Poulin B. A., Ryan J. N.,
1126 Aiken G. R., Gautier-Luneau I. and Nagy K. L. (2015) Formation of Mercury Sulfide from Hg(II)-Thiolate
1127 Complexes in Natural Organic Matter. *Environ. Sci. Technol.* **49**, 9787–9796.
- 1128 März C., Poulton S. W., Beckmann B., Küster K., Wagner T. and Kasten S. (2008) Redox sensitivity of P cycling
1129 during marine black shale formation: Dynamics of sulfidic and anoxic, non-sulfidic bottom waters. *Geochim.*
1130 *Cosmochim. Acta* **72**, 3703–3717.
- 1131 Mason R. P., Choi A. L., Fitzgerald W. F., Hammerschmidt C. R., Lamborg C. H., Soerensen A. L. and Sunderland
1132 E. M. (2012) Mercury biogeochemical cycling in the ocean and policy implications. *Environ. Res.* **119**, 101–
1133 117.
- 1134 Mason R. P., Fitzgerald W. F. and Morel F. M. M. (1994) The biogeochemical cycling of elemental mercury:
1135 Anthropogenic influences. *Geochim. Cosmochim. Acta* **58**, 3191–3198.
- 1136 Mason R. P. and Sheu G. R. (2002) Role of the ocean in the global mercury cycle. *Global Biogeochem. Cycles* **16**,
1137 40-1-40–14.
- 1138 Mercone D., Thomson J., Croudace I. . and Troelstra S. . (1999) A coupled natural immobilisation mechanism for
1139 mercury and selenium in deep-sea sediments. *Geochim. Cosmochim. Acta* **63**, 1481–1488.
- 1140 Merritt K. A. and Amirbahman A. (2009) Mercury methylation dynamics in estuarine and coastal marine
1141 environments - A critical review. *Earth-Science Rev.* **96**, 54–66.
- 1142 Mikac N., Niessen S., Ouddane B. and Wartel M. (1999) Speciation of mercury in sediments of the Seine estuary
1143 (France). *Appl. Organomet. Chem.* **13**, 715–725.
- 1144 Morel F. M. M., Kraepiel A. M. L. and Amyot M. (1998) The chemical cycle and bioaccumulation of mercury.
1145 *Annu. Rev. Ecol. Syst.* **29**, 543–566.

- 1146 Morse J. W. and Luther G. W. (1999) Chemical influences on trace metal-sulfide interactions in anoxic sediments.
1147 *Geochim. Cosmochim. Acta* **63**, 3373–3378.
- 1148 Müller P. J. and Suess E. (1979) Productivity, sedimentation rate, and sedimentary organic matter in the oceans—I.
1149 Organic carbon preservation. *Deep Sea Res. Part A. Oceanogr. Res. Pap.* **26**, 1347–1362.
- 1150 NASA Ocean Biology (OB.DAAC) (2014) Mean annual sea surface chlorophyll-a concentration for the period
1151 2009-2013 (composite dataset created by UNEP- WCMC).
- 1152 Newton R. J., Reeves E. P., Kafousia N., Wignall P. B., Bottrell S. H. and Sha J. G. (2011) Low marine sulfate
1153 concentrations and the isolation of the European epicontinental sea during the Early Jurassic. *Geology* **39**, 7–
1154 10.
- 1155 Nieuwenhuize J., Maas Y. E. M. and Middelburg J. J. (1994) Rapid analysis of organic carbon and nitrogen in
1156 particulate materials. *Mar. Chem.* **45**, 217–224.
- 1157 Ogrinc N., Monperrus M., Kotnik J., Fajon V., Vidimova K., Amouroux D., Kocman D., Tessier E., Žižek S. and
1158 Horvat M. (2007) Distribution of mercury and methylmercury in deep-sea surficial sediments of the
1159 Mediterranean Sea. *Mar. Chem.* **107**, 31–48.
- 1160 Outridge P. M., Sanei H., Stern G. A., Hamilton P. B. and Goodarzi F. (2007) Evidence for control of mercury
1161 accumulation rates in Canadian High Arctic Lake sediments by variations of aquatic primary productivity.
1162 *Environ. Sci. Technol.* **41**, 5259–5265.
- 1163 Owens J. D., Lyons T. W., Hardisty D. S., Lowery C. M., Lu Z., Lee B. and Jenkyns H. C. (2017) Patterns of local
1164 and global redox variability during the Cenomanian–Turonian Boundary Event (Oceanic Anoxic Event 2)
1165 recorded in carbonates and shales from central Italy. *Sedimentology* **64**, 168–185.
- 1166 Paschall O., Carmichael S. K., Königshof P., Waters J. A., Ta P. H., Komatsu T. and Dombrowski A. (2019) The
1167 Devonian-Carboniferous boundary in Vietnam: Sustained ocean anoxia with a volcanic trigger for the
1168 Hangenberg Crisis? *Glob. Planet. Change* **175**, 64–81.
- 1169 Pedersen T. F. and Calvert S. E. (1990) Anoxia vs. productivity: what controls the formation of organic- carbon-rich
1170 sediments and sedimentary rocks? *Am. Assoc. Pet. Geol. Bull.* **74**, 454–466.
- 1171 Percival Lawrence M. E., Bergquist B. A., Mather T. A. and Sanei H. (2021) Sedimentary Mercury Enrichments as
1172 a Tracer of Large Igneous Province Volcanism. In *Large Igneous Provinces: A Driver of Global
1173 Environmental and Biotic Changes* (eds. R. E. Ernst, A. J. Dickson, and A. Bekker). Geophysical Monograph
1174 Series, American Geophysical Union. pp. 247–262.
- 1175 Percival L. M. E. E., Ruhl M., Hesselbo S. P., Jenkyns H. C., Mather T. A. and Whiteside J. H. (2017) Mercury
1176 evidence for pulsed volcanism during the end-Triassic mass extinction. *Proc. Natl. Acad. Sci. U. S. A.* **114**,
1177 7929–7934.
- 1178 Percival L. M. E. E., Witt M. L. I. I., Mather T. A., Hermoso M., Jenkyns H. C., Hesselbo S. P., Al-Suwaidi A. H.,
1179 Storm M. S., Xu W. and Ruhl M. (2015) Globally enhanced mercury deposition during the end-Pliensbachian
1180 extinction and Toarcian OAE: A link to the Karoo-Ferrar Large Igneous Province. *Earth Planet. Sci. Lett.* **428**,
1181 267–280.
- 1182 Percival L. M. E., Jenkyns H. C., Mather T. A., Dickson A. J., Batenburg S. J., Ruhl M., Hesselbo S. P., Barclay R.,
1183 Jarvis I., Robinson S. A. and Woelders L. (2018) Does large igneous province volcanism always perturb the
1184 mercury cycle? Comparing the records of Oceanic Anoxic Event 2 and the end-cretaceous to other Mesozoic
1185 events. *Am. J. Sci.* **318**, 799–860.
- 1186 Percival L.M.E., Tedeschi L. R., Creaser R. A., Bottini C., Erba E., Giraud F., Svensen H., Savian J., Trindade R.,
1187 Coccioni R., Frontalini F., Jovane L., Mather T. A. and Jenkyns H. C. (2021) Determining the style and
1188 provenance of magmatic activity during the Early Aptian Oceanic Anoxic Event (OAE 1a). *Glob. Planet.
1189 Change* **200**, 103461.

- 1190 Pham A. L. T., Morris A., Zhang T., Ticknor J., Levard C. and Hsu-Kim H. (2014) Precipitation of nanoscale
1191 mercuric sulfides in the presence of natural organic matter: Structural properties, aggregation, and
1192 biotransformation. *Geochim. Cosmochim. Acta* **133**, 204–215.
- 1193 Pirrone N., Cinnirella S., Feng X., Finkelman R. B., Friedli H. R., Leaner J., Mason R., Mukherjee A. B., Stracher
1194 G. B., Streets D. G. and Telmer K. (2010) Global mercury emissions to the atmosphere from anthropogenic
1195 and natural sources. *Atmos. Chem. Phys.* **10**, 5951–5964.
- 1196 Pisarzowska A., Rakociński M., Marynowski L., Szczerba M., Thoby M., Paszkowski M., Perri M. C., Spalletta C.,
1197 Schönlaub H.-P. P., Kowalik N. and Gereke M. (2020) Large environmental disturbances caused by magmatic
1198 activity during the Late Devonian Hangenberg Crisis. *Glob. Planet. Change* **190**, 103155.
- 1199 Poulton S. W., Henkel S., März C., Urquhart H., Flögel S., Kasten S., Sinninghe Damsté J. S. and Wagner T. (2015)
1200 A continental-weathering control on orbitally driven redox-nutrient cycling during Cretaceous oceanic anoxic
1201 event 2. *Geology* **43**, 963–966.
- 1202 Pyle D. M. and Mather T. A. (2003) The importance of volcanic emissions for the global atmospheric mercury
1203 cycle. *Atmos. Environ.* **37**, 5115–5124.
- 1204 Racki G., Rakocinski M., Marynowski L. and Wignall P. B. (2018) Mercury enrichments and the Frasnian-
1205 Famennian biotic crisis: A volcanic trigger proved? *Geology* **46**, 543–546.
- 1206 Rakociński M., Książak D., Pisarzowska A. and Marynowski L. (2022) Mercury evidence of intense submarine
1207 volcanism and hydrothermal activity during a mid-Tournaisian anoxic event in the Carnic Alps. *Gondwana
1208 Res.* **109**, 225–238.
- 1209 Rakociński M., Marynowski L., Pisarzowska A., Beldowski J., Siedlewicz G., Zatoń M., Perri M. C., Spalletta C.
1210 and Schönlaub H. P. (2020) Volcanic related methylmercury poisoning as the possible driver of the end-
1211 Devonian Mass Extinction. *Sci. Rep.* **10**, 1–8.
- 1212 Rakociński M., Pisarzowska A., Corradini C., Narkiewicz K., Dubicka Z. and Abdiyev N. (2021) Mercury spikes as
1213 evidence of extended arc-volcanism around the Devonian–Carboniferous boundary in the South Tian Shan
1214 (southern Uzbekistan). *Sci. Rep.* **11**, 1–15.
- 1215 Ravichandran M. (2004) Interactions between mercury and dissolved organic matter - A review. *Chemosphere* **55**,
1216 319–331.
- 1217 Rohling E. J., Marino G. and Grant K. M. (2015) Mediterranean climate and oceanography, and the periodic
1218 development of anoxic events (sapropels). *Earth-Science Rev.* **143**, 62–97.
- 1219 Rumayor M., Gallego J. R., Rodríguez-Valdés E. and Díaz-Somoano M. (2017) An assessment of the environmental
1220 fate of mercury species in highly polluted brownfields by means of thermal desorption. *J. Hazard. Mater.* **325**,
1221 1–7.
- 1222 Rydberg J., Gälman V., Renberg I., Bindler R., Lambertsson L. and Martínez-Cortizas A. (2008) Assessing the
1223 Stability of Mercury and Methylmercury in a Varved Lake Sediment Deposit. *Environ. Sci. Technol.* **42**,
1224 4391–4396.
- 1225 Sabatino N., Ferraro S., Coccioni R., Bonsignore M., Del Core M., Tancredi V. and Sprovieri M. (2018) Mercury
1226 anomalies in upper Aptian-lower Albian sediments from the Tethys realm. *Palaeogeogr. Palaeoclimatol.
1227 Palaeoecol.* **495**, 163–170.
- 1228 Sanei H. and Goodarzi F. (2006) Relationship between organic matter and mercury in recent lake sediment: The
1229 physical-geochemical aspects. *Appl. Geochemistry* **21**, 1900–1912.
- 1230 Sanei H., Grasby S. E. and Beauchamp B. (2012) Latest Permian mercury anomalies. *Geology* **40**, 63–66.
- 1231 Van Santvoort P. J. M., De Lange G. J., Thomson J., Colley S., Meysman F. J. R. and Slomp C. P. (2002) Oxidation

- 1232 and origin of organic matter in surficial Eastern Mediterranean hemipelagic sediments. *Aquat. Geochemistry*
1233 **8**, 153–175.
- 1234 Scaife J. D., Ruhl M., Dickson A. J., Mather T. A., Jenkyns H. C., Percival L. M. E., Hesselbo S. P., Cartwright J.,
1235 Eldrett J. S., Bergman S. C. and Minisini D. (2017) Sedimentary Mercury Enrichments as a Marker for
1236 Submarine Large Igneous Province Volcanism? Evidence From the Mid-Cenomanian Event and Oceanic
1237 Anoxic Event 2 (Late Cretaceous). *Geochemistry, Geophys. Geosystems* **18**, 4253–4275.
- 1238 Schlanger S. O. and Jenkyns H. C. (1976) Cretaceous Oceanic Anoxic Events: Causes and Consequences. *Geol. en*
1239 *Mijnb.* **55**, 179–184.
- 1240 Schuster P. F., Krabbenhoft D. P., Naftz D. L., Cecil L. D., Olson M. L., Dewild J. F., Susong D. D., Green J. R. and
1241 Abbott M. L. (2002) Atmospheric mercury deposition during the last 270 years: A glacial ice core record of
1242 natural and anthropogenic sources. *Environ. Sci. Technol.* **36**, 2303–2310.
- 1243 Schütze M., Gatz P., Gilfedder B. and Biester H. (2021) Why productive lakes are larger mercury sedimentary sinks
1244 than oligotrophic brown water lakes. *Limnol. Oceanogr.* **66**, 1316–1332.
- 1245 Shen J., Algeo T. J., Chen J., Planavsky N. J., Feng Q., Yu J. and Liu J. (2019a) Mercury in marine
1246 Ordovician/Silurian boundary sections of South China is sulfide-hosted and non-volcanic in origin. *Earth*
1247 *Planet. Sci. Lett.* **511**, 130–140.
- 1248 Shen J., Algeo T. J., Planavsky N. J., Yu J., Feng Q., Song H. H., Song H. H., Rowe H., Zhou L. and Chen J.
1249 (2019b) Mercury enrichments provide evidence of Early Triassic volcanism following the end-Permian mass
1250 extinction. *Earth-Science Rev.* **195**, 191–212.
- 1251 Shen J., Chen J., Algeo T. J., Yuan S., Feng Q., Yu J., Zhou L., O’Connell B. and Planavsky N. J. (2019c) Evidence
1252 for a prolonged Permian–Triassic extinction interval from global marine mercury records. *Nat. Commun.* **10**,
1253 1–9.
- 1254 Shen J., Feng Q., Algeo T. J., Liu Jinling, Zhou C., Wei W., Liu Jiansi, Them T. R., Gill B. C. and Chen J. (2020)
1255 Sedimentary host phases of mercury (Hg) and implications for use of Hg as a volcanic proxy. *Earth Planet.*
1256 *Sci. Lett.* **543**, 116333.
- 1257 Shipboard Scientific Party (2004) Site 1261. In *Proceedings of the Ocean Drilling Program, 207 Initial Reports*
1258 (eds. J. Erbacher, D. C. Mosher, and M. J. Malone). Ocean Drilling Program, College Station. pp. 1–103.
- 1259 Snow L. J., Duncan R. A. and Bralower T. J. (2005) Trace element abundances in the Rock Canyon Anticline,
1260 Pueblo, Colorado, marine sedimentary section and their relationship to Caribbean plateau construction and
1261 oxygen anoxic event 2. *Paleoceanography* **20**, 1–14.
- 1262 Sprain C. J., Renne P. R., Vanderkluysen L., Pande K., Self S. and Mittal T. (2019) The eruptive tempo of Deccan
1263 volcanism in relation to the Cretaceous-Paleogene boundary. *Science (80-.)*. **363**, 866–870.
- 1264 Strode S. A., Jaeglé L., Selin N. E., Jacob D. J., Park R. J., Yantosca R. M., Mason R. P. and Slemr F. (2007) Air-
1265 sea exchange in the global mercury cycle. *Global Biogeochem. Cycles* **21**, 1–12.
- 1266 Sunderland E. M., Gobas F. A. P. C., Heyes A., Branfireun B. A., Bayer A. K., Cranston R. E. and Parsons M. B.
1267 (2004) Speciation and bioavailability of mercury in well-mixed estuarine sediments. *Mar. Chem.* **90**, 91–105.
- 1268 Sweere T., Hennekam R., Vance D. and Reichart G. J. (2021) Molybdenum isotope constraints on the temporal
1269 development of sulfidic conditions during Mediterranean sapropel intervals. *Geochemical Perspect. Lett.* **17**,
1270 16–20.
- 1271 Takahashi T., Sutherland S. C., Sweeney C., Poisson A., Metzl N., Tilbrook B., Bates N., Wanninkhof R., Feely R.
1272 A., Sabine C., Olafsson J. and Nojiri Y. (2002) Global sea–air CO₂ flux based on climatological surface ocean
1273 pCO₂, and seasonal biological and temperature effects. *Deep Sea Res. Part II Top. Stud. Oceanogr.* **49**, 1601–
1274 1622.

- 1275 Them T. R., Jagoe C. H., Caruthers A. H., Gill B. C., Grasby S. E., Gröcke D. R., Yin R. and Owens J. D. (2019)
 1276 Terrestrial sources as the primary delivery mechanism of mercury to the oceans across the Toarcian Oceanic
 1277 Anoxic Event (Early Jurassic). *Earth Planet. Sci. Lett.* **507**, 62–72.
- 1278 Tremblin M., Khozyem H., Adatte T., Spangenberg J. E., Fillon C., Grauls A., Hunger T., Nowak A., Läubli C.,
 1279 Lasseur E., Roig J.-Y., Serrano O., Calassou S., Guillocheau F. and Castellort S. (2022) Mercury enrichments
 1280 of the Pyrenean foreland basins sediments support enhanced volcanism during the Paleocene-Eocene thermal
 1281 maximum (PETM). *Glob. Planet. Change* **212**, 103794.
- 1282 Tribouillard N., Algeo T. J., Lyons T. W. and Riboulleau A. (2006) Trace metals as paleoredox and
 1283 paleoproductivity proxies: An update. *Chem. Geol.* **232**, 12–32.
- 1284 Tsikos H., Jenkyns H. C., Walsworth-Bell B., Petrizzo M. R., Forster A., Kolonic S., Erba E., Premoli Silva I., Baas
 1285 M., Wagner T. and Sinninghe Damsté J. S. (2004) Carbon-isotope stratigraphy recorded by the Cenomanian-
 1286 Turonian Oceanic Anoxic Event: Correlation and implications based on three key localities. *J. Geol. Soc.*
 1287 *London.* **161**, 711–719.
- 1288 Turgeon S. and Brumsack H. J. (2006) Anoxic vs dysoxic events reflected in sediment geochemistry during the
 1289 Cenomanian-Turonian Boundary Event (Cretaceous) in the Umbria-Marche Basin of central Italy. *Chem.*
 1290 *Geol.* **234**, 321–339.
- 1291 Ullrich S. M., Tanton T. W. and Abdrashitova S. A. (2001) Mercury in the aquatic environment: A review of factors
 1292 affecting methylation. *Crit. Rev. Environ. Sci. Technol.* **31**, 241–293.
- 1293 Villar E., Cabrol L. and Heimbürger-Boavida L. E. (2020) Widespread microbial mercury methylation genes in the
 1294 global ocean. *Environ. Microbiol. Rep.* **12**, 277–287.
- 1295 Du Vivier A. D. C., Selby D., Sageman B. B., Jarvis I., Gröcke D. R. and Voigt S. (2014) Marine 187Os/188Os
 1296 isotope stratigraphy reveals the interaction of volcanism and ocean circulation during Oceanic Anoxic Event
 1297 2. *Earth Planet. Sci. Lett.* **389**, 23–33.
- 1298 Wallace G. T. (1982) The association of copper, mercury and lead with surface-active organic matter in coastal
 1299 seawater. **11**, 379–394.
- 1300 Wang K., Liu G. and Cai Y. (2021) Possible pathways for mercury methylation in oxic marine waters. *Crit. Rev.*
 1301 *Environ. Sci. Technol.*, 1–19.
- 1302 Wang Z., Tan J., Boyle R., Wang W., Kang X., Dick J. and Lyu Q. (2020) Mercury anomalies within the lower
 1303 Cambrian (stage 2–3) in South China: Links between volcanic events and paleoecology. *Palaeogeogr.*
 1304 *Palaeoclimatol. Palaeoecol.* **558**.
- 1305 Wortmann U. G. and Chernyavsky B. M. (2007) Effect of evaporite deposition on Early Cretaceous carbon and
 1306 sulphur cycling. *Nature* **446**, 654–656.
- 1307 Xu W., Ruhl M., Jenkyns H. C., Leng M. J., Huggett J. M., Minisini D., Ullmann C. V., Riding J. B., Weijers J. W.
 1308 H., Storm M. S., Percival L. M. E., Tosca N. J., Idiz E. F., Tegelaar E. W. and Hesselbo S. P. (2018) Evolution
 1309 of the Toarcian (Early Jurassic) carbon-cycle and global climatic controls on local sedimentary processes
 1310 (Cardigan Bay Basin, UK). *Earth Planet. Sci. Lett.* **484**, 396–411.
- 1311 Zhao H., Grasby S. E., Wang X., Zhang L., Liu Y., Chen Z., Hu Z. and Huang Y. (2022a) Mercury enrichments
 1312 during the Carnian Pluvial Event (Late Triassic) in South China. *GSA Bull.*, 1–12.
- 1313 Zhao H., Shen J., Algeo T. J., Racki G., Chen J., Huang C., Song J., Qie W. and Gong Y. (2022b) Mercury isotope
 1314 evidence for regional volcanism during the Frasnian-Famennian transition. *Earth Planet. Sci. Lett.* **581**,
 1315 117412.
- 1316 Zhu G., Wang P., Li T., Zhao K., Yan H., Li J. and Zhou L. (2021) Nitrogen geochemistry and abnormal mercury
 1317 enrichment of shales from the lowermost Cambrian Niutitang Formation in South China: Implications for the

1318 marine redox conditions and hydrothermal activity. *Glob. Planet. Change* **199**, 103449.

1319